INFRARED SPECTROSCOPY AND THEORETICAL STUDIES
OF GROUP IV MOLECULES

by

Eric Gonzalez

Master of Science, 2007
Texas Christian University
Fort Worth, Texas

Bachelor of Science, 1998
University of Havana
Havana, Cuba

Submitted to the Graduate Faculty of the College of Science
and Engineering Texas Christian University in partial
fulfillment of the requirements for the degree of

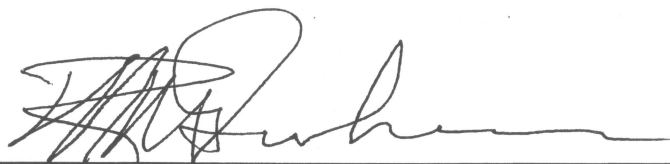Doctor of Philosophy

Texas Christian University

August 2009

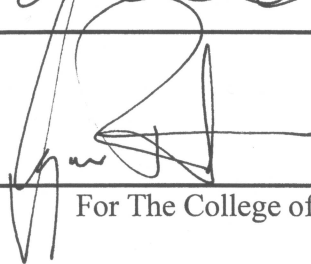# INFRARED SPECTROSCOPY AND THEORETICAL STUDIES OF
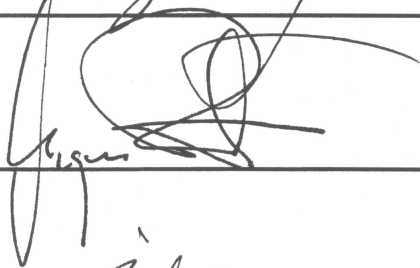# GROUP IV MOLECULES

by

Eric Gonzalez

Dissertation approved:

_____

Major Professor

_____

_____

_____

For The College of Science and Engineering

to Annita

ACKNOWLEDGEMENTS

TABLE OF CONTENTS

LIST OF FIGURES

Figure   Page

CHAPTER I

INTRODUCTION

Infrared spectroscopy has been widely used to study molecules since the pioneering work of Elmer S. Imes.[1] This and later, similar studies gave experimental support for the theoretical formulation of the physics of molecules. Also, great effort has been made in predicting molecular properties during the past decades, resulting in a great number of computational codes, which are grouped in suites of programs like *Gaussian 03*[2] that allow the computation of many molecular properties from first physical principles. These are called *ab initio* calculations. In this work, almost all experimental results will be compared with corresponding calculations.

The research described in this dissertation is mainly focused on forming novel molecules by the laser ablation of sintered rods. The elements used were carbon, silicon and germanium because of their great importance in semiconductor technology and optoelectronic devices. Also, carbon cluster are the backbone of many interstellar species, and understanding how they form by the laser ablation could provide clues to the chemical processes in astrophysical environments.

Infrared observation of the isotopic shifts of vibrational fundamentals of the synthesized molecules results in the identification of the structure of the molecule responsible for the absorptions and the assignment of vibrational fundamentals. These assignments are made upon good agreement between the experimental isotopic shifts and the calculated isotopic shifts. This allows to have a better understanding of how Group IV elements bond to form these molecules, which could be the building blocks of novel semiconductor and optoelectronic materials.

The deciphering of the structure of the molecule responsible for the isotopic shift pattern is referred as the isotopic substitution technique, which is discussed in section 2.4 of Chapter II. The limitation is that the natural abundance of ^{13}C is only 1%, so isotopic shifts might only be observed if a high yield of the carbon bearing molecule were produced. This, however, is not usually the case when a molecule is synthesized for the first time in the lab. For this reason, carbon rods with a higher concentration of ^{13}C (10-90%) were made in order to get a higher yield of carbon cluster with ^{13}C-substituted atoms; this is discussed in more detail in the section "Rod Fabrication" in Chapter II.

The silicon and germanium elements also have naturally abundant isotopes. Silicon has three natural stable isotopes ^{28}Si (92% abundance), ^{29}Si (5 %), and ^{30}Si (3%); germanium has five: ^{70}Ge (21% abundance), ^{72}Ge (28%), ^{73}Ge (8%), ^{74}Ge (36%), and ^{76}Ge (7% abundance). Thus the infrared absorptions of silicon or germanium species will result in an envelope of peaks due to the number of isotopomers of Si_n and Ge_n molecules. For germanium clusters this results in a large number of peaks spread in a small frequency interval.[3]   If the germanium or silicon atoms participate in the vibration, the isotopic absorptions of germanium-carbon or germanium-silicon-carbon molecules will also result in isotopic shifts envelopes rather than single absorptions peaks. This is observed for the second most intense infrared active fundamentals of GeC_3Ge and GeC_3Si presented in this work. To my knowledge, this is the only work which presents the infrared observation of germanium isotopic shifts. These molecules are discussed in Chapters V and VIII.

Previous studies in the TCU Molecular Physics Laboratory have reported vibrational spectra for Si_nC_m[4], Ge_nC_m,[5,6] and $Si_nC_mGe_l$[7] clusters. In early work, novel, small, silicon-carbon clusters were produced by the evaporation of mixtures of silicon and carbon from tantalum

Knudsen cells. Vibrational fundamentals were identified for a variety of Si_nC_m clusters with various structures including linear SiC_3Si,[8] cyclic Si_2C_2,[9] and planar pentagonal Si_3C_2[10]. Later investigations, using the laser ablation technique, identified for the first time vibrational fundamentals of the larger silicon-carbon clusters SiC_7[11], SiC_9[6], as well as the germanium carbon species GeC_3Ge[7], GeC_7[8], GeC_9[8], and the mixed Group IV cluster, GeC_3Si[9]. Another group[12] from Texas A&M University carried out experiments using a Knudsen effusion, mass spectrometer method measuring the partial pressures of GeC_2, Ge_2C, Ge_3C, and Ge_2C_2 above liquid germanium which was contained in a graphite Knudsen cell. The assumed ground state geometries were C_{2v} for GeC_2, Ge_2C, Ge_3C and D_{2h} for Ge_2C_2. The equilibrium geometry assumed for GeC_2 was T-shaped (C_{2v}) analogous to the silicon-carbon cluster SiC_2.[13] Later, the equilibrium geometry of GeC_2 was theoretically investigated.[14] Observation of isotopic frequency shifts could validate the L-shaped ground state geometry predicted for GeC_2. Experiments conducted as part of the present research failed to form this molecule, a task which was difficult because the yield of the C_2 molecule is lower than the C_1 monomer, and the C_3 trimer, when using the laser ablation technique.[15] SiC_2 and AlC_2[16] are the only C_2 bearing species produced by the laser ablation technique despite many experimental studies with the transition metals and germanium using the laser evaporation technique that produced species containing the C_3 trimer.

SiC_3 rhomboidal and fan structures have been detected in space,[58,59] and have been subject to extensive theoretical studies because of a controversy about what the geometry is for the global minimum (see the introduction of Chapter VI). On the other hand, this work presents experimental evidence that linear GeC_3 has been formed by the laser ablation technique. See

Chapter VI for a detailed discussion of this molecule that has been synthesized here for the first time.

This work also presents new spectroscopic data for carbon clusters in Chapter V and VI. The observation of novel combination bands of C_5 and C_9 has allowed the assignment of two symmetry stretching fundamentals of these molecules. In addition, Chapter VI presents experimental evidence and theoretical calculations which have allowed assignment of the remaining infrared active vibrational fundamentals of linear C_7 and C_8. Because these absorptions are very weak they passed undetected in many spectroscopic studies on carbon clusters done in the 90s. Their detection here also indicates the high yield of carbon clusters produced by the laser ablation technique employed in this research. With this high production of carbon clusters far infrared spectroscopy could in the future lead to the identification of bending modes which have still not all been detected yet.

Two novel molecules were produced in this research, linear GeC_5Ge and GeC_3, allowing the assignment of the $v_4(\sigma_u)$ mode of linear GeC_5Ge at 2158.0 cm^{-1}, and the $v_1(\sigma)$ and $v_2(\sigma)$ modes of linear GeC_3 at 1903.9 cm^{-1} and 1279.6 cm^{-1} respectively. New spectroscopic data was obtained for other germanium/carbon species: the $v_4(\sigma_u)$ mode of GeC_3Ge at 735.6 cm^{-1}, which exhibit germanium isotopic shifts, and the bending mode $v_6(\pi_u)$ at 580.1 cm^{-1}, the (v_1+v_4) combination band of linear C_5 at 3388.8 cm^{-1} which allows us to assign the only remaining unobserved fundamental of this molecule the $v_1(\sigma_g)$ symmetric stretch at 1946 cm^{-1}, the (v_2+v_7) combination band of linear C_9 at 3471.8 cm^{-1} which allows us to assign the previously unobserved fundamental, the $v_2(\sigma_g)$ symmetric stretch at 1870 cm^{-1}, and the weak $v_6(\sigma_u)$ asymmetric stretch for of linear C_7 at 1100.1 cm^{-1}.

Chapter VII includes a theoretical study on the calculation of infrared intensities. Carbon dioxide was used as a test case for these calculations. The results of this work suggests that if the infrared intensities are computed using the mechanical (up to the quartic term) and electrical (up to the quadratic) anharmonicities, the predictions won't be as inexact as they are using only the first derivative of the molecular dipole-moment with harmonic transition states.

CHAPTER II

EXPERIMENTAL TECHNIQUES

2.1   Experimental Apparatus

Fourier transform infrared (FTIR) spectroscopy has been widely used to analyze matter. Iin the solid, liquid or gas phase matter absorbs light in the infrared region giving a characteristic infrared signature for the sample. Figure 2.1 shows the schematic of the FTIR spectrometer that is built around a Michelson interferometer, in which a light wave is superimposed with a time-shifted copy of itself coming from the movable mirror. This spectrometer has a higher signal-to-noise ratio compared to wavelength-selective spectrometers because it measures the total intensity of the incident light not just a small band.[17]   A better signal-to-noise ratio is also achieved by averaging many interferograms. Usually 1000 interferograms are averaged and the Bartlet apodization function is used in the FFT(Fast Fourier transform) for all generated spectra involving new discoveries in this dissertation research.
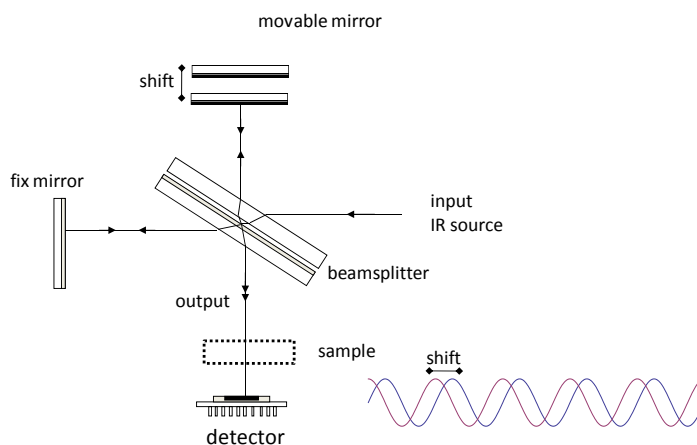
Figure 2.1.   Schematics of the Michelson interferometer.

Matrix isolation spectroscopy[18] consists of trapping molecules in a solid inert gas, *e.g.* argon at 10 K, and applying a spectroscopic technique to the sample. The trapped molecules cannot rotate, which greatly simplifies the infrared spectrum because the large number of rotational absorptions will be absent.

Figure 2.2 shows the top view of the experimental setup, within which the optical path inside the FTIR spectrometer is illustrated. An optical table with transfer optics is placed in the spectrometer's sample section to redirect the light toward the laser ablation chamber. This configuration allows two independent laser ablation chambers to share the same spectrometer. The spectrometer and the laser ablation chambers are separate with different vacuum systems at $\sim10^{-3}$ Torr and $\sim10^{-8}$ Torr respectively. A CsI window, transparent in the mid infrared (refer to the transmittance spectra in Fig. 2.3), is used to separate the laser ablation chamber from the spectrometer. A quartz window allows the laser beam (Nd:YAG 1064 nm operating in the pulse mode) into the chamber, toward the rods. 1024 nm corresponds to 9398.5 cm^{-1}, and Fig. 2.3 shows that the quartz window transmits this frequency. The separation of the spectrometer from the ablation chamber protects the spectrometer optics from graphite dust and the vapor from other elements that come from the laser ablation of the rods.

The molecules are produced by simultaneous laser ablation of carbon, germanium, or silicon rods, while these rods are rotating and vertically translating. The evaporated species are condensed in solid Ar (Matheson, 99.9995% purity) on the gold mirror previously cooled to ~10 K by a close cycle refrigeration system (ARS, Displex). During deposition an argon flow is allowed into the chamber, which condenses onto the gold mirror, and traps the molecules being formed. FTIR absorption spectra are recorded over the range of 500 to 5000 cm^{-1} at a resolution of 0.2 cm^{-1}. The beamsplitter is KBr which has a range of 500-6000 cm^{-1}. The detectors used in

this work are the MCT (Hg-Cd-Te, range ~500-12000 cm^{-1}) and InSb (range 2000-14000 cm^{-1}) detectors. The former is very sensitive at ~2000 cm^{-1}, but the later is ~7 times more sensitive in 3000-4000 cm^{-1} region. The InSb detector enabled the observation of novel combination bands of carbon clusters. Figure 2.4 shows a comparison between the InSb and MCT detectors in the vicinity of a new combination band at 3388.8 cm^{-1}, which is assigned to linear C_5, as will be discussed in detail in Chapter VI. The InSb detector was indispensable for observing the isotopic shifts of this band, which are essential in the assignment of the absorption.

Nd:YAG lasers
power range 0.2-4.0 Watts

infrared source

focusing
lenses

Michelson
interferometer

quartz window

vacuum
10^{-3} Torr

CsI window

gold-plated mirror
deposition mirror at
~10 K

The other team similar laser
ablation chamber setup

transfer optics

Vacuum
10^{-8} Torr

detector

preamplifier

output signal   -   +

rotating and
translating rods

Ar delivery system
~700 Torr

Figure 2.2.   Top view schematics of the experimental setup. The transfer optics allows two laser ablation chambers to share the same spectrometer. Drawing is not to scale.
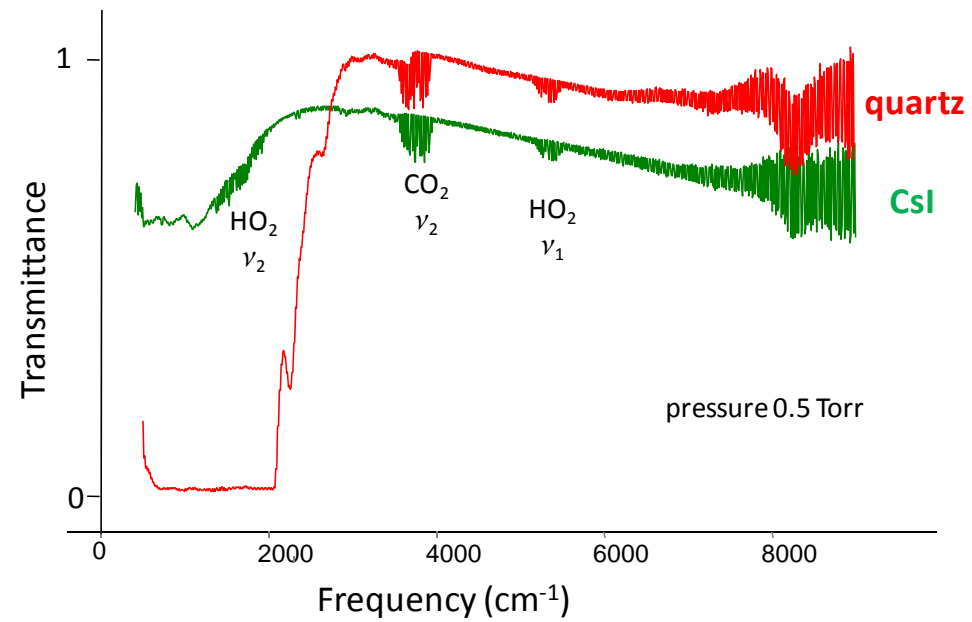
Figure 2.3.   Transmittance of CsI window (2.5 mm thickness) and the quartz window (2.0 mm thickness). The quartz window although transparent in the visible acts like a filter in the mid infrared. The spectrometer was partially evacuated up to 0.5 Torr, which accounts for the CO_2 and water absorptions.

.
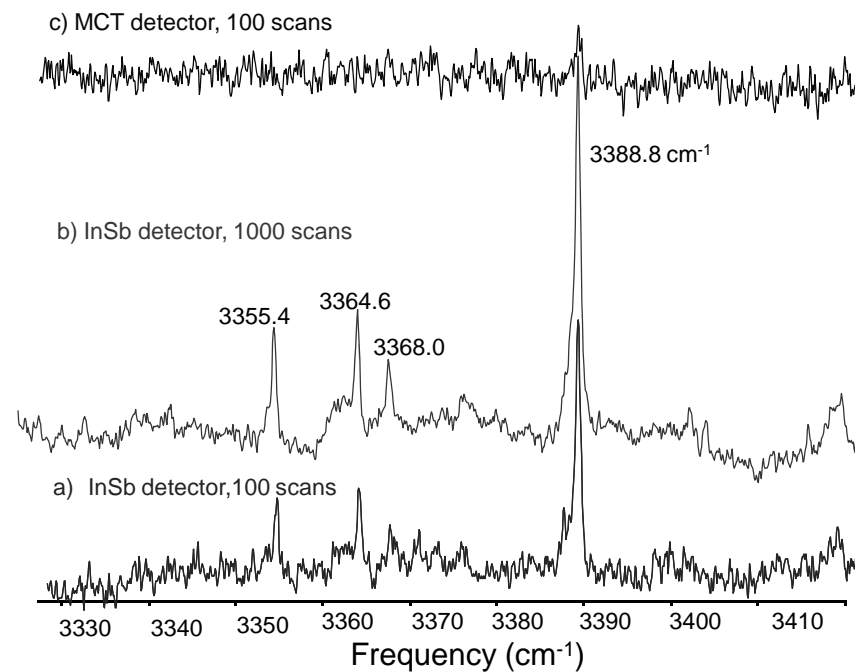
Figure 2.4.   The combination band absorption at 3388.8 cm^{-1} has been undetected in previous studies on combination bands of carbon clusters. With the MCT detector (c) the band is barely above the noise after 100 scans, but with the same number of scans using the InSb detector the signal-to-noise improves by a factor ~7 and two isotopic shifts appear to the low frequency side. After 1000 scans with the InSb detector (b) another shift shows up with intensity half of the other two. This shift pattern is what is expected for linear C_5, and is observed because of the high sensitivity of the InSb detector in the 3000 cm^{-1} region. The carbon rod used had 10% [13]C enrichment.

2.2   Rod Fabrication

In order to decipher the molecular structure and to make an unambiguous determination of the vibrational fundamentals it is crucial to measure isotopic frequency shifts. For this reason, carbon rods are fabricated using mixtures of ^{12}C (Alfa Aesar, 99.9995% purity) and ^{13}C (Isotec, 99.3% purity), the percent ratio % ^{13}C:% ^{12}C determines the shape of the intensities of the isotopic shifts which enables the determination of the symmetry of the molecule.

A pair of formulas (Eq. 2.1) have been derived to calculate the ^{13}C to ^{12}C % ratio, $r = \frac{\%^{13}C}{\%^{12}C}$:

$$M_{12} = \frac{M}{1 + r\frac{m_{13}}{m_{12}}} \qquad\qquad M_{13} = \frac{M}{1 + \frac{1}{r}\frac{m_{12}}{m_{13}}}$$

$M = M_{12} + M_{13}$ is the rod total mass

$m_{12} = 12.00000$ a.u. $m_{13} = 13.003355$ a.u.

Eq. 2.1

These formulas can be also used to make germanium-carbon or silicon-carbon rods with a desired concentration of germanium and carbon atoms in the rod (just replace m_{13} by the average m_{Ge}=72.61 a.u. or m_{Si}=20.08 a.u.). The rods used to produce the high production of GeC$_3$Ge discussed in Chapter V have 20% Ge atoms with a Ge:C mass ratio 1.5:1. On the other hand, the germanium-carbon rods used to produce the first synthesis of the GeC$_3$ molecule discussed in Chapter VI have 5-7% Ge atoms with a Ge:C mass ratio of ~0.45:1.

Also a set of formulas were derived to find the desired concentration of three element rods, see Eq. 2.2. These formulas were used to make rods having 0.07:0.86:0.07 (Ge:C:Si) desired atomic ratios, equivalent to a mass ratio 0.290:0.595:0.115. Notice that the mass of germanium in the rod is more than twice the mass of silicon. It was found that these rods produce a high yield of GeC$_3$Si, GeC$_3$Ge, and SiC$_3$Si. See section 9.6 of Chapter IX, for a

discussion of the newly observed fundamental of linear GeC_3Si. These formulas allow one to know the concentration of each element in the rod, which results in a systematic procedure for doing experiments, and permits the reproduction of experiments with other elements but with the same concentrations. For example, a nickel-carbon rod with 5-7% Ni atoms concentration might lead to the production of NiC_3 since this concentration successfully allowed the formation of GeC_3, see Chapter V. Similarly, the use of the concentration ratio that produced a high yield of GeC_3Si could be used to form other metal-C_3Si clusters, as shown by Eq. 2.2:

$$M_{Ge} = \frac{M}{1 + \dfrac{r_C}{r_{Ge}}\dfrac{m_C}{m_{Ge}} + \dfrac{r_{Si}}{r_{Ge}}\dfrac{m_{Si}}{m_{Ge}}}$$

$$M_C = \frac{M}{1 + \dfrac{r_{Ge}}{r_C}\dfrac{m_{Ge}}{m_C} + \dfrac{r_{Si}}{r_C}\dfrac{m_{Si}}{m_C}}$$

$$M_{Si} = \frac{M}{1 + \dfrac{r_C}{r_{Si}}\dfrac{m_C}{m_{Si}} + \dfrac{r_{Ge}}{r_{Si}}\dfrac{m_{Ge}}{m_{Si}}}$$

Eq. 2.2

$M = M_{Ge} + M_C + M_{Si}$ is the rod total mass

$m_{Ge} = 72.61$ a.u. $\qquad m_C = 12.00$ a.u. $\qquad m_{Si} = 28.08$ a.u

$r_{Ge} + r_C + r_{Si} = 1$

where $r_{Ge}, r_C,$ and r_{Si} are the concentration ratios of Ge, C, and Si respectively

The germanium-carbon, silicon-carbon, and germanium-silicon-carbon rods were sintered in a newly constructed vacuum furnace at temperatures close to the lower melting points of the elements involved. The high temperature furnace and high current power supply were designed respectively by Murdock[19] and Katchinska[20]. Figure 2.5 shows the new furnace power-supply. The rods were sintered at temperatures 100 ^{o}C lower than the lowest melting point of the elements present in the rod. The sintering time was between 2 to 3 days at pressures of~10^{-7} Torr. These rods were capable of resisting high laser power for long periods (1-2 hours) in more than five experiments.
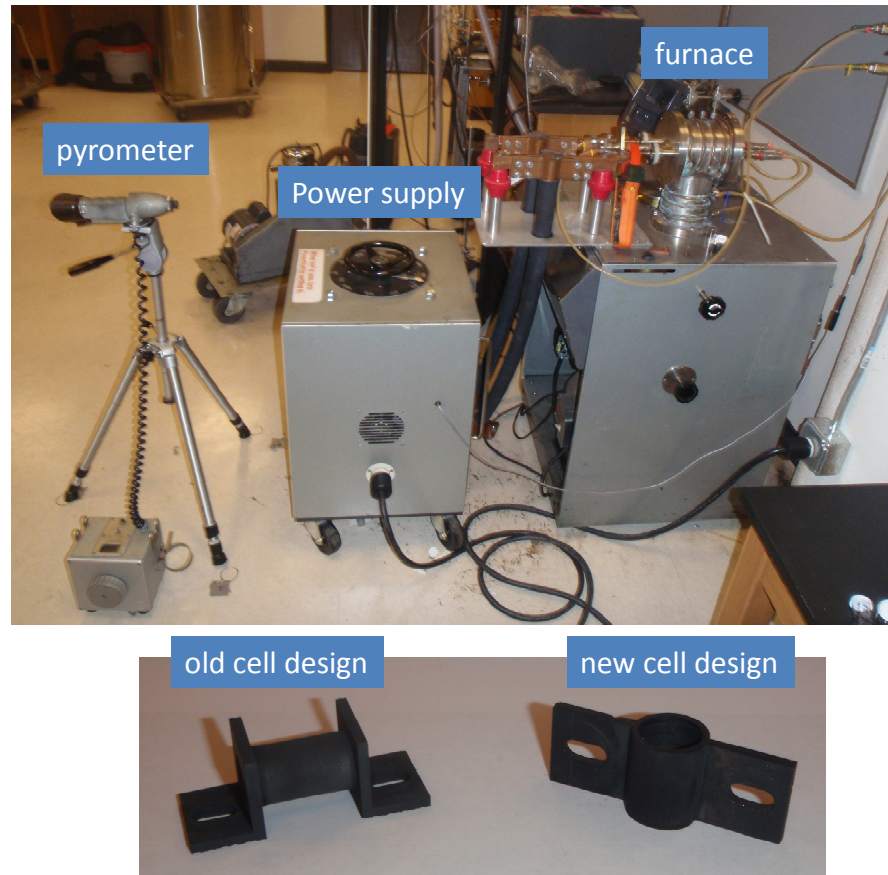
Figure 2.5   Newly built power supply (up to 650 A /5 Volts) and vacuum furnace which allows the heating of carbon rods to up ~2400 °C. The bottom figure shows a new cell designed with less volume where the center of the rod will be the hottest area.

2.3   Experimental Conditions

The experimental parameters: Ar flow rate, laser power per unit area, and deposition time have been previously discussed.[21] In this research, two types of experiments have been carried out using low and high laser power per unit area. This is controlled by increasing the laser power and the focus of the beam on the rod. For example, a loosely focused (~4-6 mm diameter spot on the rod) with high power (~3 Watts) beam gives ~5 x10^{-2} Watts/cm^2. A tightly focused (3 mm diameter spot on the rod) with relatively low laser power (~0.7 Watts) gives ~ 14 x10^{-2} Watts/cm^2. These different conditions result in increasing or decreasing the yield of particular carbon clusters. Also the plume or cloud of vapor around the spot where the laser hits the rod has a different color and shape: yellowish for a loose focused laser, violet for the tighter one, and white for very low power. The rule of thumb for which molecules are favored is: the tight focus produces a high yield of linear C_3 and C_4, and the loose focus, C_5, C_6, cyclic C_6, C_7, C_9 and C_{12} as well as many unidentified absorptions. The violet plume (tight focus and 1 Watt of laser power) produces a very large amount of C_7 and C_4. It is worth noting another manipulation of the experiment which produced a high yield of carbon clusters that allowed the observation of previously detected combination bands and weak fundamentals: the lens was rotated ~15° making an ellipsoidal spot on the rod and turning the plume color from white to yellowish. With this type of plume sputtering* was almost eliminated and the throughput (photons reaching the detector after being reflected from the gold mirror) after 30 min deposition diminished just a little. Under those conditions deposition times were up to ~ 150 min, and could be longer if the gold mirror could hold bigger Ar matrices. The deposition times were limited not because of loss of signal, but because the Ar matrix falls from the mirror at around 200 min.

---

* Sputtering produces chunks of graphite rather than evaporating atoms or molecules.

2.4   The Isotopic Substitutions Technique

The isotopic substitution technique has been used at the TCU Molecular Physics Lab since the observation of C_4.[22]   It consists of using a controlled or known concentration of the ^{13}C isotope that will produce a unique isotopic shift pattern of the vibrational fundamentals which allows deciphering the structure of the molecule responsible for the absorptions. Figures 2.6 and 2.7 present the isotopic shift patterns of the ν_3 fundamental of the linear C_3 and C_4 molecules produced by the laser evaporation of carbon rods with different concentrations of ^{13}C. In Fig. 2.6 (a), the rod with 10% ^{13}C permits the observation of the absorptions of the single ^{13}C-substituted isotopomers B and C. Calculations predict them to be the 13-12-12 and 12-13-12 isotopomers, and their intensity ratio with respect to the main band A is ~20 % for the two equivalent sites isotopomer (13-12-12 and 12-12-13) and ~10% for the unique site isotopomer (12-13-12); they are very close to expected values of 22% and 11%.[*] In Fig. 2.6 (b), the rod with 85% ^{13}C permits the observation of the single ^{12}C-substituted isotopomers, which is referred to as the mirror spectra of Fig. 2.6 (a). Notice that both absorptions have similar intensities, ~20 % the main band A′, which is attributed to not having complete randomization of ^{12}C and ^{13}C atoms resulting from the ablation process of the experiment. Figure 2.6 (c) and (d) present the 50% ^{13}C experiment and simulation. Iin this case all isotopomers have the same probability of being formed: bands B and B′ are twice intense as the others because they correspond to equivalent sites isotopomers 13-12-12 and 12-13-13 respectively. Figure 2.7 presents similar features for linear C_4.   In this case there are overlaps between the ^{13}C double substituted isotopomers13-13-12-12 and 13-12-12-13, labeled as D. The technique and analysis explained

---

[*] If the rod has 10% of the atoms ^{13}C, then the probability of evaporating a ^{13}C atom is 0.10 and a ^{12}C atom is 0.90. Thus the full ^{12}C band of linear C_3 has a probability of $(0.9)^3$ of being formed and the single substituted isotopomer $0.1*(0.9)^2$, so the ratios are 0.1/0.9 and 2(0.1/0.9) for the unique and equivalent sites isotopomers, giving 11% and 22%, respectively.

above were used in all assignments of fundamentals or combination bands in this dissertation research.
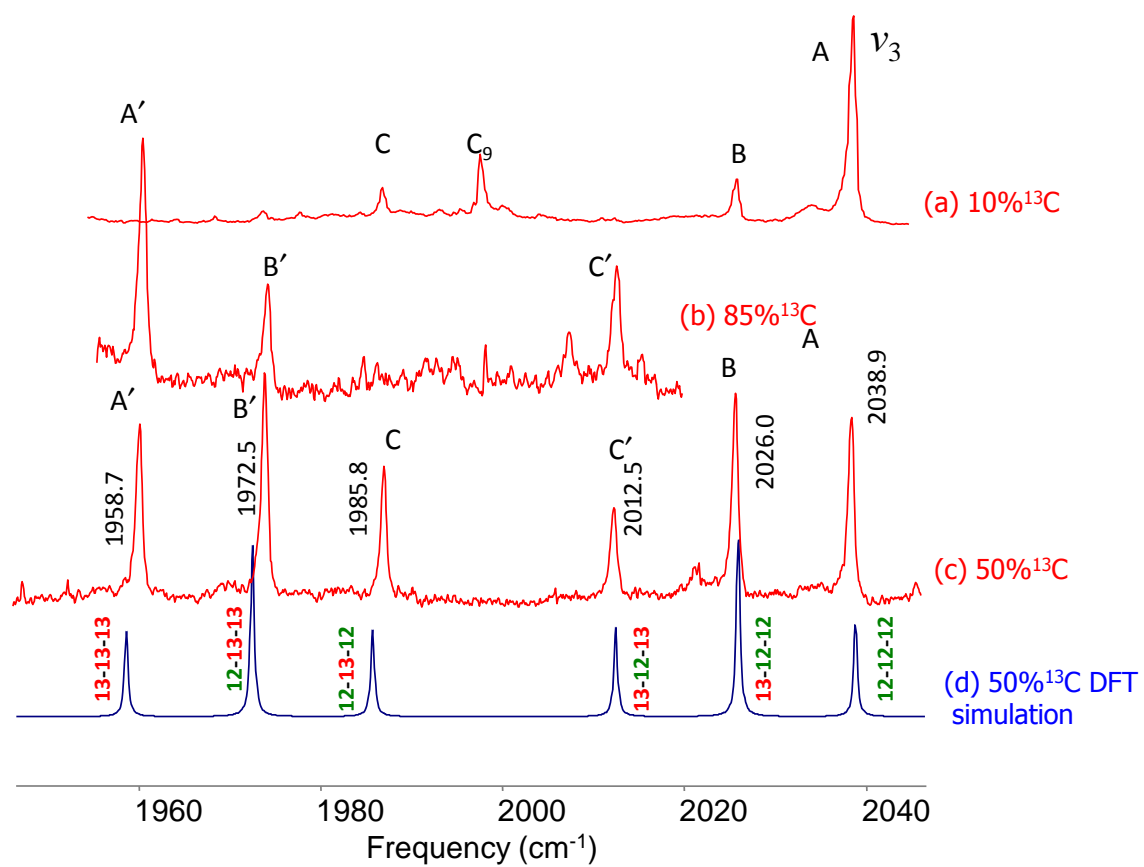
Figure 2.6   Shown above are the isotopic shift patterns for the v_3 vibrational fundamental of linear C_3 with three concentrations of ^{13}C: (a) 10%, (b) 85% and (c) 50%. The DFT simulation with (d) 50% ^{13}C is shown below. With 50% ^{13}C enrichment of the rod all isotopomers have the same probability of being formed.
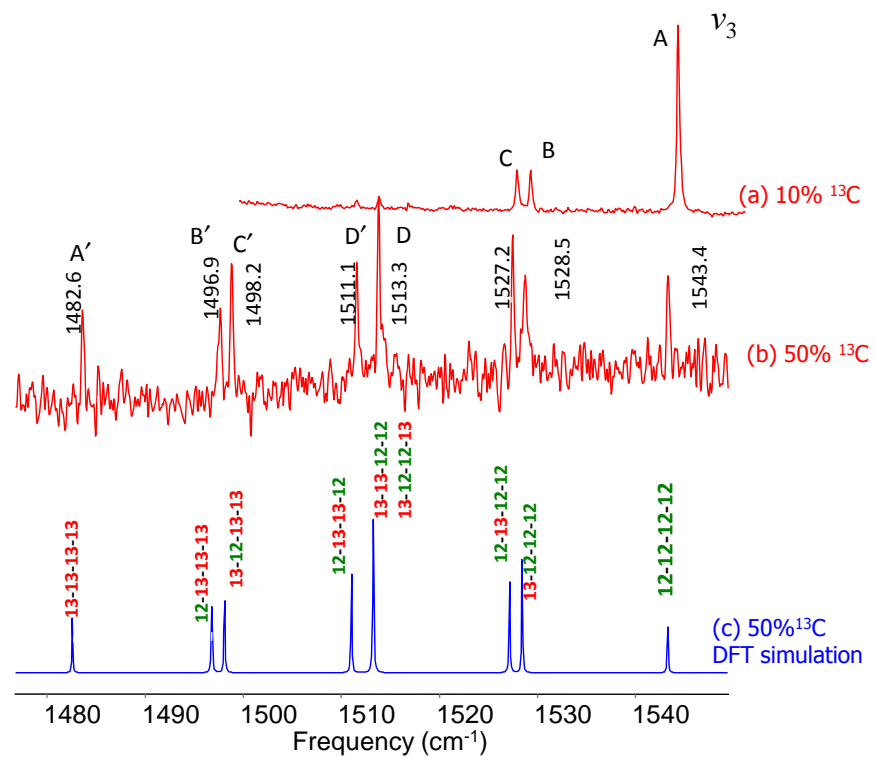
Figure 2.7   Above are the isotopic shift patterns of vibrational fundamental of linear C_4 with two concentrations of ^{13}C: (a) 10%, and (b) 50%. Below is the DFT simulation (c) with 50% ^{13}C.

CHAPTER III.

VIBRATIONAL SPECTRA OF GERMANIUM-CARBON CLUSTERS IN SOLID AR:
IDENTIFICATION OF THE $\nu_4(\sigma_u)$ MODE OF LINEAR GeC$_5$Ge

3.1. Introduction

The Group IVB molecular clusters, Si_nC_m, Ge_nC_m, and $Si_nC_mGe_l$, are of experimental and

theoretical interest because of their novel structures and potential applications in semiconductor

technology and microelectronics products.[23,24,25,26] Previously, we have reported vibrational

spectra for Si_nC_m[27], Ge_nC_m[28,29], and $Si_nC_mGe_l$[30] clusters. In early work, novel small silicon-

carbon clusters were produced by the evaporation of mixtures of silicon and carbon from

tantalum Knudsen cells. Vibrational fundamentals were identified for a variety of Si_nC_m clusters

with various structures including linear SiC_3Si,[31] cyclic Si_2C_2,[32] and planar pentagonal Si_3C_2.[33]

Later investigations, using the laser ablation technique, identified for the first time vibrational

fundamentals of the larger silicon-carbon clusters SiC_7[34] and SiC_9,[44] as well as the germanium-

carbon species GeC_3Ge,[28] GeC_7,[46] and GeC_9,[46] and the mixed Group IV cluster, GeC_3Si.[47] All of

these molecules were found to be linear, although it should be noted that in other recent matrix

work on transition-metal-carbon clusters the laser ablation technique has produced the cyclic

isomer of TiC_3[35], and in earlier work on C_n clusters,[36,37] cyclic C_6 and C_8.

FTIR matrix isolation studies of the vibrational spectra of Ge_nC_m clusters formed by laser

ablation have continued and in this paper we report a new specie, linear GeC$_5$Ge. It was

expected that GeC$_5$Ge would retain the linear structure of C_5 since previous experimental

measurements and DFT calculations have shown that the original linear carbon chain structure is

retained on the addition of a Si or Ge atom to one or both ends. For example, SiC_3Si,[48] SiC_4,[38] SiC_4Si,[39] GeC_3Ge,[28] GeC_7,[46] GeC_9,[46] and GeC_3Si[47] have all been observed to have linear structures.

This work presents experimental measurements and DFT calculations, which confirm a linear geometry for GeC_5Ge in the ground state. Based on very good agreement between ^{13}C isotopic shift measurements with the predictions of DFT calculations the $\nu_4(\sigma_u)$ fundamental of GeC_5Ge has been unambiguously assigned.

3.2. Theory

To support the identification of the vibrational spectrum of GeC_5Ge, we performed DFT calculations at the standard B3LYP/cc-pVDZ level using the *Gaussian 03* program suite.[2] The optimized geometry parameters for the $^1\Sigma_g^+$ ground state of linear GeC_5Ge are presented in Fig 3.1. The harmonic fundamental frequencies and infrared intensities of linear GeC_5Ge are given in Table 3.1. Isotopic shift calculations were performed only for the most intense stretching fundamental, $\nu_4(\sigma_u)$.
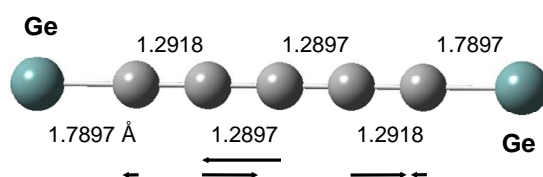
Figure 3.1   DFT predicted (B3LYP/cc-pVDZ) ground state geometry for the GeC₅Ge cluster. Arrows indicate the principal nuclear displacements for the $v_4(\sigma_u)$ mode (see Table 3.1).

Table 3.1   DFT B3LYP/cc-pVDZ predicted vibrational frequencies (cm^{-1}) and band intensities for the linear GeC₅Ge.

Vibrational mode	Frequency (cm^{-1})	Infrared intensity (km/mol)
$v_1(\sigma_g)$	2027.0	0
$v_2(\sigma_g)$	1075.3	0
$v_3(\sigma_g)$	240.8	0
$v_4(\sigma_u)$	2135.0	4592
$v_5(\sigma_u)$	1619.2	1212
$v_6(\sigma_u)$	561.9	148
$v_7(\pi_g)$	516.3	0
$v_8(\pi_g)$	121.5	0
$v_9(\pi_u)$	628.7	13
$v_{10}(\pi_u)$	237.8	7
$v_{11}(\pi_u)$	43.3	1

3.3. Experimental Procedure

GeC$_5$Ge was produced using a dual-laser ablation setup that has been described previously,[34] in which germanium and carbon rods are rotated and translated while being simultaneously ablated by two Nd:YAG lasers (CGR-11, Spectra Physics) operating at 1064 nm in the pulsed mode. The evaporated species are condensed in solid Ar (Matheson, 99.9995% purity) on a gold surfaced mirror previously cooled to ~10 K by a closed cycle refrigeration system (ARS, Displex). The mirror is enclosed in a vacuum chamber maintained at a pressure of ~10^{-8} Torr. Experimental parameters such as laser focus, laser power, and Ar flow were adjusted to favor the production of GeC$_5$Ge. For the laser ablation of the carbon rod a loosely focused beam was used with a power of 2.0 Watts; for the germanium rod (ESPI, 99.9999% purity) the beam was tightly focused with a power of 2.8 Watts. During deposition, the Ar flow rate was adjusted by opening a needle valve until the chamber pressure increased from ~10^{-8} to ~6.0×10^{-5} Torr. Typically, matrix samples were deposited for ~30 min.

In order to make an unambiguous determination of molecular structure and to identify vibrational fundamentals it is crucial to measure isotopic shifts. For this reason carbon rods were fabricated using two mixtures of ^{12}C (Alfa Aesar, 99.9995% purity) and ^{13}C (Isotec, 99.3% purity) with ~15% ^{13}C and ~85% ^{13}C enrichments to obtain single and double ^{13}C substitutions in Ge$_n$^{12}C$_n$ and the mirror image isotopic shift pattern for single and double ^{12}C substitutions in Ge$_n$^{13}C$_n$. The carbon powder mixtures were pressed into cylindrical rods (2 cm long and 1 cm in diameter) with a die pressure of ~1.5 GPa for 4 hours and then the rods were baked for 21 days at ~1950°C inside a furnace maintained under a vacuum of ~10^{-6} Torr or better.

FTIR absorption spectra of the products condensed in the Ar matrix were recorded over the range of 500-3500 cm^{-1} at a resolution of 0.2 cm^{-1} using a Bomem DA3.16 Fourier transform

spectrometer equipped with a liquid nitrogen cooled MCT (Hg-Cd-Te) detector and KBr beamsplitter. Details of the optical system have been reported previously.[40]

3.4. Results and Discussion

Figure 3.2 shows survey spectra recorded in the range 1750-2200 cm^{-1} where most of the stretching modes of germanium-carbon clusters are expected to be located. The spectrum produced by the simultaneous ablation of a carbon (~1.5% ^{13}C natural enrichment) and a Ge rod is shown in Fig. 3.2(a). For comparison, Fig. 3.2(b) shows the spectrum produced under identical experimental conditions by the ablation of a carbon rod alone. Experimental parameters were adjusted to favor the production of the relatively longer carbon chains C_5, C_6, C_7, and C_9, rather than C_3. The simultaneous ablation produced the characteristic fundamental vibrations of germanium-carbon clusters identified in our previous studies,[28,46] the $\nu_4(\sigma)$ mode of GeC_9 at 1928.3 cm^{-1}, the $\nu_1(\sigma)$ mode of GeC_7 at 2063.8 cm^{-1}, and the less intense $\nu_3(\sigma_u)$ mode of GeC_3Ge at 1920.3 cm^{-1}. In addition, two intense new absorptions at 2158.0 and 2093.2 cm^{-1} were observed. Since these bands, appeared only when germanium was ablated, the molecules responsible must certainly contain germanium. Because vibrational frequencies of pure Ge_n clusters lie below 700 cm^{-1} both of these bands are plausible candidates for Ge_nC_m molecules. The identification of the 2093.2 cm^{-1} absorption will be the subject of a future report.

In order to find the geometry and number of carbon atoms present in the Ge_nC_m cluster responsible for the 2158.0 cm^{-1} absorption, it was necessary to make ^{13}C isotopic shift measurements. Several experiments were carried out using rods made with low (~15% ^{13}C) and high (~85% ^{13}C) enrichments. The observed ratios of band intensities for isotopomers of C_5, C_6, and C_9 were generally consistent with the nominal enrichment levels in the rods.
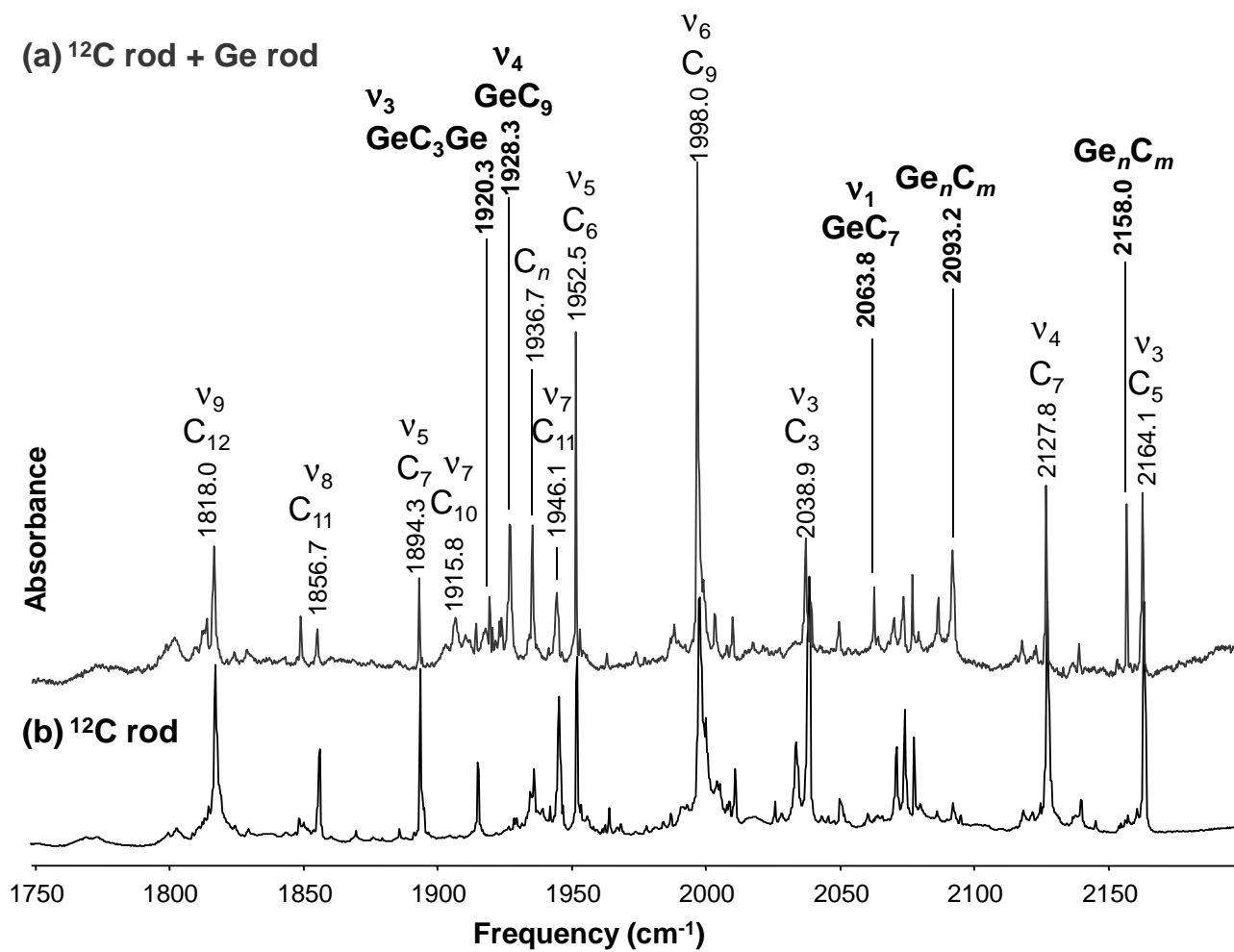
Figure 3.2   FTIR spectra produced by dual ablation of (a) Ge and ^{12}C rods and (b) a pure ^{12}C rod.

Figure 3.3(a) shows the spectrum observed when a 15% ^{13}C-enriched rod was ablated simultaneously with a Ge rod. Three bands appear in the vicinity of the 2158.0 cm^{-1} absorption, the $v_3(\sigma_u)$ mode of C$_5$ at 2164.1 cm^{-1},[42] the $v_7(\sigma_u)$ mode of C$_{12}$ at 2140.0 cm^{-1},[41] and the $v_4(\sigma_u)$ mode of C$_7$ at 2127.9 cm^{-1}.[43] Shifts corresponding to single and double ^{13}C-substituted isotopomers for C$_5$ and C$_7$ are labeled[42,43] as well as a feature at 2123.4 cm^{-1} that belongs to an as yet, unidentified C$_n$ species. Thus three prominent absorptions are left as potential single ^{13}C substitution shifts for the 2158.0 cm^{-1} absorption (A), the bands at 2155.1 (B), 2142.3 (C) and 2116.8 cm^{-1} (D). Bands B and C are ~30% of the intensity of the 2158.0 cm^{-1} while band D is ~15 % of its intensity. These intensity ratios observed with a ^{13}C enrichment of 15% indicate that the molecule contains one carbon at a unique site and two pairs of equivalent carbons, as would be the case for GeC$_5$Ge.

Figure 3.4(a) shows the mirror spectrum corresponding to single and double ^{12}C substitutions in Ge$_n$^{13}C$_n$ obtained by simultaneously ablating an 85% ^{13}C-enriched rod and a Ge rod. The absorption at 2074.7 cm^{-1}, which is a factor $\sim\sqrt{12/13}$ of the 2158.0 cm^{-1} frequency, is readily identified as belonging to the fully ^{13}C-substituted isotopomer and is probably a carbon-carbon stretch mode. All known absorptions of carbon chains bands and their isotopic shifts are labeled leaving two obvious candidates for single ^{12}C-substituted isotopic shifts from the 2074.7 cm^{-1} band at 2077.8 (B′) and 2098.8 (C′), and a possible third band at ~2117 cm^{-1} (D′). With 15% ^{12}C isotopic abundance, the B′ and C′ bands are ~30% as intense as the 2074.7 cm^{-1} band, which is analogous to the candidates for the single ^{13}C shift, B and C bands in Fig. 3.3(a) produced with 15% ^{13}C isotopic abundance. This behavior confirms that there are two pairs of equivalent carbons in the carrier molecule. The isotopomer corresponding to a ^{12}C in the central position is unfortunately, overlapped by the corresponding single ^{12}C isotopomer band shifted from the v_4
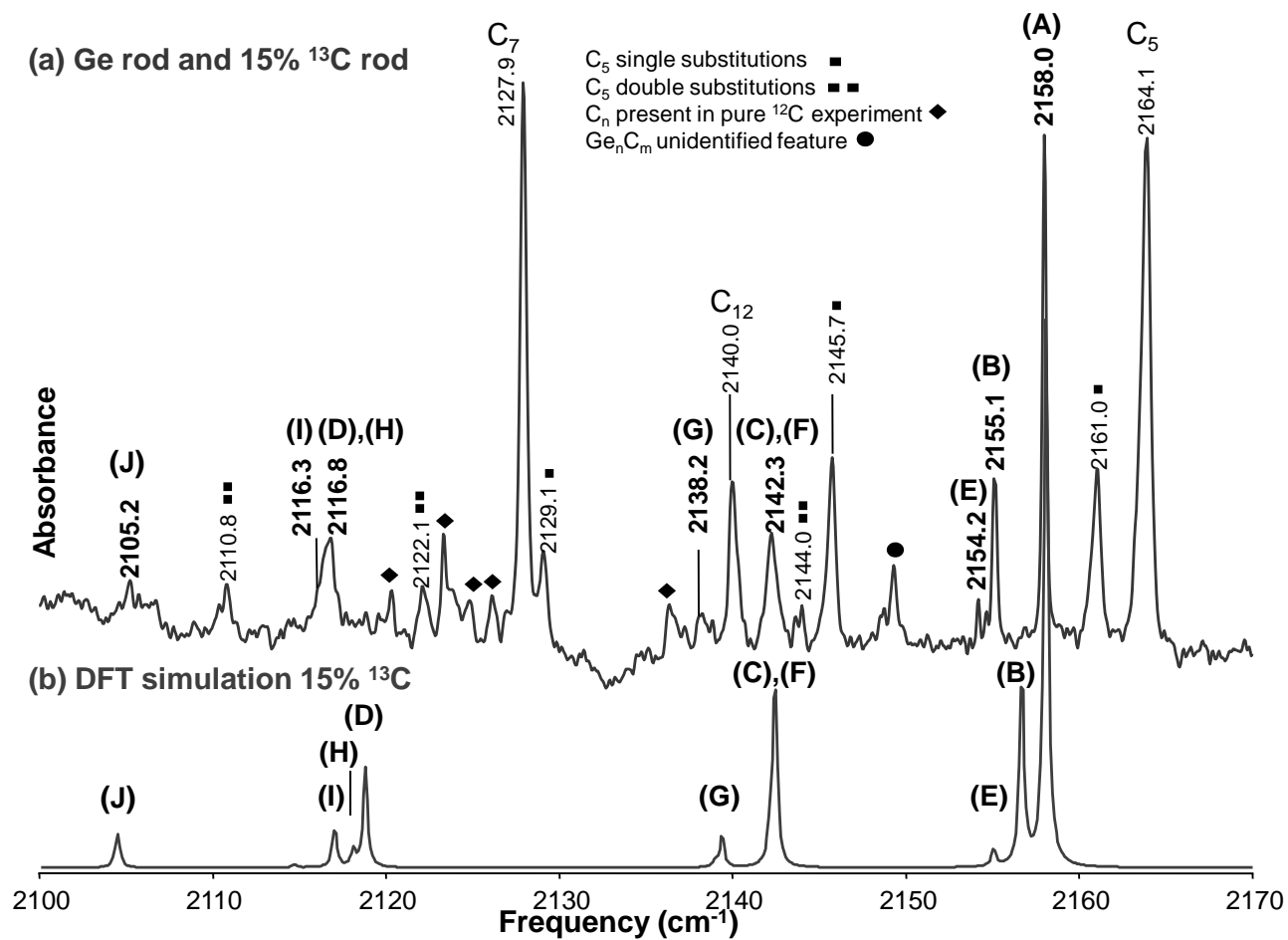
Figure 3.3   Comparison of the FTIR spectra of the $\nu_4(\sigma_u)$ mode of linear GeC_5Ge and its ^{13}C isotopic shifts (a) produced by the simultaneous evaporation of a Ge rod and carbon rods with 15% [13]C enrichment, with (b) a simulation for 15% [13]C enrichment derived from DFT calculations at the B3LYP/cc-pVDZ level. The letters correspond to the single and double ^{13}C-substituted isotopomers listed in Table 3.2

Table 3.2   Comparison of observed vibrational frequencies (cm^{-1}) of the $v_4(\sigma_u)$ mode for ^{13}C- substituted isotopomers of linear GeC$_5$Ge with the predictions of B3LYP/cc-pVDZ level calculations.

Isotopomer		Observed	B3LYP/ cc-pVDZ	Scaled[a]	Difference
Ge-C-C-C-C-C-Ge		v	v	v	Δv
74-12-12-12-12-12-74	(A)	2158.0	2135.0	2158.0	…
74-13-12-12-12-12-74	(B)	2155.1	2133.6	2156.6	1.5
74-12-13-12-12-12-74	(C)	2142.3	2119.5	2142.3	0.0
74-12-12-13-12-12-74	(D)	2116.8	2096.3	2118.9	2.1
74-13-12-12-12-13-74	(E)	2154.2	2132.0	2154.9	0.7
74-13-13-12-12-12-74	(F)	---[b]	2119.3	2142.1	---
74-13-12-12-13-12-74	(G)	2138.2	2116.5	2139.2	1.0
74-12-13-12-13-12-74	(H)	---[c]	2095.5	2118.0	--
74-13-12-13-12-12-74	(I)	2116.3	2094.4	2117.0	0.7
74-12-13-13-12-12-74	(J)	2105.2	2082.1	2104.4	-0.8

[a]Results of the DFT-B3LYP/cc-pVDZ calculation scaled by a factor of 2158.0/2135.0=1.01076.

[b]Overlapped by band C.

[c]Overlapped by band D.
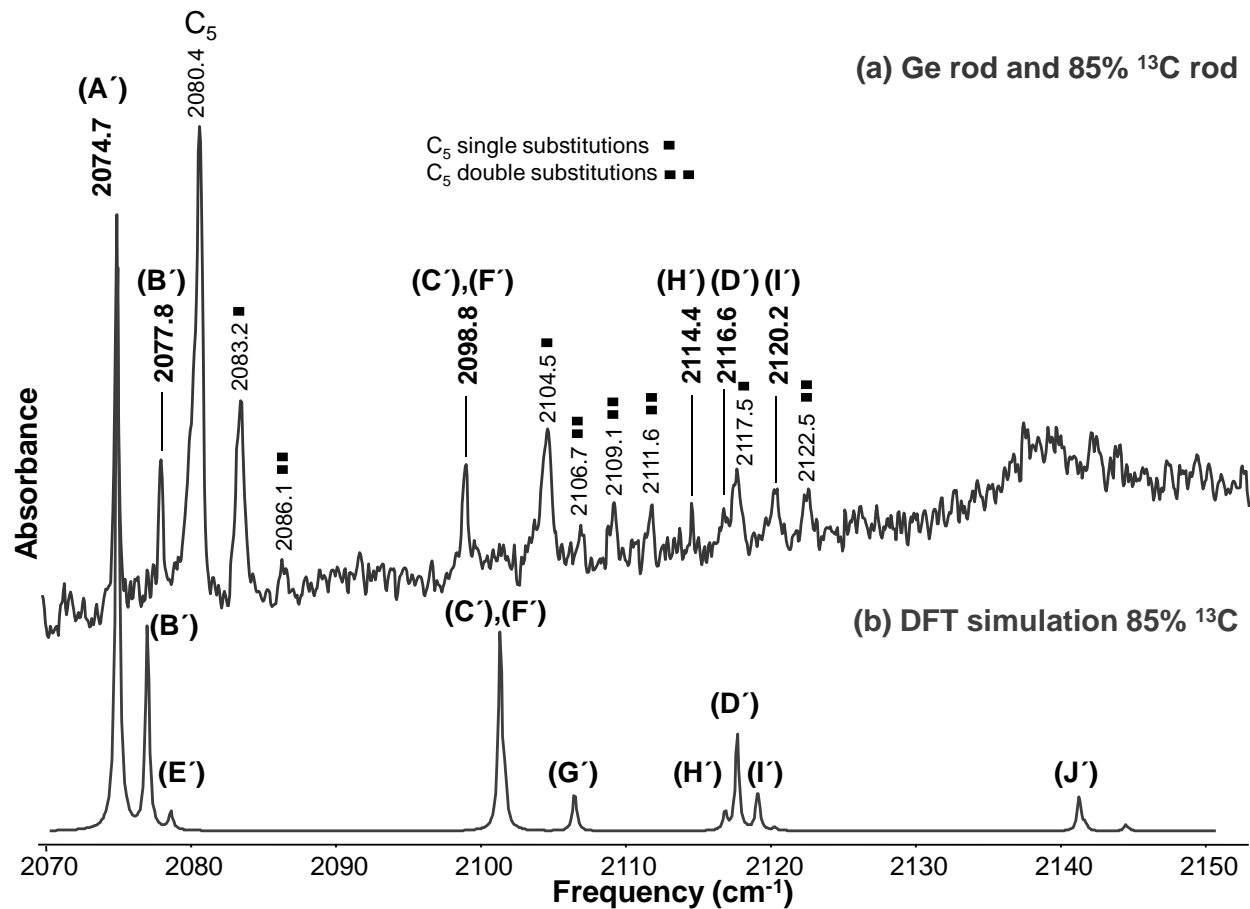
Figure 3.4 Comparison of the FTIR spectra of the $\nu_4(\sigma_u)$ mode of linear GeC$_5$Ge and its ^{12}C isotopic shifts (a) produced by the simultaneous evaporation of a Ge rod and carbon rods with 85% [13]C enrichment, with (b) a simulation for 85% [13]C enrichment derived from DFT calculations at the B3LYP/cc-pVDZ level. The letters correspond to the single and double ^{12}C-substituted isotopomers listed in Table 3.3.

Table 3.3   Comparison of observed vibrational frequencies (cm^{-1}) of the $\nu_4(\sigma_u)$ mode for ^{12}C- substituted isotopomers of linear GeC$_5$Ge with the predictions of B3LYP/cc-pVDZ level calculations.

Isotopomer Ge-C-C-C-C-C-Ge		Observed ν	B3LYP/ cc-pVDZ ν	Scaled[a] ν	Difference $\Delta\nu$
74-13-13-13-13-13-74	(A′)	2074.7	2051.0	2074.7	---
74-12-13-13-13-13-74	(B′)	2077.8	2053.0	2076.8	-1.0
74-13-12-13-13-13-74	(C′)	2098.8	2076.9	2101.0	2.2
74-13-13-12-13-13-74	(D′)	2116.6	2093.0	2117.2	0.6
74-12-13-13-13-12-74	(E′)	---[b]	2054.6	2078.3	---
74-12-13-13-12-13-74	(F′)	2098.8	2077.2	2101.2	2.4
74-12-12-13-13-13-74	(G′)	---[c]	2081.9	2106.0	---
74-13-12-13-12-13-74	(H′)	2114.4	2092.1	2116.3	1.9
74-12-13-12-13-13-74	(I′)	2120.2	2094.3	2118.5	-1.7
74-13-12-12-13-13-74	(J′)	---	2116.1	2140.6	---

[a]Results of the DFT-B3LYP/ cc-pVDZ calculation scaled by a factor of 2074.7/2051.0=1.0116.
[b]Overlapped by $\nu_3(\sigma_u)$ mode of ^{13}C$_5$.
[c]Overlapped by C$_5$ double-^{12}C isotopomer shift.

mode of $^{13}C_5$ at 2117.5 cm^{-1}. On the low frequency side of this mode, a band observed at 2116.6 cm^{-1} (D′) very likely belongs to the isotopomer with a centrally substituted ^{12}C. Deconvolution of the two partially overlapped bands gives an estimate of ~20% for the intensity of the 2116.6 cm^{-1} absorption compared to the 2074.7 cm^{-1} absorption (A′) belonging to the fully ^{13}C-substituted isotopomer. Although this is only a rough estimate, given the uncertainty in establishing the line profiles with the signal-to-noise ratio in this region, it is reasonably close to the 15% expected for the isotopomer with a centrally substituted ^{12}C.

The observed isotopic shift pattern for single ^{13}C-substituted isotopomers in Fig. 3.3(a) and the "mirror" pattern for single ^{12}C isotopomers in Fig. 3.4(a) provide evidence for at least five carbon atoms, two pairs of equivalent atoms and one unique atom in the unknown molecule. A linear GeC$_m$Ge ($m \geq 5$) geometry is consistent with the above arguments and with the previous observation of the Group IVB central symmetric molecules, SiC$_3$Si, SiC$_4$Si, and GeC$_3$Ge. Isotopic shift patterns for $^{12}C/^{13}C$ isotopic ratios of 85/10% and 10/90% were therefore simulated using the results of the DFT calculations at the B3LYP/cc-pVDZ level for linear GeC$_5$Ge. These simulations, which are presented in Fig. 3.3(b) and 3.4(b), show very good agreement with the observed isotopic shift patterns in Fig. 3.3(a) and 3.4(a). Although the lower signal-to-noise ratio makes the assignments of the doubly substituted isotopomers in Fig. 3.3 (a) and 3.4(a) more difficult, the relative intensities are in reasonable agreement. For example, the I′ isotopomer in Fig. 3.4 is calculated to be twice the intensity of the H′ isotopomer, compared with the observed ratio of 1.6. There are five naturally occurring isotopes of Ge (21.2% ^{70}Ge, 27.7% ^{72}Ge, 7.7% ^{73}Ge, 35.9% ^{74}Ge, and 7.4% ^{76}Ge), however, as suggested by the nuclear displacements for the $\nu_4(\sigma_u)$ fundamental shown in Fig. 3.1, Ge does not participate in this vibration and the spectra for all Ge isotopes thus occur at the same frequency. More detailed comparisons between the predicted and

observed ^{13}C shift frequencies are shown in Tables 3.2 and 3.3, which also include the data for double substitution shifts. The observed differences between the calculated and observed shifts are comparable to those observed for previously identified Ge_nC_m molecules such as GeC_3Ge and GeC_7.[28,46] The excellent agreement between experimental and theoretical results thus confirms the identification of the $\nu_4(\sigma_u)$ fundamental vibration of linear GeC_5Ge at 2158.0 cm^{-1}.

3.5. Conclusion

The linear GeC_5Ge germanium-carbon chain has been detected for the first time through the dual laser evaporation of graphite and germanium. FTIR isotopic shift measurements and DFT calculations at the B3LYP/cc-pVDZ level confirm the identification of the $\nu_4(\sigma_u)$ vibrational fundamental at 2158.0 cm^{-1}.

CHAPTER IV

FTIR IDENTIFICATION OF THE $\nu_4(\sigma_u)$ AND $\nu_6(\pi_u)$ MODES OF LINEAR GeC$_3$Ge

4.1   Introduction

Previously, our group has reported vibrational spectra for Si$_n$C$_m$,[44,45] Ge$_n$C$_m$,[1,46] and Si$_n$C$_m$Ge$_l$[47] clusters. In early work, novel small silicon-carbon clusters were produced by the evaporation of mixtures of silicon and carbon from tantalum Knudsen cells. Vibrational fundamentals were identified for a variety of Si$_n$C$_m$ clusters with various structures, including linear SiC$_3$Si,[48] cyclic Si$_2$C$_2$,[49] and planar pentagonal Si$_3$C$_2$.[50] Later investigations, using the laser ablation technique, identified for the first time vibrational fundamentals of the larger silicon-carbon clusters SiC$_7$ and SiC$_9$,[44,45] as well as the germanium-carbon species GeC$_3$Ge,[5] GeC$_7$ and GeC$_9$,[46] and the mixed Group IV cluster, GeC$_3$Si.[47]

FTIR matrix isolation studies on the vibrational spectra of Ge$_n$C$_m$ clusters formed by laser ablation have continued. Efforts have been directed toward increasing the production of GeC$_3$Ge in order to be able to detect the next most intense infrared active modes, which were not detectable when the $\nu_3(\sigma_u) = 1920.7$ cm^{-1} fundamental was produced for the first time by Dr. D.L. Robbins. This was achieved by sintering a germanium-carbon rod which upon laser ablation produced a very high yield of the molecule. By using hard, sintered Ge-C rods evaporation was enhanced over sputtering, allowing long deposition times which resulted in trapping more molecules in the matrix.

Since Ge participates in the next most intense $\nu_4(\sigma_u)$ vibrational mode (see Figure 4.1), and has five natural isotopes with relative abundances of 21.2 % ^{70}Ge, 27.7 % ^{72}Ge, 7.7 % ^{73}Ge, 35.9

% ^{74}Ge, and 7.4 % ^{76}Ge, there are 15 possibly observable isotopomers of GeC$_3$Ge even in the absence of ^{13}C isotopic substitutions. The natural abundances of the Ge isotopes produce a Ge isotopic shift pattern on the envelope of the $v_4(\sigma_u)$ absorption that is consistent with the presence of two equivalent Ge atoms.

Ge   Ge

$v_3(\sigma_u)$ 2028.1 cm^{-1}

Intensity: 2225.7 km/mole

$v_4(\sigma_u)$ 740.0 cm^{-1}

Intensity: 217.3 km/mole

$v_6(\pi_u)$ 575.4 cm^{-1}

Intensity: 16.4 km/mole

$v_7(\pi_u)$ 69.1 cm^{-1}

Intensity: 3.7 km/mole
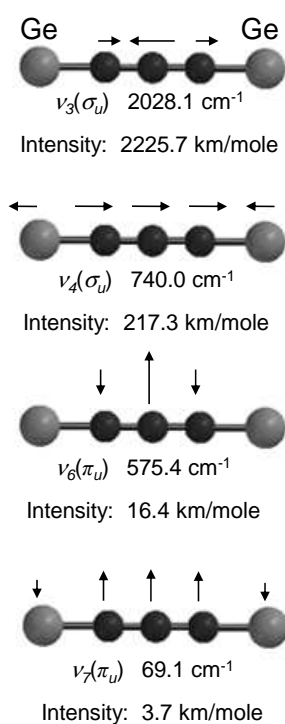
Figure 4.1.   FT-B3LYP/cc-pVDZ predicted infrared active vibrational frequencies (cm^{-1}) and band intensities for $^1\Sigma_g^+$ ground state of linear GeC$_3$Ge. Arrows indicate the principal nuclear displacements for each mode.

In comparing measured isotopic shifts to the pattern predicted by DFT calculations, our group usually scales the theoretical shifts by multiplying by the ratio of the experimental and calculated main band frequencies. In general, the criterion for good agreement is that the differences between the experimental and scaled theoretical frequencies shifts are less than 2 cm^{-1}. Since the Ge isotopic shift envelope extends to only a few cm^{-1}, this criterion could not be used in the present work. Instead, a new way to correlate the theoretical frequency shifts was used to compare experiment and theory, which is presented in the theory section.

This work presents experimental measurements and DFT calculations, which corroborate the linear geometry already determined for GeC_3Ge in its ground state. Based on very good agreement between $^{70,72,73,74,76}Ge$ and ^{13}C isotopic shift measurements and the predictions of DFT calculations the $v_4(\sigma_u)$ and $v_6(\pi_u)$ fundamentals of GeC_3Ge have now been unambiguously assigned at 735.3 and 580.1 cm^{-1}, respectively.

4.2   Theoretical Predictions

The B3LYP[51,52,53] functional (Becke type 3 exchange and the correlation functional of Lee, Yang, and Parr) with cc-pVDZ basis was used in calculations with the *Gaussian 03* program suite.[2] Table 4.1 lists the predicted harmonic fundamental frequencies and infrared intensities. The infrared active vibrations, showing normal mode displacements are presented in Fig. 4.1. In our earlier work on GeC_3Ge (Ref. 5) the 6-31G* basis was used, while in later studies on GeC_7 and GeC_9[46] and GeC_3Si[47] the basis set used was cc-pVDZ. It should be noted that with the 6-31G* basis set the bending fundamentals are generally predicted at considerably higher frequencies than when using the cc-pVDZ basis. Accordingly, the $v_6(\pi_u)$ fundamental of

GeC$_3$Ge, which is predicted at 933 cm^{-1} with the 6-31G* basis set (see Ref. 5) is calculated at 575.4 cm^{-1} with the cc-pVDZ basis set. In extensive studies of many carbon,[54,55] silicon-carbon,[44,45] and germanium-carbon[46] species it has been found that calculations with the cc-pVDZ basis set provide a good description of geometries and vibrational fundamentals. Experimental measurement of the $v_6(\pi_u)$ mode of GeC$_3$Ge in the present work confirms the superiority of the cc-pVDZ basis over the 6-31G* (see Results and Analysis). State of the art theoretical studies[56] on Ge$_2$C$_3$ using DFT, MP2, and CCSD(T) with larger basis sets predicts the linear GeC$_3$Ge as the lowest energy isomer.

Table 4.1.   DFT-B3LYP/cc-pVDZ predicted vibrational frequencies (cm^{-1}) and band intensities for linear GeC$_3$Ge.

Vibrational mode	Frequency (cm^{-1})	Infrared intensity (km/mol)
$v_1(\sigma_g)$	1520.4	0
$v_2(\sigma_g)$	277.2	0
$v_3(\sigma_u)$	2028.1	2226
$v_4(\sigma_u)$	740.0	217
$v_5(\pi_g)$	190.4	0
$v_6(\pi_u)$	575.4	16
$v_7(\pi_u)$	69.1	4

4.3   Perturbative Approach for Calculating Isotopic Shifts

The standard approach when calculating isotopic shifts for carbon clusters is to obtain them from the diagonalization of the appropriately mass-weighted force constant matrix. When anharmonic effects as well as effects due to couplings with other vibrational modes are small such shifts typically agree with experiment to within a few tenths of cm^{-1}. Larger errors can be attributed to inaccuracies in the force constant matrix giving rise to errors in the normal mode coordinates for the vibrational fundamental being observed. Below we have calculated the isotopic shifts resulting from ^{13}C substitution using this standard approach.

The proposed identification of the $v_4(\sigma_u)$ fundamental of GeC_3Ge however allows us to consider the shifts due to the various isotopes of germanium using a different approach. The perturbation[145] resulting from changes in the molecule's nuclear masses caused by isotopic substitution is the difference between the kinetic energy of the final mass, $m_n(f)$ and the initial mass, $m_n(i)$ for all K isotopically substituted atoms,

$$W(i \rightarrow f) = \sum_{n=1}^{K} \left[\frac{\hbar^2}{2m_n(i)} \nabla_n^2 - \frac{\hbar^2}{2m_n(f)} \nabla_n^2 \right] \qquad \text{Eq. 4.1}$$

Using this perturbation and neglecting coupling between other vibrational modes, the harmonic frequency ω, shifted from the unperturbed frequency ω_o, resulting from an isotopic substitution can be derived to infinite order to be given by

$$\omega = \left[1 - \sum_{n=1}^{K} \left(1 - \frac{m_n(i)}{m_n(f)} \right) |\mathbf{u}_n|^2 \right]^{\frac{1}{2}} \omega_o \qquad \text{Eq. 4.2}$$

where $\mathbf{u}_n$ is the normal mode displacement vector of atom n in normalized mass weighted coordinates. Within the harmonic aproximation therefore, the inexactness in Eq. 4.2 originates

only with the values of the normal mode displacements providing the interaction with other fundamentals can be neglected. In the case of the germanium shifts of the $v_4(\sigma_u)$ fundamental of GeC$_3$Ge, Eq. 4.2 was found to be applicable since the isotopic shifts calculated using Eq. 4.2 agreed to within 0.01 cm^{-1} with the shifts calculated using the standard method employing the full force constant matrix. In addition, since the two germanium atoms are equivalent , Eq. 4.2 now provides a simple one-parameter model by which we can fit calculated isotopic shifts to experimental shifts, thus giving us an improved value of the mass-weighted normal mode displacement.

4.4   Experimental Procedures

The objective of this research was to increase the yield of linear GeC$_3$Ge in order to improve the signal-to-noise ratio and enable the measurement of $v_4(\sigma_u)$ and $v_6(\pi_u)$ that are predicted to be the next most intense vibrational fundamentals after the $v_3(\sigma_u)$ fundamental already reported. GeC$_3$Ge was first produced by simultaneously ablating the surfaces of a pair of continuously rotating and translating germanium and carbon rods; however, in the present work, this dual laser ablation approach was replaced by evaporating a single rod made from a mixture of Ge and C. The ablation of a rod containing a mixture of Ge, Si, and C was first used to produce GeC$_3$Si.[47]   In the present work, optimizing the Ge:C mass ratio of the germanium-carbon rod was crucial to achieving a high yield of GeC$_3$Ge. From a series of experiments testing different ratios to enhance the production of this molecule; it was concluded that Ge:C= 1.5:1 was optimum.

A single rod with one Nd:YAG laser (Spectra Physics) operating at 1064 nm in pulse mode was used. The evaporated species were condensed in solid Ar (Matheson, 99.9995% purity) on a

gold surfaced mirror previously cooled to ~10 K by a closed refrigeration system (ARS, Displex). The mirror was enclosed in vacuum chamber maintained at a pressure of ~10^{-8} Torr. Experimental parameters such as the laser focus, laser power, and Ar flow were adjusted to favor the production of GeC_3Ge. For the laser ablation of the rod a beam with a power of 3.0 Watts, loosely focused on an area of ~25 mm^2, was used. During deposition, the Ar flow rate was adjusted by opening a needle valve until the chamber pressure increased from ~10^{-8} to ~6.0×10^{-5} Torr. Typically, matrix samples were deposited for ~120 min.

In order to make an unambiguous determination of molecular structure and to identify vibrational fundamentals it is crucial to measure isotopic shifts. For this reason Ge-C rods were fabricated with mixtures of ^{12}C (Alfa Aesar, 99.9995% purity) and ^{13}C (Isotec, 99.3% purity). Since, as mentioned earlier, Ge has five naturally occurring isotopes, Ge isotopic enrichment were unnecessary. Two rods were fabricated with the mass ratio Ge:C=1.5:1, one with ^{12}C and the other having an appropriate ^{13}C enrichment to obtain the ^{13}C isotopic shifts necessary to determine the number of carbon atoms present and the geometry of the molecule.

4.5   Results and Discussion

Figure 4.2 shows survey spectra recorded in the range 1800-2200 cm^{-1} where the most intense stretching modes of germanium-carbon clusters are expected to be located. The spectrum produced by the ablation of a germanium-carbon rod is shown in Fig. 4.2(a). For comparison, Fig. 4.2(b) shows the spectrum produced under identical experimental conditions by the ablation of a carbon rod alone. The ablation of the germanium-carbon rod produced the characteristic fundamental vibrations of germanium-carbon clusters identified in our previous studies, the $v_4(\sigma)$ mode of GeC_9 at 1928.2 cm^{-1}, the $v_4(\sigma_u)$ mode of GeC_5Ge at 2158.0 cm^{-1}, and the $v_3(\sigma_u)$ mode of

GeC_3Ge at 1920.7 cm^{-1}. In addition, other new absorptions at 2087.7, 2093.3 and 2116.6 cm^{-1} were observed, which are currently under investigation and will be the subjects of future reports. Figure 4.3 shows the spectra in the range of 500-800 cm^{-1} where three other new bands appear, a sharp pair of lines at 579.1 and 580.1 cm^{-1} and a broader band at 736.0 cm^{-1} which we will consider first.
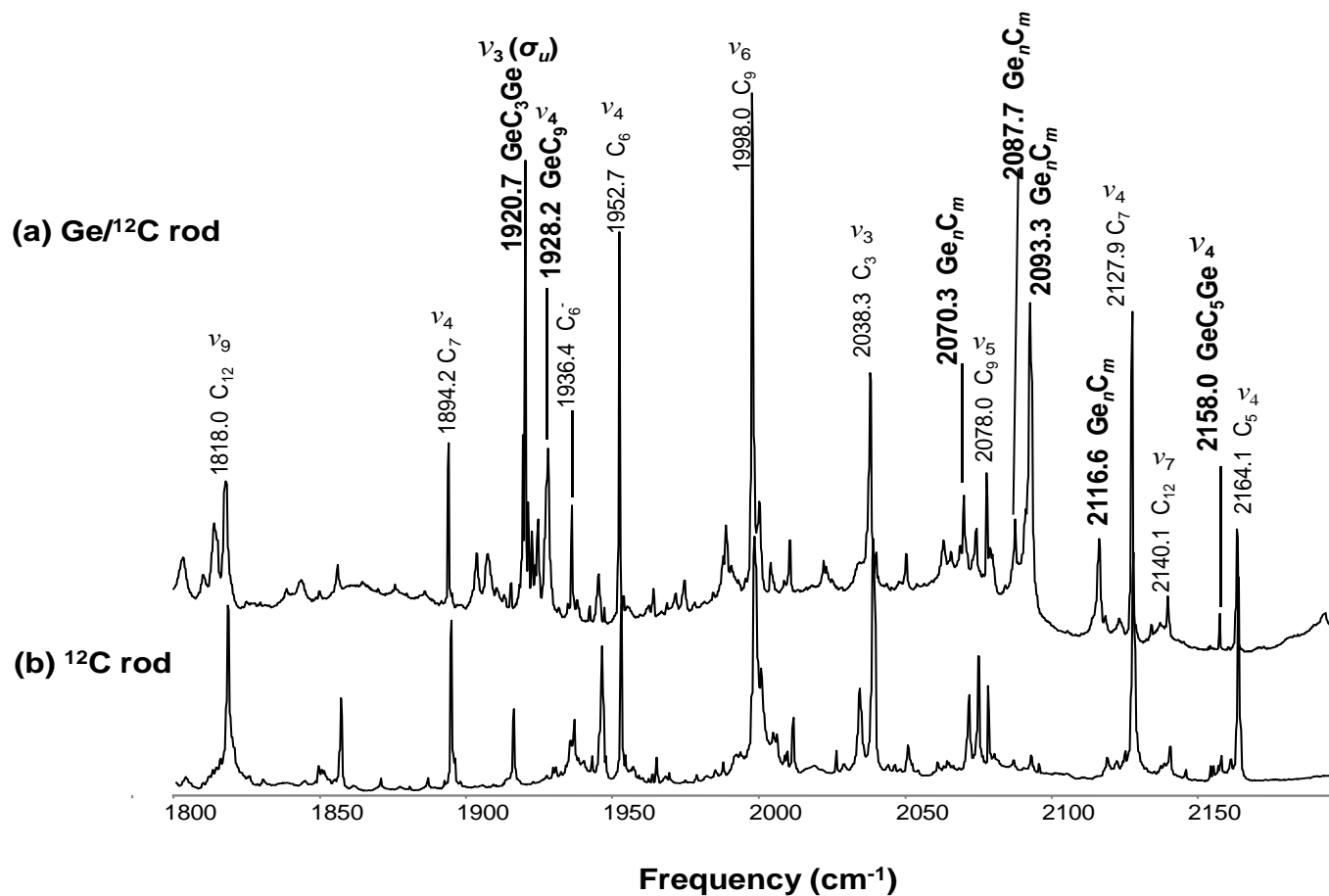
Figure 4.2   FTIR spectra produced by the ablation of (a) a germanium-carbon rod and (b) a pure ^{12}C rod in the 1800-2150 cm^{-1} frequency region.
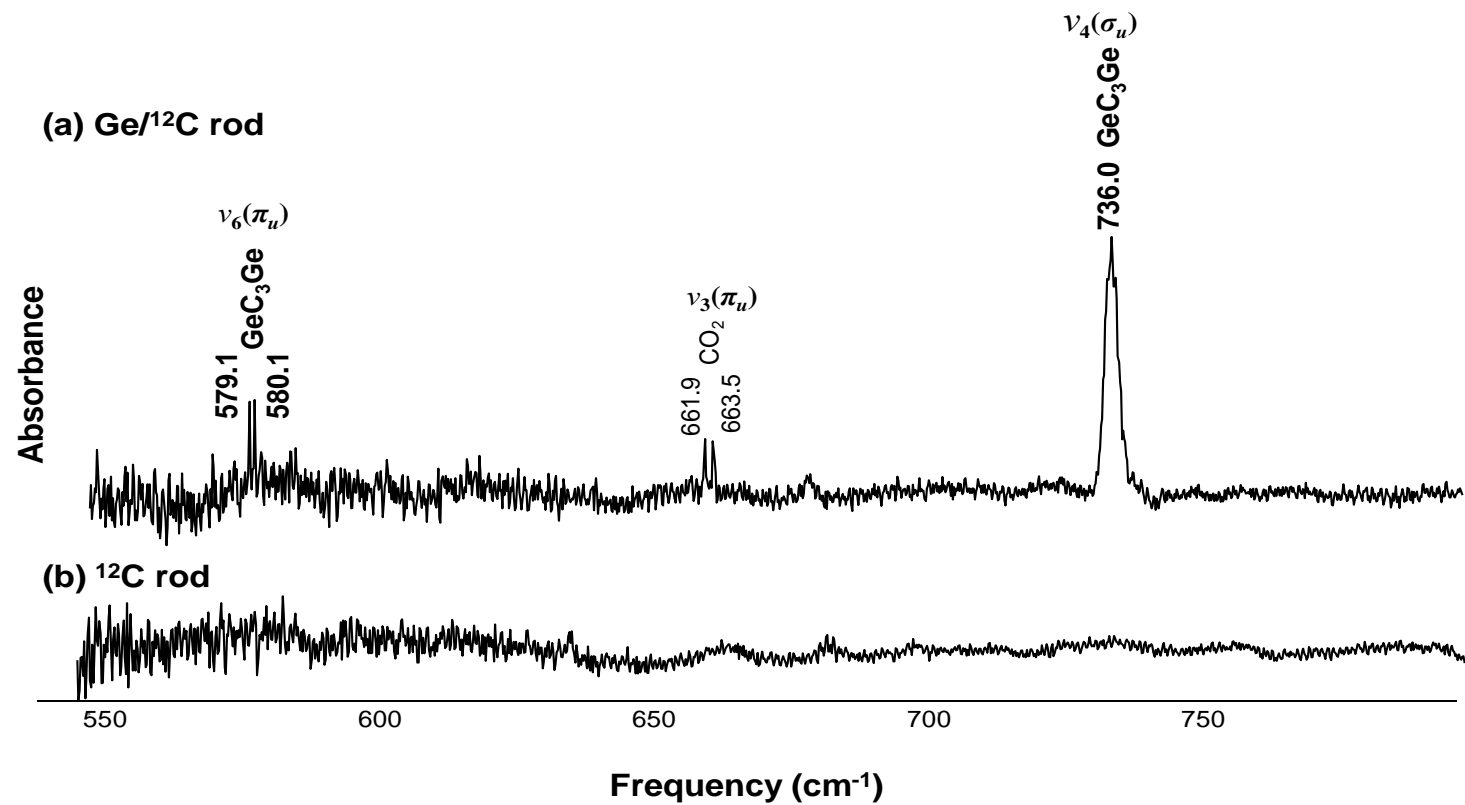
Figure 4.3. FTIR spectra produced by the ablation of (a) a germanium-carbon rod and (b) a pure ^{12}C rod, in the 550-750 cm^{-1} frequency region.

GeC$_3$Ge is the most prominent species in the spectrum judging by the intensity of the most intense mode of GeC$_3$Ge at $v_3(\sigma_u)$ =1920.7 cm^{-1} in Fig. 4.2 compared with the absorptions of other species. The 736.0 cm^{-1} absorption is close to the 740.0 cm^{-1} frequency predicted for the $v_4(\sigma_u)$ fundamental, and the ratio of its intensity to the $v_3(\sigma_u)$ band is 0.3, reasonably close to the ratio of 0.1 calculated from the predicted intensities of the fundamentals shown in Table 4.1. It thus appears possible that this band corresponds to the $v_4(\sigma_u)$ stretching fundamental of linear GeC$_3$Ge.

The absorption envelope of the $v_4(\sigma_u)$ fundamental of linear GeC$_3$Ge would be expected to contain several peaks and extend over ~5 cm^{-1}. The envelope's characteristic shape would result from the Ge atoms' participation in the vibration, the frequency, the normal mode displacement vector u (see Eq. 4.2), and the line widths of the germanium isotopomer peaks contributing to the absorption envelope. The presence of two equivalent germanium atoms in the molecule would produce 15 isotopomers, each with a different probability of being formed. For example, the 74-12-12-12-72, 74-12-12-12-70, and 74-12-12-12-74 isotopomers have probabilities, 0.20, 0.15, and 0.13, respectively, while the 76-12-12-12-76 and 76-12-12-12-73 isotopomers have relatively lower probabilities, 0.006 and 0.01, respectively. Consequently, the peaks of some isotopomers would be more intense than others because of their greater abundances. The vibrational frequency value and u determines the spread of the absorption envelope. In the 700 cm^{-1} region it is spread over only ~5 cm^{-1}, compared with tens of cm^{-1} if the absorption were in the 2000 cm^{-1} region. The peak linewidths determine the number of peaks resolved. If linewidths are close to the spectrometer resolution (0.2 cm^{-1}) all peaks would be resolved but, if linewidths are greater than the resolution and the envelope extends only a few cm^{-1}, many peaks would be unresolved.

Table 4.2.   Observed vibrational frequencies (cm^{-1}) of the $v_4(\sigma_u)$ mode for [70,72,73,74,76]Ge-substituted isotopomers of linear GeC$_3$Ge, DFT predictions at B3LYP/cc-pVDZ level of theory, and theoretical predictions given by Eq. (2) using the optimized mass weighted normal mode displacement found by minimizing the RMS deviation of the observed frequencies.

Isotopomer Ge-C-C-C-Ge		Observed (cm^{-1}) v_e	B3LYP/ cc-pVDZ	Scaled[a]	Theoretical[b] v_t	Difference $v_e - v_t$
76-12-12-12-76	(A)	…	738.1	733.4	733.9	…
76-12-12-12-74	(B)	734.5	739.1	734.4	734.6	-0.1
76-12-12-12-73	(C)	…	739.6	734.9	735.0	…
74-12-12-12-74	(D)	735.3[c]	740.0	735.3	735.3	…
76-12-12-12-72	(E)	735.3	740.1	735.4	735.3	0.0
74-12-12-12-73	(F)	…	740.5	735.8	735.7	…
73-12-12-12-73	(G)	…	741.0	736.3	736.0	…
74-12-12-12-72	(H)	736.0	741.0	736.3	736.0	0.0
76-12-12-12-70	(I)	…	741.2	736.5	736.1	…
73-12-12-12-72	(J)	…	741.5	736.8	736.4	…
72-12-12-12-72	(K)	736.7	742.0	737.3	736.7	0.0
74-12-12-12-70	(L)	736.7	742.1	737.4	736.8	0.1
73-12-12-12-70	(M)	…	742.6	737.9	737.1	…
72-12-12-12-70	(N)	737.5	743.1	738.4	737.5	0.0
70-12-12-12-70	(O)	738.3	744.2	739.5	738.3	0.0

[a]Results of the DFT-B3LYP/ cc-pVDZ calculation scaled by a factor of 735.3/740.1=0.993514; [c]Considered to be the unperturbed frequency in Eq. 4.2, [b]Results of scaling by minimizing the RMS deviation of the observed frequencies and the theoretical predictions given by Eq. 4.2.

With the assumption that the spectrum originates from the $v_4(\sigma_u)$ fundamental of linear GeC$_3$Ge we chose the unperturbed frequency in Eq. 4.2 to correspond to the 74-12-12-12-74 isotopomer observed at 735.3 cm^{-1} (see Table 4.2). Using the normal mode displacement from our DFT calculation proved to result in an absorption envelope that was substantially broader than the one observed in the experimental spectrum. To ascertain if our assignment was still consistent with our assumption that the spectrum resulted from two equivalent germanium atoms we calculated the isotopic shifts using Eq. 4.2, minimizing the root mean square (RMS) deviation between the calculated and observed frequencies. The optimized mass weighted normal mode displacement was found to be 0.2656, considerable lower than the DFT calculated value of 0.3124. The former value of the normal mode displacement was used to generate the semi-empirical values for the germanium isotopic shifts shown in the "Theoretical" column of Table 4.2 and the simulated spectrum exhibited in Fig 4.4(b). The lower value of the normal mode displacement of the germanium atoms indicates, due to normalization condition of the normal mode vector, that the normal modes displacements of some or all the carbon atoms are larger than the DFT predictions. Thus it is expected that the observed ^{13}C absorptions should appear at lower frequencies than what is predicted by the DFT calculations. We will find below that such is indeed also the case (*e.g.* see Fig. 4.5).

In Fig. 4.4(b) the spectrum is simulated using Lorentzian profiles for the isotopomer shifts at the scaled frequencies given in Table 4.2. Each line profile is scaled by the predicted intensity of the isotopomer and its probability, given the natural abundances of the germanium isotopes. Table 4.2 compares the observed frequencies with the calculated scaled isotopomer frequencies and shows very good agreement between theory and experiment.
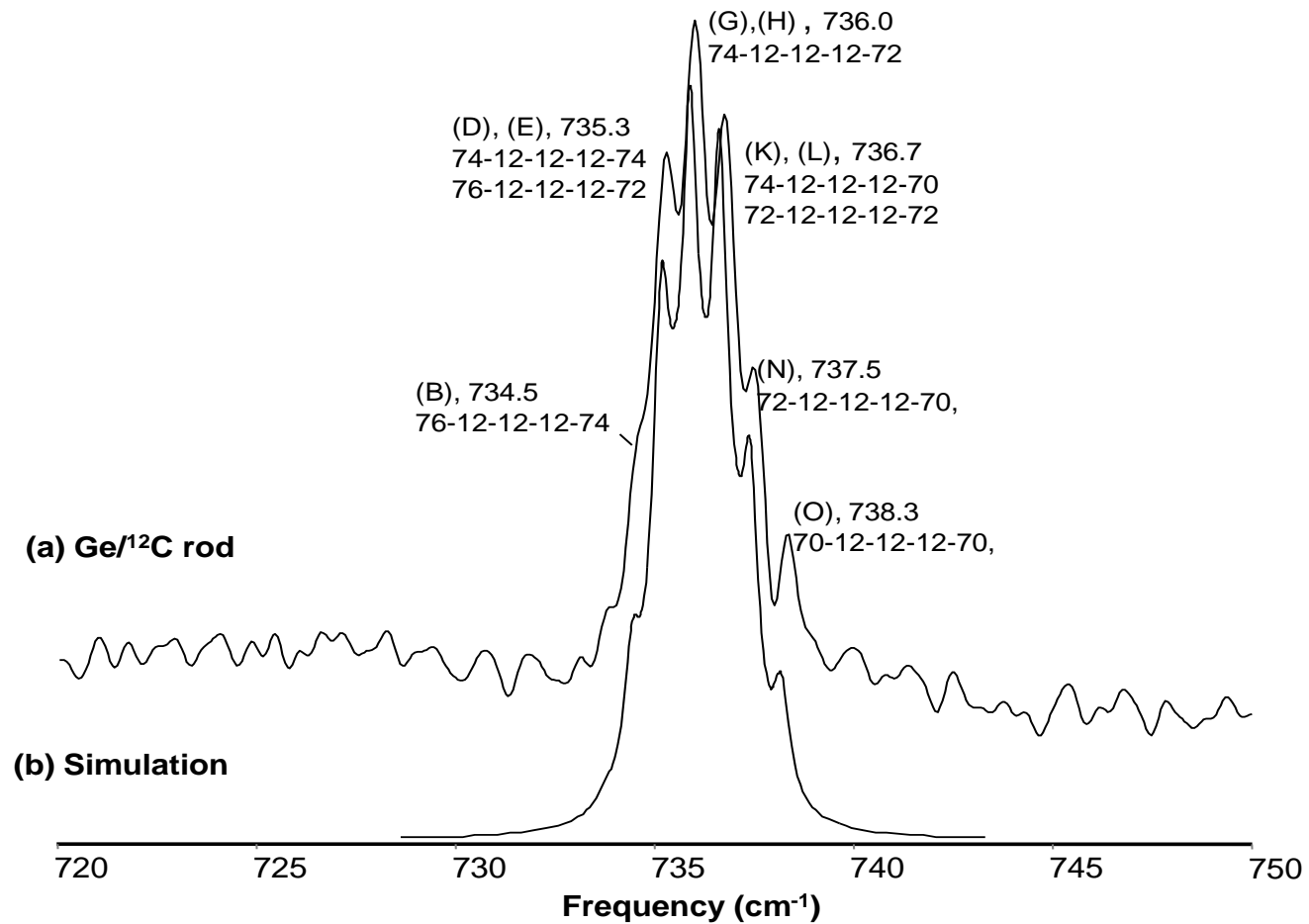
Figure 4.4   Comparison of the FTIR spectra of the $\nu_4(\sigma_u)$ mode of linear GeC$_3$Ge and its [70,72,73,74,76] Ge isotopic shifts (a) produced by the simultaneous evaporation of a germanium-carbon rod, with (b) a simulated spectrum calculated using Eq. 4.2 and the calculated displacement vector of the Ge atoms obtained from minimizing the RMS error between experimental frequencies and the ones obtained using Eq. 4.2.
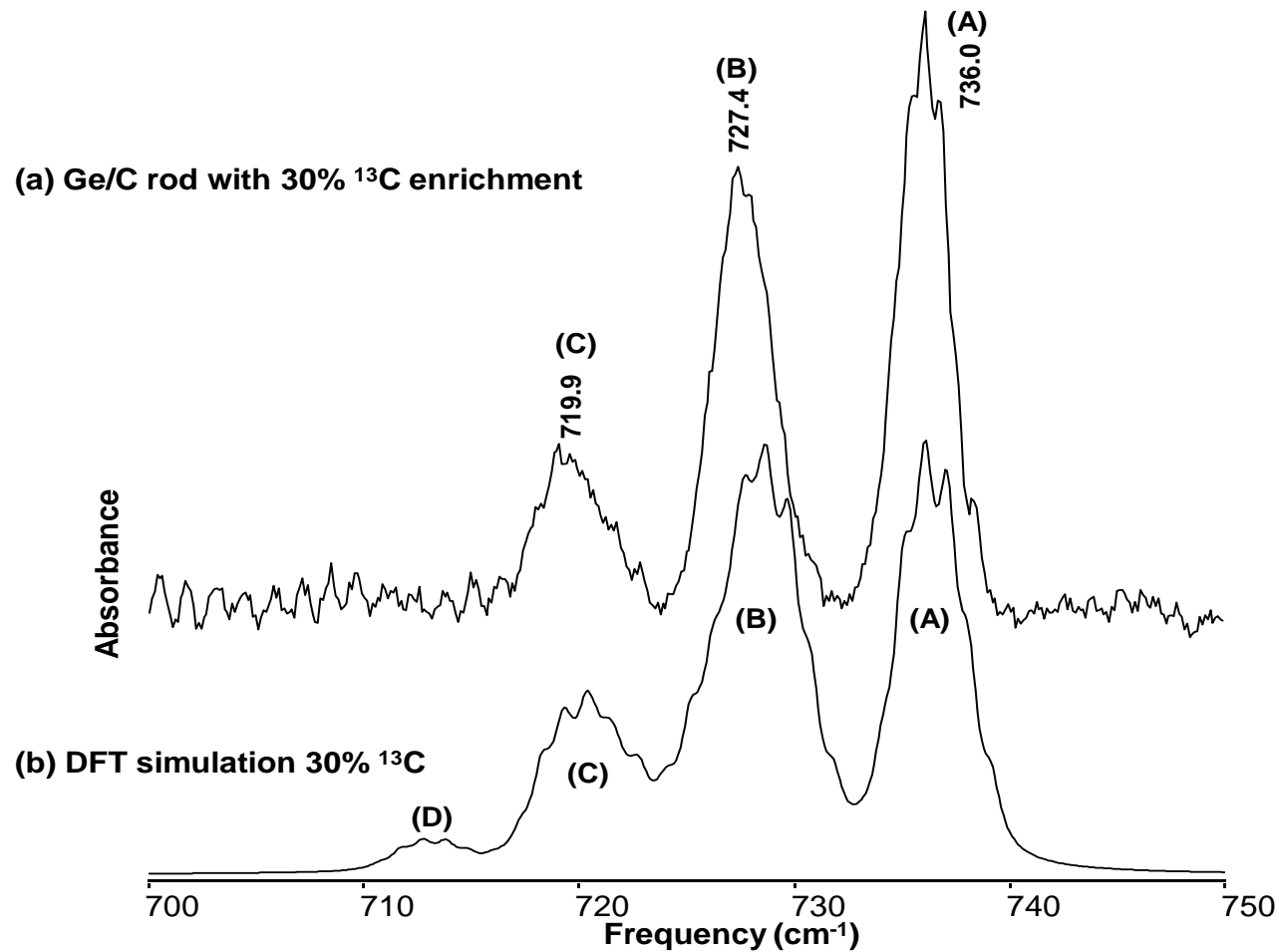
Figure 4.5   Comparison of the FTIR spectra of the $v_4(\sigma_u)$ mode of linear GeC_3Ge and its ^{13}C isotopic shifts (a) produced by the simultaneous evaporation of a germanium-carbon rod with 30% ^{13}C enrichment, with (b) a simulation for 30% ^{13}C and $^{70,72,73,74,76}Ge$ isotopomers derived from DFT calculations at the B3LYP/cc-pVDZ level. The letters correspond to the single and double ^{13}C-substituted isotopomers listed in Table 4.3.

The germanium isotopic shifts observed on the profile of the 736.0 cm^{-1} absorption band in Fig. 4.4 prove that two germanium atoms participate in the vibration, but no conclusion can be drawn about the number of carbon atoms present. The presence of several unidentified germanium-carbon bands in the 1800-2200 cm^{-1} region, 2087.7, 2093.2, and 2116.6 cm^{-1}, raises the possibility that one of the species responsible for these bands might be responsible for the 736.0 cm^{-1}. Since DFT predicted intensities can sometimes deviate from experimentally observed intensities, the argument presented earlier linking the absorption at 736.0 cm^{-1} and the $v_3(\sigma_u) = 1920.7$ cm^{-1} fundamental of GeC$_3$Ge based on their intensity ratio, is not conclusive. An experiment using a germanium-carbon rod enriched with ^{13}C was therefore carried out to establish the presence of three carbon atoms in a linear structure. The spectrum in Fig. 4.5(a) was obtained with 30% ^{13}C enrichment two new absorptions labeled B and C appear. Figure 4.5 (b) shows the DFT simulated for linear GeC$_3$Ge spectrum for comparison. The absorption labeled A corresponding to Ge-12-12-12-Ge contains all the $^{70,\ 72,\ 73,\ 74,\ 76}$Ge isotopomer absorptions as already discussed and shown in Fig. 4.4. The ^{13}C isotopic shifts are responsible for the absorptions labeled B (Ge-13-12-12-Ge and Ge-12-13-12-Ge), C (Ge-13-13-12-Ge and Ge-13-12-13), and D (Ge-13-13-13-Ge). The envelope corresponding to D was not observed since at 30% ^{13}C enrichment the abundance of the fully substituted isotopomer falls below the noise level. The DFT simulation predicts envelopes A, B, and C broader than those observed since the B3LYP/cc-pVDZ calculation predicts a higher value of the displacement vectors for the terminal germanium atoms. As can be seen in Fig. 4.5 the observed carbon shifts are closer to the main band indicating that some or all the normal mode displacements of the carbon atoms are higher than the DFT predictions, as discussed above.

The envelope of the B absorption includes 27 isotopomers but only the feature at 727.4 cm^{-1} is clearly resolved. At the 0.2 cm^{-1} resolution the following isotopomers with their predicted abundances shown in parentheses could contribute to this feature: 74-13-12-12-72 (1.5%), 74-12-12-13-72 (1.5%), 76-13-12-12-70 (0.2%), 76-12-12-13-70 (0.2%), and 73-13-12-12-73 (0.09%). Since the absorption envelope labeled C and centered at 719.9 cm^{-1}, is not resolved; no specific isotopomer assignments can be made in this case

The results of isotopic shift calculations for linear GeC$_3$Ge structure are presented in Table 4.3 which together with Fig. 5(b) shows the very good agreement between the observed and DFT calculated isotopomer frequencies. Comparison of measured ^{13}C and ^{70,72,73,74,76}Ge isotopic shifts with DFT predictions thus confirms that the absorption at 735.3 cm^{-1} (74-12-12-12-74) is the $v_4(\sigma_u)$ stretching mode of linear GeC$_3$Ge

.

Table 4.3. Comparison of observed vibrational frequencies (cm^{-1}) of the $v_4(\sigma_u)$ mode for ^{13}C- substituted isotopomers of linear GeC$_3$Ge with the predictions of B3LYP/cc-pVDZ level calculations.

Isotopomer Ge-C-C-C-Ge		Observed (cm^{-1})	B3LYP/ cc-pvDZ	Scaled[a]	Difference
Ge-12-12-12-Ge	(A)	736.0[b]	741.0[b]	736.0	…
Ge-13-12-12-Ge	(B)	727.4[c]	733.7[c]	728.7	1.3
Ge-12-13-12-Ge					
Ge-13-13-12-Ge	(C)	719.9[d]	725.4[e]	720.5	0.6
Ge-12-13-12-Ge					
Ge-13-13-13-Ge	(D)	…	717.7[f]	712.8	…

[a] Results of the DFT-B3LYP/ cc-pVDZ calculation scaled by a factor of 736.0/741.0=0.9933
[b] 74-12-12-12-72 isotopomer frequency
[c] 74-13-12-12-72, 74-12-12-13-72, 76-13-12-12-70, and 76-12-12-13-70 isotopomer frequencies (see text)
[d] center of the envelope
[e] 74-12-13-13-70 isotopomer frequency
[f] 74-13-13-13-72 isotopomer frequency
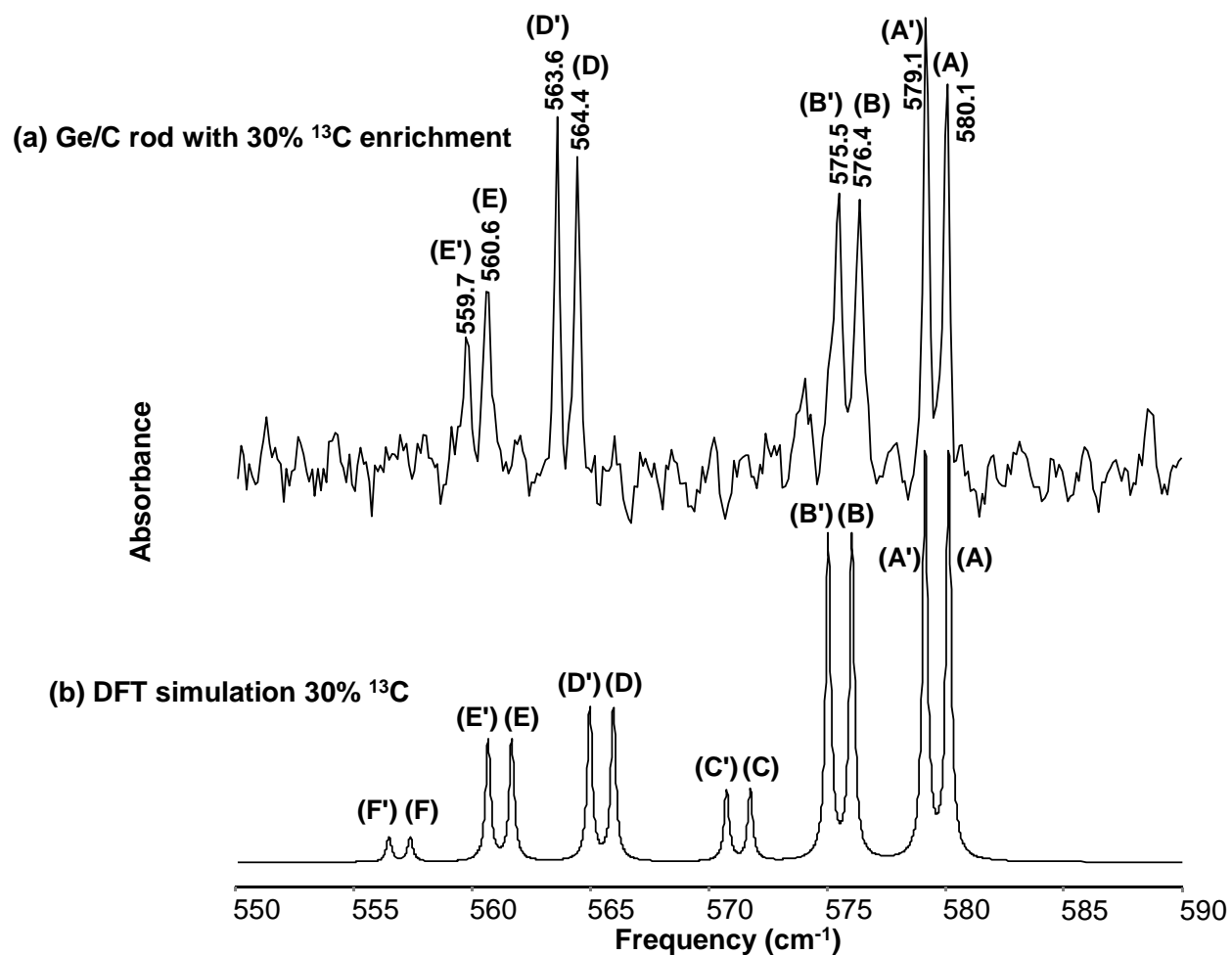
Figure 4.6   Comparison of the FTIR spectra of the $v_6(\pi_u)$ mode of linear GeC_3Ge and its ^{13}C isotopic shifts (a) produced by the simultaneous evaporation of a germanium-carbon rod with 30% [13]C enrichment, with (b) a DFT simulation for 30% [13]C enrichment derived from DFT calculations at the B3LYP/cc-pVDZ level. The letters correspond to the ^{13}C-substituted isotopomers listed in Table 4.4.

Table 4.1 indicates that the DFT calculations for linear GeC_3Ge predict the $v_6(\pi_u)$ bending mode at 575.4 cm^{-1}. Germanium atoms do not participate in this vibration, so a relatively sharp band is expected. As shown in Fig. 4.3(a) the spectrum resulting from the evaporation of a $Ge/^{12}C$ rod has a pair of relatively narrow absorptions at 579.1 and 580.1 cm^{-1} that are obvious candidates for the $v_6(\pi_u)$ fundamental. The intensity ratio of this pair to the $v_4(\sigma_u)$=735.3 cm^{-1} fundamental is 0.1, reasonably close to the 0.07 predicted. The 0.03 intensity ratio of the 580 cm^{-1} pair compared to the $v_3(\sigma_u)$=1920.7 cm^{-1} fundamental is somewhat larger than the 0.007 predicted but, since the intensity ratio of 0.3 observed for $v_4(\sigma_u)$ to $v_3(\sigma_u)$ is also somewhat more than the 0.1 predicted, we suspect that the intensity predicted for the $v_3(\sigma_u)$ mode is a little high.

The 579.1, 580.1 cm^{-1} pair of absorptions persist after annealing at 20 and 40 K, leading us to discount two trapping sites as their origin and to consider the possibility that the degeneracy of the bending mode is broken. Similar splitting occurred[57] when the $v_5(\pi_u)$ bending mode of linear C_4 was measured, and was attributed to the presence of two matrix trapping sites in the face centered cubic solid Ar. As can be seen in the spectrum in Fig. 4.3(a) similar splitting is also observed for the $v_3(\pi_u)$ bending mode of CO_2, see Fig. 4.3 (a). If in the present case the splitting corresponds to a single molecule rather than to two different species, the splitting should also be observed in the ^{13}C isotopic shifts. The overlapping shift patterns for different species would not be expected to produce equidistant pairs. Figure 4.6 (a) shows the spectrum when a germanium-carbon rod having 30% ^{13}C enrichment was used. The intensity ratios of isotopomer and main band are calculated assuming that, consistent with the ^{13}C isotopic enrichment, the probability of evaporating a ^{12}C atom is 70% and a ^{13}C atom is 30%. As expected, the isotopic shifts appear in pairs that are approximately equidistant. The intensity of the pair labeled B, B′ corresponding to the Ge-13-12-12-Ge isotopomer is ~80% of the main, Ge-12-12-12-Ge band labeled A,

compared with the expected 86%. The intensity of the D, D' pair (Ge-12-13-12-Ge) is ~62% of the intensity of the main band, compared to the expected 43% and the E, E′ pair (Ge-13-13-12-Ge) is ~38 % compared to the expected 37%. The C, C′ (Ge-13-12-13-Ge) and F, F′ pairs (Ge-13-13-13-Ge), which should be respectively, 18% and 8 % as intense as the main band, fall below the noise level and cannot be observed. In general, the observed ratios are close to the expected values with a somewhat larger deviation for the D, D′ pair that could be a consequence of incomplete randomization during the laser evaporation process or rod fabrication. This isotopic shift spectrum thus confirms the presence of three carbon atoms in a central symmetric structure.

The ^{13}C isotopic shifts calculated for the $v_6(\pi_u)$ bending mode of linear GeC$_3$Ge are shown in Table 4.4. Agreement between theoretically predicted and experimentally measured isotopic shifts is very good. In addition, Figure 4.6 shows that the experimentally observed spectrum matches the DFT simulated spectra very well. This close agreement, together with the small difference between the theoretical and experimental intensity ratios for the three observed fundamentals, makes it possible to unambiguously assign the $v_6(\pi_u)$ bending mode of linear GeC$_3$Ge at 580.1 cm^{-1} .

4.6   Conclusions

Two new vibrational fundamentals of linear GeC$_3$Ge, $v_4(\sigma_u) = 735.3$ cm^{-1} and $v_6(\pi_u) = 580.1$ cm^{-1}, have been assigned based on the results ^{13}C and ^{70,72,73,74,76}Ge isotopic shift measurements and comparison with the predictions of DFT calculations at the B3LYP/cc-pVDZ level. This is apparently the first observation of germanium isotopic shifts in vibrational spectra.

Table 4.4   Comparison of observed vibrational frequencies (cm^{-1}) of the $v_6(\pi_u)$ mode for ^{13}C-substituted isotopomers of linear GeC$_3$Ge with the predictions of B3LYP/cc-pVDZ level calculations.

Isotopomer Ge-C-C-C-Ge		Observed (cm^{-1})	B3LYP/ cc-pVDZ	Scaled	Difference
74-12-12-12-74	(A)	580.1	575.4	580.1[a]	…
	(A')	579.1	575.4	579.1[b]	…
74-13-12-12-74	(B)	576.4	571.3	576.0	-0.4
	(B')	575.5	571.3	575.0	-0.5
74-13-12-13-74	(C)	…	567.1	571.7	…
	(C')	…	567.1	570.7	…
74-12-13-12-74	(D)	564.4	561.3	565.9	1.5
	(D')	563.6	561.3	564.9	1.3
74-13-13-12-74	(E)	560.6	557.0	561.6	0.9
	(E')	559.7	557.0	560.6	0.9
74-13-13-13-74	(F)	…	552.8	557.3	…
	(F')	…	552.8	556.4	…

[a]Results of the DFT-B3LYP/ cc-pVDZ calculation scaled by a factor of 580.1/575.4=0.99189
[b]Results of the DFT-B3LYP/ cc-pVDZ calculation scaled by a factor of 579.1/775.4=0.99361

CHAPTER V

INFRARED OBSERVATION OF LINEAR GeC$_3$

5.1   Introduction

The interest in small Group IV molecules like SiC$_2$, GeC$_2$, GeC$_3$, GeSiC$_3$, and SiC$_2$, is fed

by the potential application of their unusual electronic properties in optoelectronic and

semiconductor materials. Silicon-carbides have the added attraction that they have been detected

in the interstellar medium and circumstellar sources.[58,59] The present paper is concerned with the

first detection of the vibrational spectrum of GeC$_3$ and the determination of its structure. This

molecule is interesting not only because of the still limited experimental and theoretical studies

on germanium-carbon species, but also because of its relation to C$_4$ and to SiC$_3$, which have been

the focus of considerable discussion concerning their ground state structures.

Linear, triplet C$_4$, was first detected by EPR in an Ar matrix.[60]   Later, infrared

measurements of the $\nu_3(\sigma_u)$ and $\nu_5(\pi_u)$ vibrational fundamentals were reported in solid Ar[61,62] and

then in the gas phase.[63,64] Coupled cluster calculations by the Bartlett group have predicted[65,66]

that a cyclic isomer with transannular bond is nearly isoenergetic with the linear structure;

however, the cyclic isomer has so far eluded spectroscopic detection.

In the case of SiC$_3$, early coupled cluster calculations by the Schaefer group[67] using

configuration interaction calculations with single and double excitations (CISD) predicted a

singlet, four-member, ring structure with transannular C-C bond for the global minimum, lying

~4 kcal/mol below both the singlet ring structure with transannular Si-C bond and the $^3\Sigma$, $C_{\infty v}$,

linear structure. This prediction was followed by the observation of both ring structures by

Fourier transform microwave spectroscopy in the laboratory[68,69] and the detection of the isomer with transannular C-C bond in the envelope of the carbon star IRC +10216.

Subsequent CCSD(T) (coupled cluster with single and double substitutions and including triple excitations non-iteratively) calculations[70] were in agreement with the singlet isomer containing transannular C-C bond as the global minimum, and placed the isomer with transannular Si-C bond and linear isomer respectively, 6.2 and 7.5 kcal/mol higher. In contrast, a study utilizing MCSCF (multiconfigurational self-consistent-field) geometries[71] predicted the $C_{\infty v}$ linear triplet isomer to be the global minimum and the singlet ring structures with C-C and Si-C transannular bonds lying respectively, 4.3 and 7.4 kcal/mol higher. However, more advanced CCSD(T) calculations by Sattelmeyer *et al.*[72] reconfirmed the isomer with transannular C-C bond as the global minimum, finding the linear isomer to be energetically less stable by 7.5 and 1.3 kcal/mol than the rings with C-C and Si-C transannular bonds, respectively. Later, Gordon *et al.*[73] also concluded that the ring isomer with transannular C-C bond is more stable than the linear and the ring with Si-C transannular bond, 2.2 and 4.7 kcal/mol respectively; this has been the most advanced calculation on SiC_3 It is interesting that in photoelectron spectroscopy experiments, the Lineberger group[74] produced both linear and cyclic forms of the SiC_3 *anion* but reached no conclusion on the global minimum.

In the case of GeC_3, the subject of this paper, only one theoretical study[75] has so far appeared. At the CCSD(T) (coupled cluster with single and double substitutions and including triple excitations non-iteratively) level of theory, the ring isomer with transannular C-C bond is found to be the global minimum while the ring with transannular Ge-C bond and linear isomer are respectively 2 and 9 kcal/mol less stable (see Fig. 5.1). No experimental observation of GeC_3 has so far been reported although several small Ge_nC_m clusters have been detected mass

spectrometrically in the gas phase[76] and in this lab, GeC_3Ge,[77,78] GeC_5Ge,[79] GeC_7 and GeC_9,[80] have been formed by laser ablation in solid Ar and their vibrational fundamentals assigned. The present study on GeC_3 formed by trapping the products of the laser ablation of Ge and C has been motivated by interest in the ground state structures of tri-carbides of the Group IV elements and by our recent formation in solid Ar and identification of linear and cyclic isomers for metal tri-carbides that are characterized by a competition between the two isomers for the ground state structure. Vibrational fundamentals were observed for linear CrC_3,[81] CoC_3,[82] and AlC_3 (Ref. [83]) and for a ring isomer with transannular Si-C bond for TiC_3 (Ref. [84]) and ScC_3.[85] It is also worth noting that in our experiments the laser ablation of carbon produces both linear[86] and cyclic C_6 (D_{3h}),[87] as well as linear[88] and cyclic C_8 (C_{4h}).[89]

This work presents experimental measurements and DFT calculations, which support a linear geometry for GeC_3 in its ground state. Based on very good agreement between ^{13}C isotopic shift measurements and the predictions of DFT calculations the $v_1(\sigma)$ and $v_2(\sigma)$ fundamentals of GeC_3 have been unambiguously assigned at 1903.9 and 1279.6 cm^{-1} respectively.

5.2   Theory

As noted earlier, $CCSD(T)$[75] calculations indicate that the ring structure with transannular C-C bond is the global minimum for GeC_3 followed by the isomer with transannular GeC bond at +2.1 kcal/mol, and the linear isomer at +9.1 kcal/mol.

Table 5.1 lists the DFT-predicted harmonic fundamental frequencies and infrared intensities for the three GeC_3 isomers using the B3LYP[51,52,53] (Becke type 3 exchange and the correlation functional of Lee, Yang, and Parr) functional with cc-pVDZ basis in the *Gaussian 03*

suite of programs.[2] DFT calculations, which are generally less accurate in predicting electronic energies compared to coupled cluster methods, predict the linear isomer as the global minimum followed by the rings with transannular C-C bond (+11.2 kcal/mol), and Ge-C bond (+12.0 kcal/mol). However, the purpose of the DFT calculation is for the subsequent calculation of isotopic shift frequencies by the diagonalization of an appropriate mass-weighted force constant matrix. Our experience with B3LYP/cc-pVDZ level of theory indicates that it is adequate for this purpose.

Judging by the strength of the vibrational fundamentals of linear C_3, C_6, C_9, and C_{12} in our spectra it is reasonable to think that metal-C_3 molecules are formed predominantly by collisions between linear C_3 and the metal atom. This is illustrated in Schemes I and II in Fig. 5.1 where two different initial conditions converge to the linear geometry and the ring structure with transannular Ge-C bond. Scheme III illustrates the scenario for forming the structure with transannular C-C bond, which is unlikely in our experiments, since GeC_2 is not produced in detectable quantities by the laser ablation technique. As reported earlier, in experiments using this technique to form metal-carbides[81-85], there was no spectroscopic evidence of the ring with transannular C-C bond. By these arguments the preferred structures for GeC_3 produced by the laser ablation of germanium and carbon rods are thought to be the linear isomer or the ring with transannular Ge-C bond.

initial geometry   optimized geometry

Scheme I

2.8 Å
135°
1.3

linear
180°
1.31   1.29   1.83

Scheme II

105°   2.8
1.3

fan
2.20
2.02
1.35

Scheme III

1.5
1.3
2.2

kite
1.96
1.49
1.44
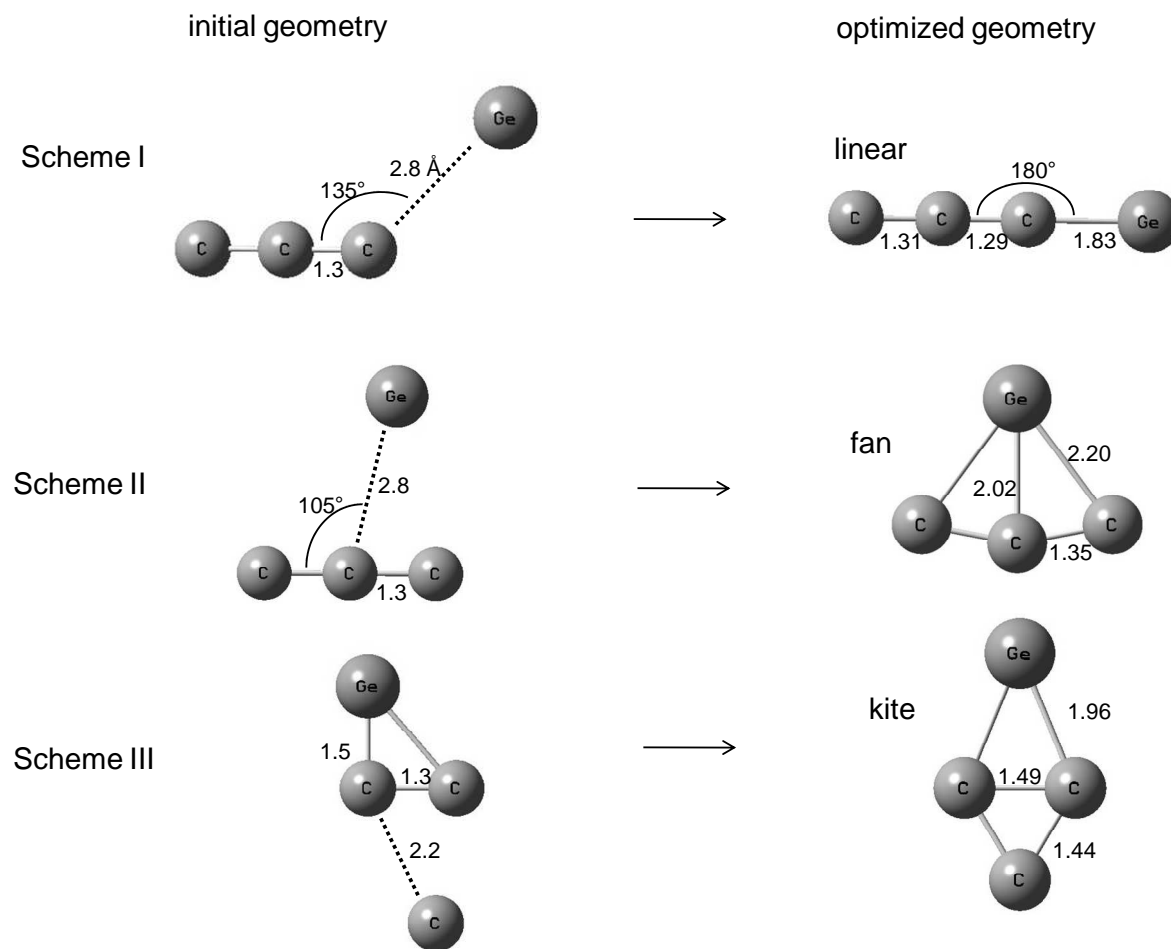
Figure 5.1   DFT-B3LYP/cc-pVDZ initial and optimized geometries. In Scheme I, a Ge atom initially at 2.8 Å and 135° from linear C_3, converges to linear GeC_3. In Scheme II a Ge atom initially at 2.8 Å and 105° from linear C_3, converges to cyclic GeC_3 with transannular Ge-C bond. In Scheme III the initial GeC_2 geometry given in Ref. 17, with a carbon atom at 2.2 Å, converges to cyclic GeC_3 with transannular C-C bond.

Table 5.1   DFT-B3LYP/cc-pVDZ predicted vibrational frequencies (cm^{-1}) and band intensities (km/mol) for GeC$_3$ isomers.

GeC$_3$ isomer	Vibrational mode	Frequency (cm^{-1})	Infrared intensity (km/mol)
$^3\Sigma$ linear	$v_1(\sigma)$	1986	197
	$v_2(\sigma)$	1300	37
	$v_3(\sigma)$	466	11
	$v_4(\pi)$	408	24
	$v_5(\pi)$	143	4
$^1A_1$ (transannular Si-C bond) +12.0 kcal/mol	$v_1(a_1)$	1136	4
	$v_2(a_1)$	696	29
	$v_3(a_1)$	393	19
	$v_4(b_1)$	217	40
	$v_5(b_2)$	1623	84
	$v_6(b_2)$	313	4
$^1A_1$ (transannular C-C bond) +11.2 kcal/mol	$v_1(a_1)$	1409	155
	$v_2(a_1)$	921	28
	$v_3(a_1)$	505	40
	$v_4(b_1)$	192	11
	$v_5(b_2)$	1011	3
	$v_6(b_2)$	323	31

5.3   Experimental Procedure

In attempting to produce GeC_3 by the laser ablation technique two different approaches were used: one consisted of simultaneously ablating the surfaces of a pair of continuously rotating and translating germanium and carbon rods, the other, of evaporating a single rod made from a sintered mixture of Ge and C powder. The ablation of a rod containing a sintered mixture of Ge, Si, and C was first used to produce GeC_3Si.[90] In the present work, optimization of the Ge:C mass ratio in the germanium-carbon rod was crucial to achieving a high yield of GeC_3. From a series of experiments testing different ratios, it was concluded that a mass ratio of Ge:C= 0.45:1 was optimum, in contrast to Ge:C=1.5:1 for GeC_3Ge (Ref. 78).

The evaporation of germanium and carbon was carried out using two Nd:YAG lasers (Spectra Physics) operating at 1064 nm in the pulse mode. The evaporated species were condensed in solid Ar (Matheson, 99.9995% purity) on a gold surfaced mirror previously cooled to ~10 K by a closed refrigeration system (ARS, Displex). The mirror was enclosed in a vacuum chamber maintained at a pressure of $\sim 10^{-8}$ Torr. Experimental parameters such as the laser focus, laser power, and Ar flow were adjusted to favor the production of GeC_3. For the laser ablation of the sintered germanium-carbon rod a beam with a power of 2.5 Watts, loosely focused on an area of ~25 mm^2 was used. Alternatively, a low power of ~0.6 Watts was used for the dual ablation of germanium and carbon rods.[84] During deposition, the Ar flow rate was adjusted by opening a needle valve until the chamber pressure increased from $\sim 10^{-8}$ to $\sim 6.0 \times 10^{-5}$ Torr. Typically, matrix samples in the experiments discussed here were deposited for ~90 min.

In order to unambiguously determine the molecular structure and identify vibrational fundamentals it is crucial to measure isotopic shifts. For this reason Ge-C rods were fabricated

with mixtures of ^{12}C (Alfa Aesar, 99.9995% purity), ^{13}C (Isotec, 99.3% purity), and germanium (ESPI, 99.9999% purity). Two rods were fabricated with mass ratio Ge:C=0.45:1, one with ^{12}C and the other having an appropriate ^{13}C enrichment to obtain the ^{13}C isotopic shifts necessary for determining the number of carbon atoms present and the geometry of the molecule.

FTIR absorption spectra of the products trapped in the Ar matrix were recorded over the range of 500-3500 cm^{-1} at a resolution of 0.2 cm^{-1}, using a Bomem DA3.16 Fourier transform spectrometer equipped with a liquid-nitrogen cooled Hg-Cd-Td (MCT) detector and a KBr beamsplitter. Details of the optical system have been reported previously.[40]

5.4   Results and Discussion

Table 5.1 indicates that the most intense infrared active modes of the three isomers of GeC$_3$ are at 1986 cm^{-1} for the linear geometry, and at 1623 and 1409 cm^{-1} for the cyclic structures, with transannular Ge-C and C-C bonds, respectively. A careful examination of the regions in the vicinity of ~1600 cm^{-1} and ~1400 cm^{-1} in the spectra taken of the evaporated products shows no evidence of carbon-germanium absorptions. The only absorptions present belong to carbon clusters and traces of water in the ~1600 cm^{-1} region. In contrast, Fig. 5.2(a) shows survey spectra recorded in the range 1880-1970 cm^{-1} where two unidentified bands appear at 1903.9 and 1924.2 cm^{-1}. Of the remaining bands, several have already been identified as the linear carbon molecules, C$_6$,[91] C$_6^-$,[92] and C$_7$,[93] which as shown in Fig. 5.2(c), are also present when only the carbon rod is ablated. The spectrum in Fig. 5.2(a) from the simultaneous ablation of carbon and germanium rods also exhibits absorptions of GeC$_3$Ge (Ref. 77, 78) and GeC$_9$ (Ref. 80) at 1920.7 and 1928.3 cm^{-1}, respectively. An absorption of GeCO (Ref. 94) at 1907.7 cm^{-1} that appears on the simultaneous ablation of C and Ge rods or of a Ge rod alone [Fig. 5.2(b)], is absent on the

ablation of a C rod [Fig. 5.2(c)]. Since it does not appear in the spectrum recorded when only an Ar matrix is deposited, GeCO likely originates with CO contamination in the Ge rod (ESPI, 99.9999% purity). The unidentified band at 1924.2 cm^{-1} in the spectrum in Fig. 2(a) obtained from simultaneous ablation disappears on annealing the matrix at a higher temperature of ~33 K and is not consistently present in all experiments. The 1903.9 cm^{-1} absorption is thus left as the only viable candidate for the $v_1(\sigma)$ mode of linear GeC$_3$.
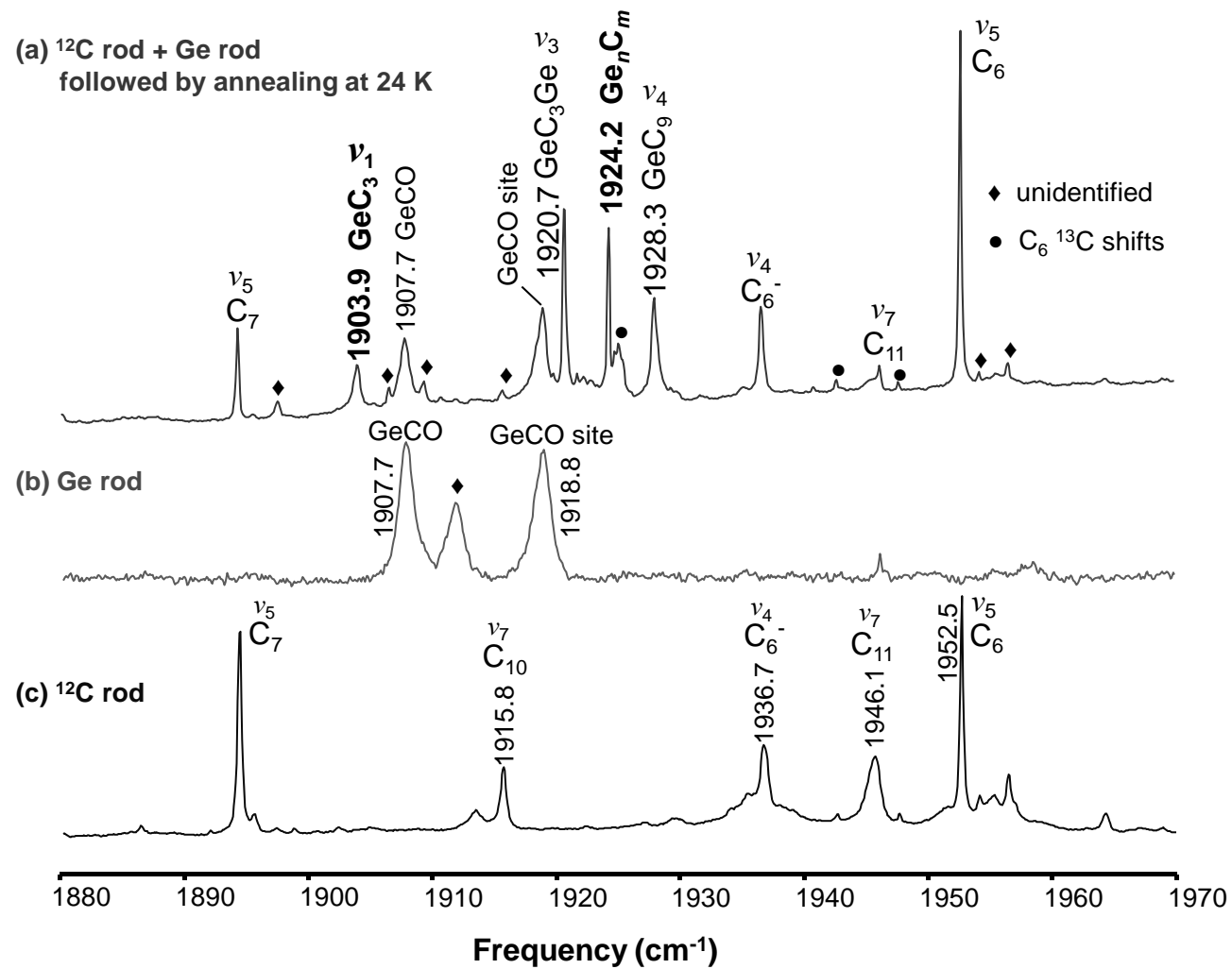
Figure 5.2   FTIR spectra produced by (a) the dual laser ablation of germanium and carbon rods, (b) laser ablation of the germanium rod used in (a), and (c) laser ablation of the carbon rod used in (a).

Figure 5.3(a) shows the spectrum obtained in an experiment very similar to the one presented in Fig. 5.2(c), but with 10% ^{13}C isotopic enrichment of the carbon. Although the spectrum is relatively complex with a substantial number of ^{13}C isotopomer bands, these are readily eliminated from consideration on the basis of previously reported isotopic studies. All of the ^{13}C isotopic shifts for the very intense v_3 mode of GeC$_3$Ge are observed,[77] as well as the absorptions of the single ^{13}C-substituted isotopomers for the v_5 mode of C$_7$ (Ref. 93), and several new isotopomer bands corresponding to double ^{13}C substitutions for this mode. The latter features are labeled + in Fig. 5.3(a) and match the DFT-predicted shifts. The single and double ^{13}C substitutions for the v_4 mode of C$_6$ and the Ge^{13}CO, and Ge^{13}CO isotopomer bands can similarly be identified.[94]

Three remaining features at 1856.5, 1885.1, and 1895.6 cm^{-1} labeled B, C, and D, respectively, are possible bands corresponding to the single ^{13}C-substituted isotopomers since they are each ~10% of the intensity of the 1903.9 cm^{-1} band that is a candidate for a fundamental of GeC$_3$. The absorptions at 1875.3 and 1848.3 cm^{-1} labeled E and F, respectively, are possible bands of the double ^{13}C-substituted isotopomers, and the very weak 1828.9 cm^{-1} absorption is tentatively thought to be the fully ^{13}C-substituted isotopomer. Figure 5.3(b) shows the DFT-simulated spectrum for all the ^{13}C –substituted isotopomers of linear GeC$_3$ calculated at the B3LYP/cc-pVDZ level of theory. The labels identify the isotopomer bands for each mass
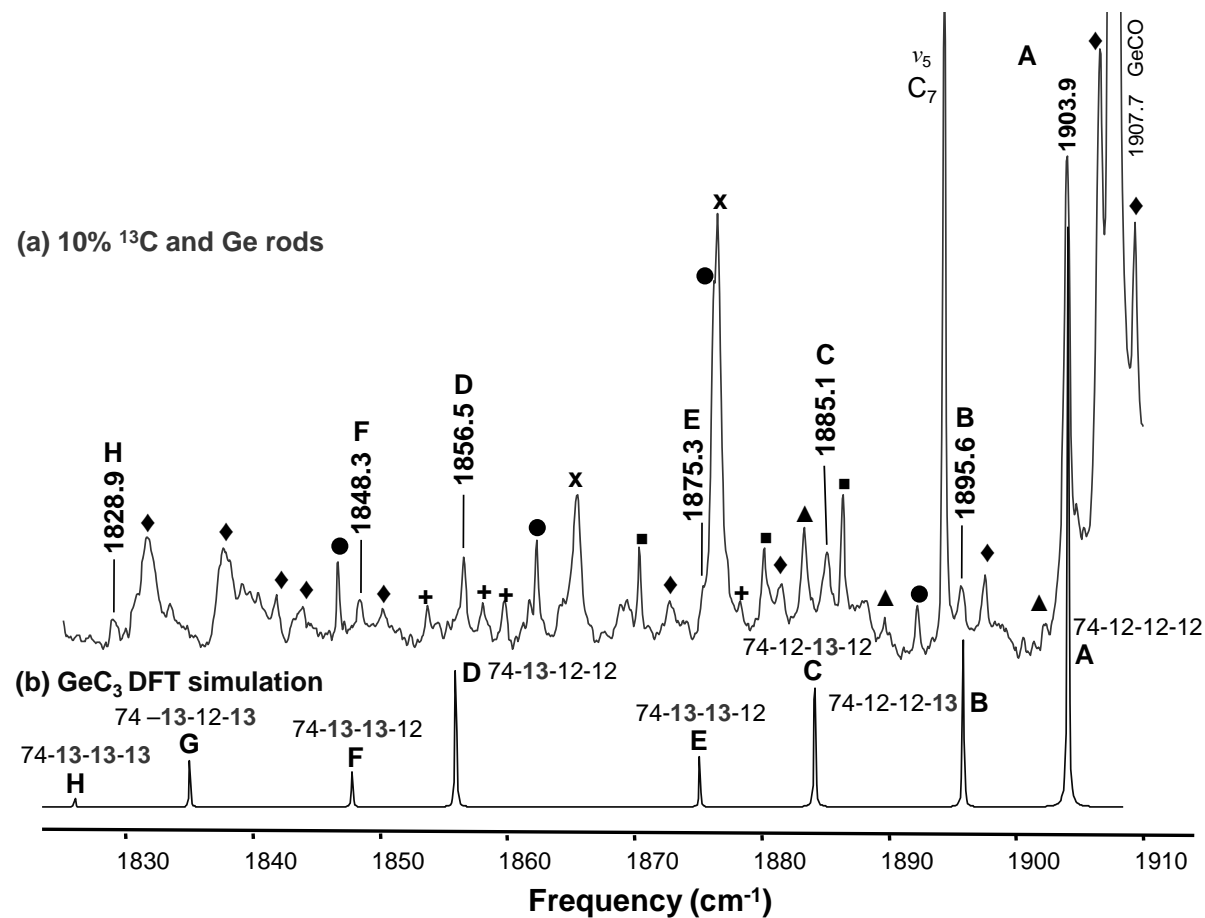
Figure 5.3   (a) FTIR spectra produced by the dual laser ablation of a germanium rod and a carbon rod with 10% ^{13}C enrichment. ♦ unidentified features present in the carbon rod ablation experiment, ▲ ^{13}C isotopic shifts for the ν_4 fundamental of C_6 (Ref. 38), ▪ single ^{13}C substitution shifts for the ν_5 fundamental of C_7 (Ref. 40), x ^{13}C isotopic shifts for the ν_1 fundamental of GeCO at two trapping sites (Ref. 41), • ^{13}C isotopic shifts for the ν_3 fundamental of GeC_3Ge (Ref. 19), + double ^{13}C substitution shifts for the ν_5 fundamental of C_7 (see text). (b) DFT- B3LYP/cc-pVDZ simulated spectrum for the $\nu_1(\sigma)$ fundamental of linear GeC_3.

Table 5.2   Comparison of the observed vibrational frequencies of the single ^{13}C-substituted isotopomers of the $v_1(\sigma)$ mode of linear GeC$_3$ for with the predictions of B3LYP/cc-pVDZ calculations.

Isotopomer Ge-C-C-C		Observed (cm^{-1}) v	B3LYP/ cc-pVDZ ω	Scaled[a] ω_{scaled}	Difference $v - \omega_{scaled}$
74-12-12-12	(A)	1903.9	1985.7	1903.9	…
74-12-12-13	(B)	1895.6	1977.4	1895.9	-0.3
74-13-12-12	(C)	1885.1	1965.8	1884.8	0.3
74-12-13-12	(D)	1856.5	1937.5	1857.6	-1.1
74-13-12-13	(E)	1875.3	1956.7	1876.0	-0.7
74-12-13-13	(F)	1848.3	1929.4	1849.8	-1.5
74-13-13-12	(G)	overlapped[b]	1916.6	1837.6	…
74-13-13-13	(H)	1828.9	1907.6	1828.9	…

[a]DFT calculations scaled by two scaling parameters function (details provided in ref. 95)

$$\omega_{scaled} = s(\omega)\omega$$

$$s(\omega) = \frac{s_{12} - s_{13}}{\omega_{12} - \omega_{13}}\omega + s_{12} - \frac{s_{12} - s_{13}}{\omega_{12} - \omega_{13}}\omega_{12} \quad \text{with} \quad s_{12} = \frac{v_{12}}{\omega_{12}} = \frac{1903.9}{1985.7}, \quad s_{13} = \frac{v_{13}}{\omega_{13}} = \frac{1828.9}{1907.6}$$

[b]Overlapped with an unidentified feature labeled ⬧ in Fig. 3(a), which is also observed in pure carbon experiments.
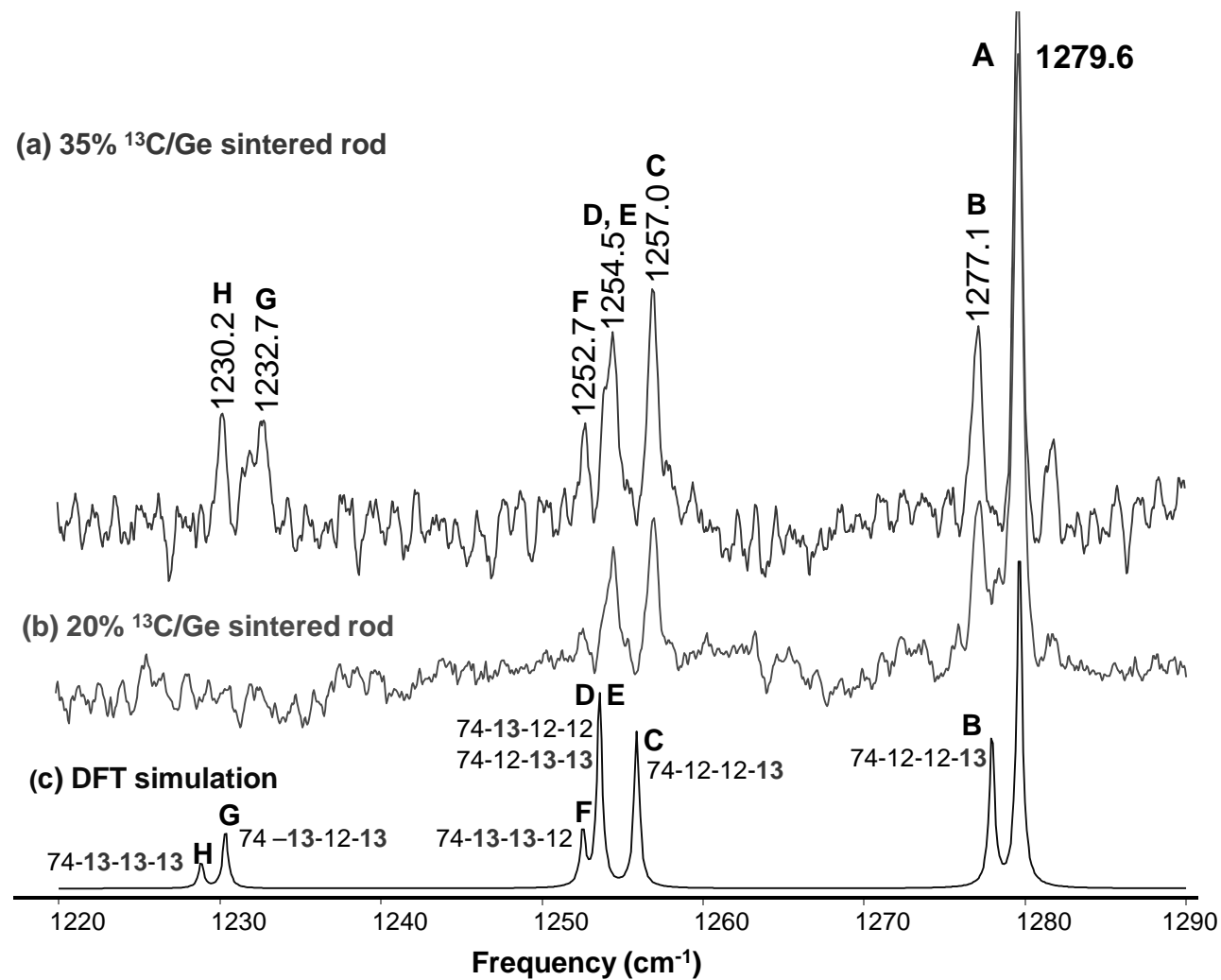
Figure 5.4   (a) FTIR spectra produced by the ablation of sintered germanium-carbon rod, the carbon powder used had 35% [13]C enrichment. (b) FTIR spectra produced by the ablation of sintered germanium-carbon rod, the carbon powder used had 20% [13]C enrichment.   (c) DFT simulation with B3LYP/cc-pVDZ level of theory for the $\nu_2(\sigma)$ fundamental of linear GeC_3.

Table 5.3   Comparison of the observed vibrational frequencies (cm^{-1}) of the $\nu_2(\sigma)$ mode for all ^{13}C substituted isotopomers of linear GeC$_3$ with the predictions of B3LYP/cc-pVDZ calculations.

Isotopomer Ge-C-C-C		Observed (cm^{-1}) ν	B3LYP/ cc-pvDZ ω	Scaled[a] ω_{scaled}	Difference $\nu - \omega_{scaled}$
Ge-12-12-12	(A)	1279.6	1299.6	1279.6	…
Ge-12-13-12	(B)	1277.1	1297.9	1277.9	-0.8
Ge-12-12-13	(C)	1257.0	1275.9	1256.6	0.4
Ge-13-12-12	(D)	1254.5	1273.6	1254.3	0.2
Ge-12-13-13	(E)	1254.5	1273.6	1254.3	0.2
Ge-13-13-12	(F)	1252.7	1272.5	1253.3	0.6
Ge-13-12-13	(G)	1232.7	1250.4	1231.8	0.9
Ge-13-13-13	(H)	1230.2	1248.8	1230.2	…

[a]DFT calculations scaled by two scaling parameters function (details in ref. 95):

$$\omega_{scaled} = s(\omega)\omega$$

$$s(\omega) = \frac{s_{12} - s_{13}}{\omega_{12} - \omega_{13}}\omega + s_{12} - \frac{s_{12} - s_{13}}{\omega_{12} - \omega_{13}}\omega_{12} \text{ with } s_{12} = \frac{\nu_{12}}{\omega_{12}} = \frac{1279.6}{1299.6}, \quad s_{13} = \frac{\nu_{13}}{\omega_{13}} = \frac{1230.2}{1248.8}$$

arrangement. In Table 5.2 the observed frequencies are compared to the calculated isotopomer frequencies which have been scaled with a two-parameter scaling function for carbon chains discussed earlier.[95] This scaling procedure can be used in the present case for the GeC_3 fundamental because the Ge atom doesn't participate in the vibration and the molecule is small, confining the spread of the shifts to only a few tens of cm^{-1}. Quadratic scaling avoids favoring the isotopic shifts of isotopomers that are closer to the full $^{12}C_n$ or $^{13}C_n$ bands, which occurs with simple linear scaling when the ratio of the observed to predicted frequencies for either the full $^{12}C_n$ or $^{13}C_n$ bands is used. The latter procedure makes the selection of the appropriate ratio for absorptions in the middle region between these bands ambiguous.   The very good agreement between the measured ^{13}C isotopic shifts and the DFT predicted frequencies confirms that the absorption at 1903.9 cm^{-1} is the $v_1(\sigma)$ stretching mode of linear GeC_3.

The DFT calculations for linear GeC_3 predict the next most intense fundamental $v_1(\sigma)$, to be at ~1300 cm^{-1}, with a relatively low intensity of 37 km/mol. In the dual laser ablation experiments that produced the spectra shown in Fig. 5.2 and 5.3, a band is observed at 1279.6 cm^{-1} with an intensity ratio of ~1/6 with respect to the 1903.9 cm^{-1} band. This is relatively close to the ~1/5 ratio predicted (see Table I). Unfortunately, the yield of linear GeC_3 was not high enough in the dual ablation experiments to observe the isotopic shifts of the band. This circumstance led us to do experiments with sintered germanium-carbon rods which were successful in producing a high yield of GeC_3Ge. As reported earlier,[78] this experimental strategy enabled the observation of two new vibrational fundamentals of linear GeC_3Ge, $v_4(\sigma_u)$ = 735.3 cm^{-1} and $v_6(\pi_u)$ = 580.1 cm^{-1}, which are predicted to have relatively low intensities, of 217 and 16 km/mol, respectively.[78] In the present experiments on GeC_3 the sintered rod has a lower percentage of germanium with a Ge:C mass ratio of 0.45:1 as discussed earlier in section 5.3.

Figure 5.4(a) shows a typical spectrum obtained in experiments using sintered Ge-C rods with 35% ^{13}C enrichment. To the low frequency side of the 1279.6 cm^{-1} absorption all of the isotopic shifts are observed and are labeled B-H. Calculation of the normal mode vectors shows that Ge does not participate in the vibration, so the fully substituted ^{13}C isotopomer (Ge-13-13-13) should scale approximately by the $\sqrt{12/13}$ mass ratio, which applied to the 1279.6 cm^{-1} band gives 1229.4 cm^{-1}. This approximate value is in fact, very close to the frequency of the band observed at 1230.2 cm^{-1} and labeled H in Fig. 5.4(a). Fig. 5.4(b) shows the spectrum recorded in an experiment which produced the best yield of GeC$_3$. The 20% ^{13}C enrichment used in this experiment resulted in the single ^{13}C-substituted isotopomer bands B, C, and D having better signal-to-noise ratio than in Fig. 5.4(a). The isotopic shift pattern for an isotopic ratio ^{12}C/^{13}C=35/75 was simulated using the results of DFT calculations at the B3LYP/cc-pVDZ level of theory for linear GeC$_3$. Fig. 5.4(c) shows very good agreement between the simulated isotopic shift spectrum and the observed isotopic shift pattern in Fig. 5.4(a) and (b). A quantitative comparison between the predicted and observed ^{13}C shift frequencies is given in Table 5.3. The excellent agreement between experimental results and theoretical predictions confirms the identification of the $v_2(\sigma)$ fundamental vibration of linear GeC$_3$ at 1279.6 cm^{-1}. It worth noting that sintered rod experiments giving a high yield of GeC$_3$, as indicated by the intensity of the 1279,6 cm^{-1} band, also produce a high yield of carbon chains with many absorptions in the vicinity of the $v_1(\sigma)$ stretching at 1903.9 cm^{-1}, thus unfortunately, preventing the observation of isotopic shifts using this technique.

Further corroboration of the proposed assignment of the $v_1(\sigma)$=1930.9 and $v_2(\sigma)$=1279.6 cm-1 fundamentals is provided by the ratio of their intensities which as noted earlier, is reasonably close to the theoretically predicted value of 5.3 (see Table 5.1) and remains constant

under a variety of experimental conditions. Figure 5.5 shows the correlation between the intensities of $\nu_1(\sigma)$ and $\nu_2(\sigma)$ for a series of experiments in which the laser power per unit area on the rod, the Ar flow, and annealing temperatures were varied to give different yields of GeC_3 in the matrix. Although the agreement is approximate since the intensity calculations are inexact, this correlation strengthens the assignments.

5.5   Conclusions

Linear GeC_3 has been formed by the dual laser ablation of germanium and carbon rods and by single laser ablation of a sintered germanium-carbon rod, and trapped in Ar matrices. Two vibrational fundamentals of linear GeC_3, $\nu_1(\sigma) = 1903.9$ cm^{-1} and $\nu_2(\sigma) = 1279.6$ cm^{-1}, have been assigned based on the comparison of ^{13}C isotopic shift measurements and the predictions of DFT calculations at the B3LYP/cc-pVDZ level. Although the $\nu_1(\sigma) = 1903.9$ cm^{-1} mode lies in a congested region that makes is analysis more complicated, the $\nu_2(\sigma) = 1279.6$ cm^{-1} mode is in a region with no other absorptions making its assignment straightforward and presenting unambiguous experimental evidence that linear GeC_3 has been synthesized.

Evidence accumulated from previous studies indicates that the laser ablation technique favors the formation of linear structures and cyclic structures with transannular metal-carbon bond over cyclic structures with transannular C-C bond. In the present work there is no spectroscopic evidence of cyclic structures for GeC_3 with either the transannular Ge-C or C-C bond although at the coupled cluster level of theory they are both predicted to be ~7-9 kcal/mol lower in energy than the linear isomer. This result suggests a need for further theoretical studies of GeC_3 to see if the cyclic isomers are indeed more stable than the linear.

Figure 5.5   Intensity correlation plot for the $\nu_1(\sigma)$ and $\nu_2(\sigma)$ fundamentals of linear GeC$_3$ at 1903.9 cm^{-1} and 1279.6 cm^{-1}, respectively. The integrated intensities are in arbitrary units.

CHAPTER VI

INFRARED OBSERVATION AND ISOTOPIC STUDY OF NEW COMBINATION BANDS
OF CARBON CHAINS C_5 AND C_9

6.1   Introduction

Carbon clusters have been of spectroscopic interest for many years, particularly because of their roles in the chemistry of the interstellar medium and circumstellar shells. Understanding their structures and how they bond has been a challenge for theorists and experimentalists alike. In the first systematic experimental investigation Weltner and McLeod[96] reported infrared fundamentals for C_n species formed by trapping the products of graphite evaporation in Ne matrices. Later, the discovery of C_{60} fullerene[97] stimulated renewed interest in carbon chains, rings and clusters.

Linear C_5 has been extensively studied with several spectroscopic techniques both in the gas phase and in matrices.[98-111] All the fundamentals have been assigned except for the $v_1(\sigma_g^+)$ symmetric stretch. The present work presents spectroscopic measurements and theoretical calculations which enable the assignment of the $(v_1 + v_4)$ combination band of linear C_5, and since the $v_4(\sigma_u^+)$ fundamental has been previously observed in an Ar matrix,[110] it is possible to obtain a frequency for the $v_1(\sigma_g)$ fundamental. Linear C_9 has similarly been the subject of many spectroscopic studies,[98,106,109,112-119] and only the three symmetric stretching modes, $v_1(\sigma_g^+)$, $v_2(\sigma_g^+)$, and $v_8(\sigma_u^+)$, have yet to be observed. In the present study, the (v_2+v_7) combination band has been measured, and using the frequency of the $v_7(\sigma_u^+)$ mode reported earlier in an Ar matrix,[43] a frequency for the $v_2(\sigma_g^+)$ fundamental has been obtained.

74

Earlier isotopic studies of carbon clusters trapped in Ar by Vala and co-workers have included measurements of combination bands of C_3 (ref. 120) and C_n ($n=5,6,7,9$).[121]

6.2 Theory

Currently, the *Gaussian 03* suite of programs[2] does not include calculations of the anharmonic corrections to the fundamentals, combination bands, or overtones of molecules having a point group with degenerate irreducible representations. Since this is the case for linear molecules, we slightly bend the chain to give a C_{2v} symmetry structure. The global minima for the bent structures of C_5 and C_9 are shifted only -2×10^{-3} and -4×10^{-4} kcal/mol from those of the linear structures. The frequencies of the stretching modes of the bent isomers differ by only ~0.1 cm^{-1} from their linear counterparts. Using these C_{2v} structures permits the calculation of anharmonic corrections for the fundamentals, combination bands, and overtones.

Table 6.1 lists the harmonic fundamentals calculated for linear C_5 and the anharmonic fundamentals, for the corresponding bent isomer. The anharmonic bending modes frequencies are not shown; a singularity occurs because pairs of close lying energy levels, which is a result of the bent structures. Table 6.2 gives similar results calculated for C_9. The level of theory used was the B3LYP[51,52,53] functional (Becke type 3 exchange and the correlation functional of Lee, Yang, and Parr) with cc-pVDZ basis set. The isotopic shifts for the combination bands ($v_1 + v_4$) of C_5 and (v_2+v_7) of C_9, which are presented in Tables 6.3 and 6.4, were computed using the bent structures.

A binary combination band is related to the fundamentals and the anharmonicity constant χ_{ij} via[122]

$$\left(\nu_i + \nu_j\right) = \nu_i(\sigma_g) + \nu_j(\sigma_u) - 2\chi_{ij} \qquad \text{Eq. 6.1}$$

If the observed combination band involves an observed asymmetric stretching fundamental the infrared inactive $\nu_j(\sigma_u)$ fundamental can be calculated using Eq. 6.1, giving a frequency within a few wave numbers of the actual value. Tables 6.1 and 6.2 present in the fifth column the frequencies expected to be observed that have been calculated using the relation

$$\nu_{\text{observed}} = 0.92673\,\nu_{\text{anharmonic-B3LYP/cc-pVDZ}} + 70.3 \qquad \text{Eq. 6.2}$$

which was derived[124] from a linear fit of a plot of the experimental frequencies for C_{2n+1} (n=1-4) linear carbon chains versus the calculated B3LYP-cc-PVDZ anharmonic results, Equation 6.2 predicts the frequencies expected to be observed within a few cm^{-1} of those actually measured. This relation can also provide valuable information for high resolution gas phase laser spectroscopy studies because it predicts the observed frequencies of odd carbon chains within a few cm^{-1}. For example, the fundamentals $\nu_1(\sigma_g)$, and $\nu_8(\sigma_u)$ modes of C_9 have not been observed, and the frequency of the $\nu_3(\sigma_g)$ fundamental has been measured only to within ± 50 cm^{-1} in a photon electron spectroscopy experiment.[123] As shown in Table 6.2, Eq. 6.2 predicts the frequencies of these modes to be respectively, 2144, 1300, and 899 cm^{-1} to within few wave numbers.

6.3   Experimental Procedure

Carbon clusters were evaporated from carbon rods using a Nd:YAG laser (Spectra Physics) operating at 1064 nm in pulse mode. The evaporated species were condensed in solid Ar

(Matheson, 99.9995% purity) on a gold surfaced mirror previously cooled to ~10 K by a closed refrigeration system (ARS, Displex). The mirror was enclosed in vacuum chamber maintained at a pressure of ~10^{-8} Torr. The carbon rod was ablated with a pulsed beam of ~2.8 Watts power, loosely focused on an area of ~25 mm^2. During the deposition, the Ar flow rate entering the chamber was ~1 mmol/h for depositions lasting 1½ hours.

The measurement of ^{13}C isotopic shifts enables the determination of the structure and the assignment of vibrational fundamentals or combination bands. For this reason carbon rods were made with mixtures of ^{12}C (Alfa Aesar, 99.9995% purity) and ^{13}C (Isotec, 99.3% purity).

FTIR absorption spectra of the products condensed in the Ar matrix were recorded over the range 500–5000 cm^{-1}, at a resolution of 0.2 cm^{-1} using a Bomem DA3.16 Fourier transform spectrometer equipped with a liquid nitrogen cooled Hg–Cd–Te (MCT) detector, KBr beamsplitter, and Globar source. For the combination bands the spectra were also recorded in the 1800-5000 cm^{-1} region using a liquid nitrogen cooled InSb detector, which improved the signal-to-noise ratio a factor of 7. This enhancement was indispensable to the observation of isotopic frequency shifts for the new combination bands identified in the present work since the combination bands are ~100 times weaker in intensity than the most intense fundamentals. Details of the optical system and experimental apparatus have been reported previously.[40]

Table 6.1   Observed   and   DFT-B3LYP/cc-pVDZ   predicted   vibrational   frequencies, combination bands (cm^{-1}) and band intensities for linear and bend structures of C_5.

Infrared active Combination bands	Observed (cm^{-1})	Frequency linear structure	Anharmonic frequency of the bend structure	Expected observed frequency using Eq. (2) of ref. 124	Infrared intensity (km/mol)
$v_1(\sigma_g)$	1946[a]	2046	2015	1938	0
$v_2(\sigma_g)$	776[b]	800	799	811	0
$v_3(\sigma_u)$	2163.9[c]	2270	2228	2174	2539
$v_4(\sigma_u)$	1446.6[d]	1499	1481	1443	122
$v_5(\pi_g)$	218±13[e]	280	…	…	0
$v_6(\pi_u)$	535±10[e]	676	…	…	3
$v_7(\pi_u)$	118±3[e]	138	…	…	14
$v_1(\sigma_g)+v_3(\sigma_u)$	?	4316	4230	4112	…
$v_1(\sigma_g)+v_4(\sigma_u)$	3388.8[a]	3545	3486	3381	…
$v_2(\sigma_g)+v_3(\sigma_u)$	2939.9[b]	3070	3018	2985	…
$v_2(\sigma_g)+v_4(\sigma_u)$	?	2299	2282	2254	…

[a] This work, [b] ref. 96, [c] ref. 98, 99, [d] ref. 93, [e] ref. 98, 99

Table 6.2   Observed and DFT-B3LYP/cc-pVDZ predicted vibrational frequencies, combination bands (cm^{-1}) and band intensities for linear and bent structures of C$_9$.   The combination bands involving $v_8(\sigma_u)$ were excluded because it has not been observed

Infrared active Combination bands	Observed (cm^{-1})	Frequency linear structure C$_9$ (cm^{-1})	Anharmonic frequency of the bend structure of C$_9$	Expected obs.freq. using Eq. (2), ref. 124	Infrared intensity (km/mol)
$v_1(\sigma_g)$	?	2276	2237	2144	0
$v_2(\sigma_g)$	**1870**[a]	**1970**	**1943**	**1870**	**0**
$v_3(\sigma_g)$	1258±50[c]	1294	1327	1300	0
$v_4(\sigma_g)$	448[b]	464	492	526	0
$v_5(\sigma_u)$	2078.1[d]	2217	2184	2095	4074
$v_6(\sigma_u)$	1998.0[d]	2132	2095	2011	6526
$v_7(\sigma_u)$	1601.0[e]	1670	1652	1602	393
$v_8(\sigma_u)$	?	895	894	899	0.2
$v_1(\sigma_g)+v_{5/6/7}(\sigma_u)$	?	4493/4408/3946	4415/4321/3883	4239	…
$v_2(\sigma_g)+v_{5/6}(\sigma_u)$	?	4187/4102	4121/4030	3965	…
$v_2(\sigma_g)+v_7(\sigma_u)$	**3471**[a]	**3640**	**3587**	**3472**	**…**
$v_3(\sigma_g)+v_{5/6/7}(\sigma_u)$	?	3511/3426/2964	3508/3415/2977	3395	…
$v_4(\sigma_g)+v_5(\sigma_u)$	2525.7[b]	2681	2675	2621	…
$v_4(\sigma_g)+v_6(\sigma_u)$	2443.0[b]	2596	2587	2537	…
$v_4(\sigma_g)+v_7(\sigma_u)$	?	2134	2145	2128	…

[a] this work, [b] Ref. 96,98, [c] Photoelectron spectroscopy ref. 98, [d] refs. 106,109,107-124, [e] 119

6.4   Results and Discussion

Figure 6.1 shows a section of a survey spectrum recorded in the range 500-5000 cm^{-1} using the MCT detector. The combination bands appeared after 45 min of deposition. Although the InSb detector gives a better signal-to-noise ratio over the MCT, it is limited to frequencies above ~2000 cm^{-1}. In this region there is only the $v_3(\sigma_u)$ fundamental of linear C_5, , and none of the fundamentals of linear C_9. Thus, the spectrum recorded with the MCT was necessary for correlating combination bands with fundamentals using the experimental intensity ratios of their absorptions, which should remain constant if both absorptions result from the same molecule. From the intensity ratios measured for several experiments producing different yields of carbon clusters, it was found that the absorption at 3388.8 cm^{-1}, labeled A in Fig. 6.2(a), is correlated to both the $v_3(\sigma_u)$ and $v_4(\sigma_u)$ fundamentals of linear C_5.[110] Similarly, the absorption at 3471.8 cm^{-1}, labeled A in Fig. 6.3(a), is correlated to both the $v_6(\sigma_u)$ and $v_7(\sigma_u)$ fundamentals of linear C_9.[119] Tables 6.1 and 6.2 list the calculated values for the harmonic and anharmonic fundamentals of linear C_5 and C_9, respectively. These predictions suggest that the observed 3388.8 and 3471.8 cm^{-1} absorptions are the (v_1+v_4) and (v_2+v_7) combination bands of linear C_5 and C_9, respectively. By itself this argument is not conclusive because the yields of different carbon chains could be correlated; there are many close lying fundamentals for different clusters; and there are traces of H_2O, CO, and CO_2 that could bond to carbon chains and produce additional absorptions. Thus it is necessary to have isotopic shift measurements in order to unambiguously assign the combination bands.

Figure 6.2(a) shows a region to the low frequency side of the 3388.8 cm^{-1}, absorption where new bands emerge when a carbon rod with 10% ^{13}C enrichment is used. For comparison, Fig.

6.2(b) shows the identical region recorded with no ^{13}C enrichment. Three new absorptions appear in Fig. 6.2(a) labeled B, C, and D, which have intensity ratios with respect to the 3388.8 cm^{-1} band of ~20, 20, and 10%, respectively. This is what would be expected for the isotopic frequency shift profile of linear C_5 when 10% ^{13}C enrichment is used. A detailed comparison of these shifts with the theoretical predictions for linear C_5 is presented in Table 6.3. As expected, the absorptions labeled B and C correspond to the 13-12-12-12-12 and 12-13-12-12-12 isotopomers, each with two equivalent sites, and D is the absorption of the 12-12-13-12-12 isotopomer with the unique central site. As seen in Table 6.3, the agreement between the measured isotopic shifts and the DFT predictions is good, confirming the assignment of the (v_1+v_4) combination band of linear C_5 at 3388.8 cm^{-1}. Using the frequency of the previously assigned[110] $v_4(\sigma_u)$ fundamental at 1446.6 cm^{-1}, Eq 1 allows us to calculate the frequency of the symmetric stretching mode $v_1(\sigma_g)$, of linear C_5 as 1946 cm^{-1} to within few cm^{-1}

Figure 6.3(a) shows the spectrum of the region to the low frequency side of the absorption at 3471.8 cm^{-1}, which was obtained using a carbon rod with 10% ^{13}C enrichment. For comparison, Fig. 6.3(b) shows the identical region of the spectrum obtained using a ^{12}C rod. The new absorptions shown in Fig. 6.3(a), labeled B, C, D, and E-F, have intensity ratios with respect to the main 3471.8 cm^{-1} band of ~ 20, 20, 20, and 30 respectively. This is the expected case when having 10% ^{13}C enrichment in the profile of linear C_9 if there is an overlap of the unique-site isotopomer 12-12-12-12-13-$\cdots$ with a pair of equivalent-sites isotopomer. The theoretical predictions of the combination band (v_2+v_7) of linear C_9 has this feature, see Table 6.4 for the detailed comparison. As expected the isotopomer 12-12-12-12-13-$\cdots$ is predicted at 16.9 cm^{-1} from the main band and there is a pair equivalent-sites isotopomer, 12-12-12-13-12-$\cdots$, which are predicted at 16.5 cm^{-1}, confirming previous assumption. Table 6.4 shows the good

agreement between the predicted and observed shifts, confirming the identification of the $(v_1 + v_4)$ combination band of linear C_9 at 3471.8 cm^{-1}. Using the frequency of the previously assigned[119] $v_7(\sigma_u)$ fundamental of linear C_9 at 1601.0 cm^{-1}, the frequency of the symmetric stretching mode $v_2(\sigma_g)$ of linear C_9 is calculated as 1870 cm^{-1} to within few cm^{-1}.

It is also important to note that eq 2 predicts from the anharmonic DFT calculation that the $v_1(\sigma_g)$ fundamental for linear C_5 should be observed in the gas phase at 1938 cm^{-1} and the $v_2(\sigma_g)$ fundamental for C_9, at 1870 cm^{-1}. These values are very close to the frequencies 1946 cm^{-1} for the $v_1(\sigma_g)$ mode of linear C_5 and 1870 cm^{-1} for the $v_2(\sigma_g)$ mode of linear C_9 derived from the measurement of combination bands in the present work.
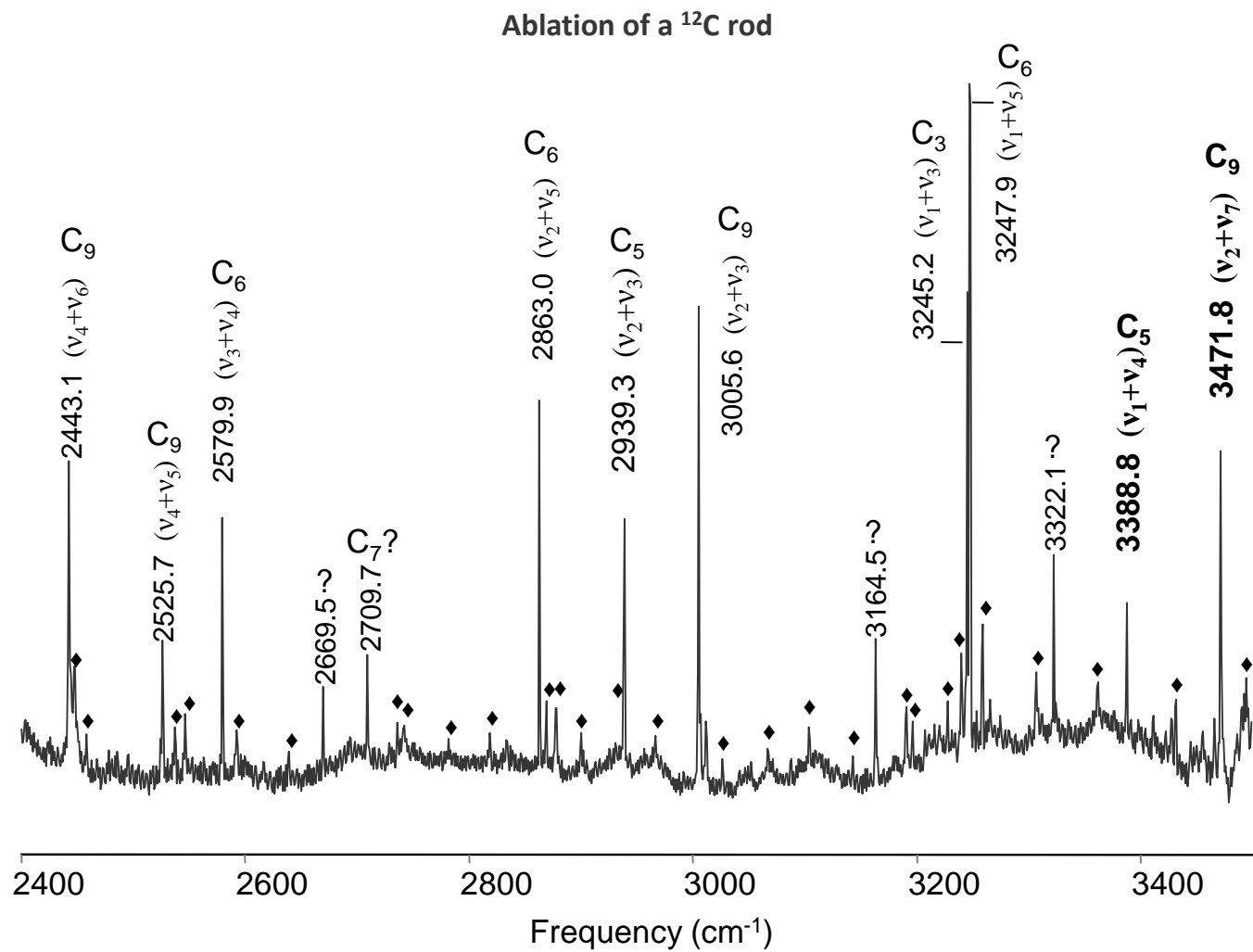
Figure 6.1   FTIR spectra produced by the laser ablation of a ^{12}C rod in the 2400-3500 cm^{-1} frequency region.   The weak absorptions labeled with ◆ could be triple or quadruple combination bands.
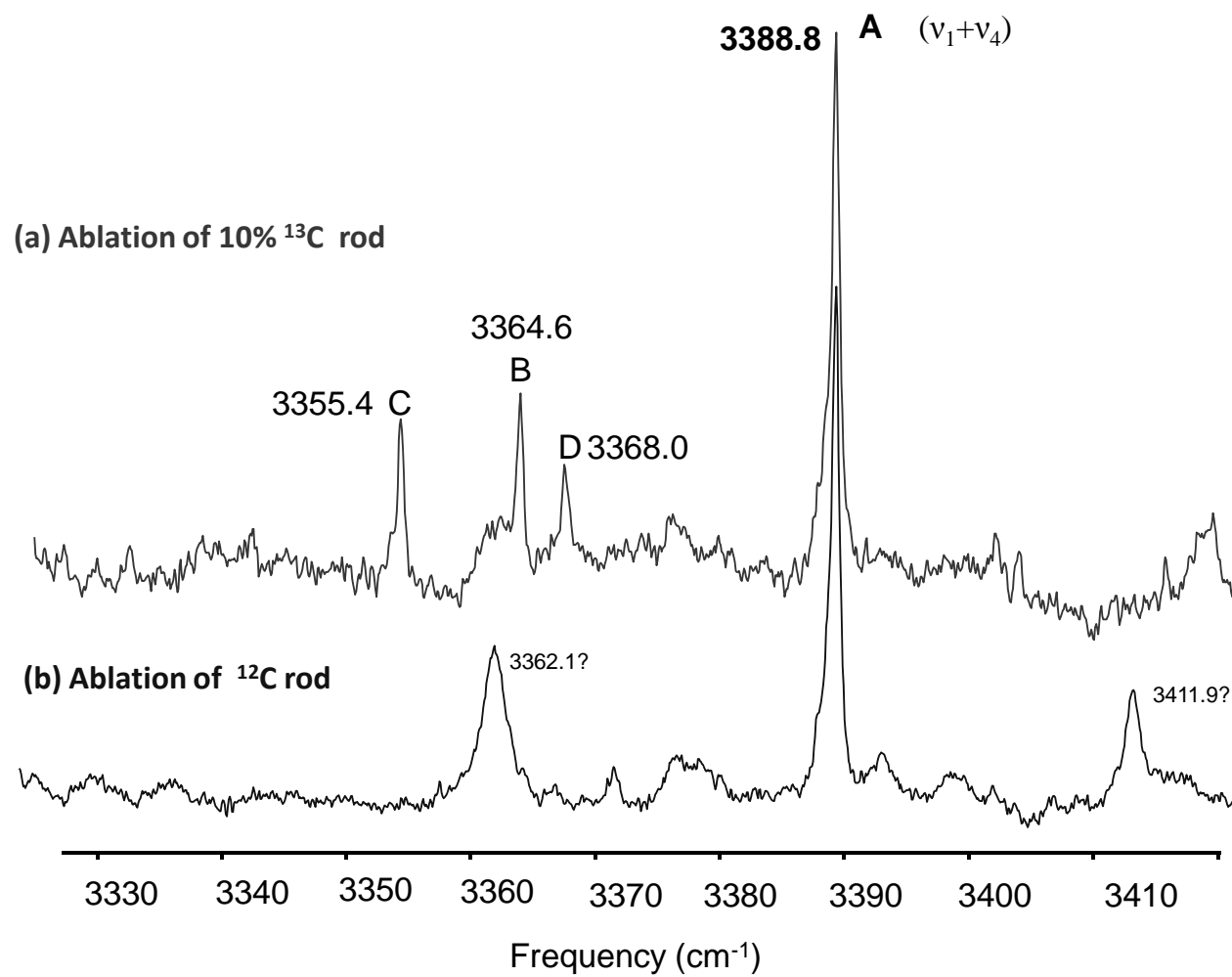
Figure 6.2　　The combination band $(\nu_1+\nu_4)$ of linear C_5. FTIR spectra produced by the laser ablation of (a) a carbon rod having 10% [13]C enrichment and (b) a ^{12}C rod.
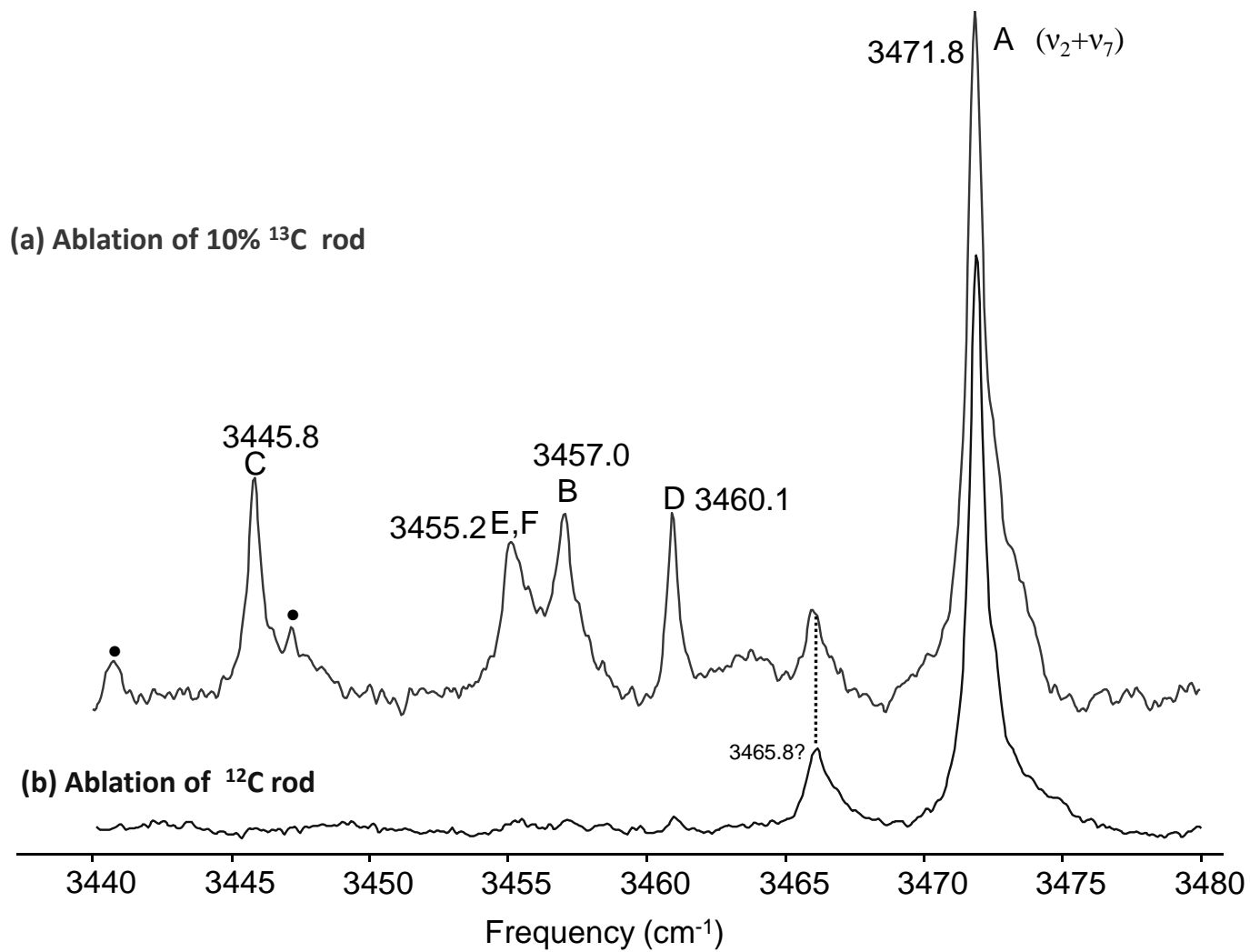
Figure 6.3   The combination band ($\nu_2+\nu_7$) of linear C_9. FTIR spectra produced by the laser ablation of (a) a carbon rod having 10% ^{13}C enrichment and (b) a ^{12}C rod.

Table 6.3   Comparison of observed vibrational frequencies (cm^{-1}) of the (v_1+v_4) combination band for single ^{13}C-substituted isotopomers of linear C_5 with the predictions of B3LYP/cc-pVDZ level calculations.

Isotopomer C-C-C-C-C		Observed (cm^{-1})	B3LYP/cc-pVDZ harmonic linear C_5 $v_1(\sigma_g)+v_4(\sigma_u)$	B3LYP/cc-pVDZ anharmonic bend C_5 (v_1+v_4)	B3LYP/cc-pVDZ anharmonic scaled[a] (v_1+v_4)	Differences obs.- scaled
12-12-12-12-12	A	3388.8	3544.8	3486.7	…	
13-12-12-12-12	B	3364.6	3519.0	3461.8	3464.6	0.0
12-13-12-12-12	C	3355.4	3510.0	3452.6	3355.7	-0.4
12-12-13-12-12	D	3368.0	3521.3	3464.5	3367.2	0.8

[a]Results of the DFT-B3LYP/ cc-pVDZ calculation scaled by a factor of 3388.8/3486.7

Table 6.4   Comparison of observed vibrational frequencies (cm^{-1}) of the (v_2+v_7) combination band for single ^{13}C-substituted isotopomers of linear C$_9$ with the predictions of B3LYP/cc-pVDZ level calculations.

Isotopomer C-C-C-C-C-…		Observed (cm^{-1})	B3LYP/cc-pVDZ harmonic linear C$_9$ $v_1(\sigma_g)$+$v_4(\sigma_u)$	B3LYP/cc-pVDZ anharmonic bend C$_9$ (v_1+v_4)	B3LYP/cc-pVDZ anharmonic scaled[a] (v_1+v_4)	Difference obs -scaled
12-12-12-12-12-…	A	3471.8	3640.7	3587.8	…	…
13-12-12-12-12-…	B	3457.0	3625.3	3573.1	3457.6	-0.6
12-13-12-12-12-…	C	3445.8	3616.4	3563.9	3448.7	-2.9
12-12-13-12-12-…	D	3460.1	3628.4	3575.9	3460.3	-0.2
12-12-12-13-12-…	E	3455.2	3623.9	3571.3	3455.8	-0.6
12-12-12-12-13-…	F	3455.2	3624.0	3571.7	3456.2	-1.0

[a] Results of the DFT-B3LYP/ cc-pVDZ calculation scaled by a factor of 3471.8/3587.8

6.5   Conclusions

New combination bands of carbon chains have been observed, $(v_1+v_4) = 3388.8$ cm^{-1} of linear C_5 and $(v_2+v_7) = 3471.8$ cm^{-1} of linear C_9. These assignments are based on very good agreement between measured isotopic shifts and DFT predictions at the B3LYP/cc-VDZ level of theory and the correlation of the intensities of the combination bands with vibrational fundamentals of the same molecule Since the asymmetric stretching modes involved in these absorptions have been measured previously[110,119] it has been possible to assign the infrared inactive symmetric stretching modes, the $v_1(\sigma_g)$ mode of linear C_5 at 1942 cm^{-1} and the $v_2(\sigma_g)$ mode of linear C_9 at 1870 cm^{-1}. The close agreement of the measured $v_1(\sigma_g)$ fundamental of linear C_5 and $v_2(\sigma_g)$ of linear C_9 and the frequencies predicted by Eq 6.2 from the B3LYP anharmonic calculation gives further support to the identifications of the fundamentals and combination bands.

In the course of this work isotopic data has also been acquired for the combination bands of linear C_5, C_6, and C_9 presented in ref. 125 $(v_2 + v_3) = 2939.3$ cm^{-1} for C_5, $(v_1 + v_5) = 3247.9$ cm^{-1}, $(v_2+v_5) = 2863.0$ cm^{-1}, and $(v_3 + v_4) = 2579.9$ cm^{-1} for C_6, and $(v_4 + v_5) = 2525.7$ cm^{-1} and $(v_4+v_6) = 2443.1$ cm^{-1} for C_9 with only minor discrepancies in the last figure. Although we have a high yield of carbon clusters, there are no absorptions in the 4000-4400 cm^{-1} indicating that for carbon chains the intensities of infrared active combination band of $v_1(\sigma_g)$ and the most intense asymmetric stretching modes are very weak. Surprisingly, in this region the first overtones reported in ref. 88 have not been observed.

CHAPTER VII

INFRARED OBSERVATION OF THE v_6 MODE OF LINEAR C_7

7.1 Introduction

Linear C_7 has been extensively studied with several spectroscopic techniques both in the gas phase and in matrices.[43,98,88,126,127,128,129,130,131,132,133,134] All infrared active stretching modes have been assigned except for the $v_6(\sigma_u)$ fundamental. This mode may have remained undetected in many infrared spectroscopy studies because its intensity is very weak. This work presents spectroscopic measurements and theoretical calculations which enable the assignment of the $v_6(\sigma_u)$ fundamental of linear C_7 at 1100.1 cm^{-1}. This assignment is based on very good agreement between ^{13}C isotopic shift measurements with the predictions of DFT calculations and the intensity correlation of this mode with previously observed $v_4(\sigma_u)$ and $v_5(\sigma_u)$ fundamentals at 2127.9 cm^{-1} and 1984.3 cm^{-1}.[43]

7.2 Theoretical Calculations

To support the identification of the $v_6(\sigma_u)$ fundamental of linear C_7, we performed DFT calculations at the standard B3LYP/cc-pVDZ level using the *Gaussian 03* program suite.[2] The harmonic fundamental frequencies and infrared intensities for linear C_7 fundamentals are given in Table 7.1. Also included are the observed fundamentals. Notice that $v_4(\sigma_u)$ and $v_5(\sigma_u)$ are predicted to be 291 and 81 times more intense than the $v_6(\sigma_u)$ fundamental.

Table 7.1   Observed and DFT-B3LYP/cc-pVDZ predicted vibrational frequencies and band intensities for linear C_7.

Vibrational mode	Observed (cm^{-1})	Frequency (cm^{-1})	Infrared intensity (km/mol)
$v_1(\sigma_g)$	?	2221.4	0
$v_2(\sigma_g)$	?	1609.5	0
$v_3(\sigma_g)$	548±90[a]/582[b]	588.8	0
$v_4(\sigma_u)$	2138.315[c]/2134.6[d]/2127.8[e]	2258.2	4656
$v_5(\sigma_u)$	1898.376[f]/1894.3[e]	1988.4	1303
$v_6(\sigma_u)$	**1100.1[g]**	**1118.8**	**16**
$v_7(\pi_g)$	496±110[a]	574.4	0
$v_8(\pi_g)$	?	190.2	0
$v_9(\pi_u)$	?	708.0	(6.1)2
$v_{10}(\pi_u)$	?	293.1	(6.2)2
$v_{11}(\pi_u)$	?	80.1	(9.9)2

[a] Gas ref. 98; [b] Ar ref. 88; [c] gas ref.126,127,128; [d] Ne ref. 129,130; [e] Ar ref.43; [f] gas ref.126; [g] this work

7.3   Experiments

Carbon clusters were evaporated from carbon rods using a Nd:YAG laser (Spectra Physics) operating at 1064 nm in the pulsed mode. The evaporated species were condensed in solid Ar (Matheson, 99.9995% purity) on a gold surfaced mirror previously cooled to ~10 K by a closed refrigeration system (ARS, Displex). The mirror was enclosed in vacuum chamber maintained at a pressure of ~10^{-8} Torr.

The measurement of ^{13}C isotopic shifts enables the determination of the structure and the assignment of vibrational fundamentals or combination bands. For this reason carbon rods were made with mixtures of ^{12}C (Alfa Aesar, 99.9995% purity) and ^{13}C (Isotec, 99.3% purity).

FTIR absorption spectra of the products condensed in the Ar matrix were recorded over the range 500–5000 cm^{-1}, at a resolution of 0.2 cm^{-1} using a Bomem DA3.16 Fourier transform spectrometer equipped with a liquid nitrogen cooled Hg–Cd–Te (MCT) detector, KBr beamsplitter, and Globar source. Details of the optical system and experimental apparatus have been reported earlier.[40]

In the present experiments the carbon rod was ablated with a pulsed beam with power of ~0.5-3.5 Watts, loosely or tightly focused on the rod with areas of ~2 mm^2 and ~25 mm^2 respectively. During the deposition, the Ar flow rate entering the chamber was ~1 mmol/h for depositions lasting up1½ hours. It was found that the optimal condition for producing linear C_7 is a tightly focused beam of 1.0 Watts. The experiments used a sintered rod doped with silicon or germanium which produced the highest yield of this molecule, which allowed the first observation of the isotopic shifts pattern. These rods were subject to high laser powers of up to 3.5 Watts for extended depositions.

7.5   Results and Discussions

Figure 7.1 shows a survey spectrum recorded in the 1050-1250 cm^{-1} region of the evaporated products and showing an unidentified absorption at 1100.1 cm^{-1}. The DFT calculation for linear C$_7$, presented in Table 7.1, predicts the $v_6(\sigma_u)$ fundamental at 1118 cm^{-1} making the absorption a good candidate for this mode. In addition, judging from the strengths of the $v_4(\sigma_u)$ and $v_5(\sigma_u)$ absorptions of linear C$_7$ this experiment with the conditions mentioned above produced a high yield of the C$_7$ molecule; when the production of C$_7$ is low, this band never appears. Figure 7.2 shows the intensity correlation between $v_4(\sigma_u)$ and $v_5(\sigma_u)$ with the new band at 1100.1 cm^{-1}, indicating that C$_7$ might be the molecule responsible for the absorption. As mentioned in the previous chapter this argument is not conclusive because the yields of different carbon chains can be correlated; there are many close lying fundamentals for different clusters; and there are traces of H$_2$O, CO, and CO$_2$ that could bond to carbon chains and produce additional absorptions. Thus it is necessary to have isotopic shift measurements in order to unambiguously assign the fundamental. Observing the isotopic shifts of this band was impossible by ablating only the ^{13}C enriched rod. The yield diminishes making undetectable the isotopic shifts of this very weak absorption. Recall that the 1100.1 cm^{-1} absorbance is 1/50 as intense as the $v_5(\sigma_u)$ absorbance and 1/108 as intense as the $v_4(\sigma_u)$ absorbance (see Fig. 7.2). The DFT predictions are 1/81 and 1/291 respectively (see Table. 7.1). As mentioned above, the best signal-to-noise ratio for the isotopic shifts pattern was observed when ablating sintered silicon or germanium doped rods having 10% ^{13}C enrichment. Figure 7.3(a) shows the best of the experiments with sintered silicon/germanium-carbon rods. Five new absorptions appear in Fig. 7.3(a) labeled B, C, D, and F, which have intensity ratios with respect to the 1100.1 cm^{-1} band of ~20, 20, 20 and 10%, respectively. This is what would be expected for the isotopic shifts
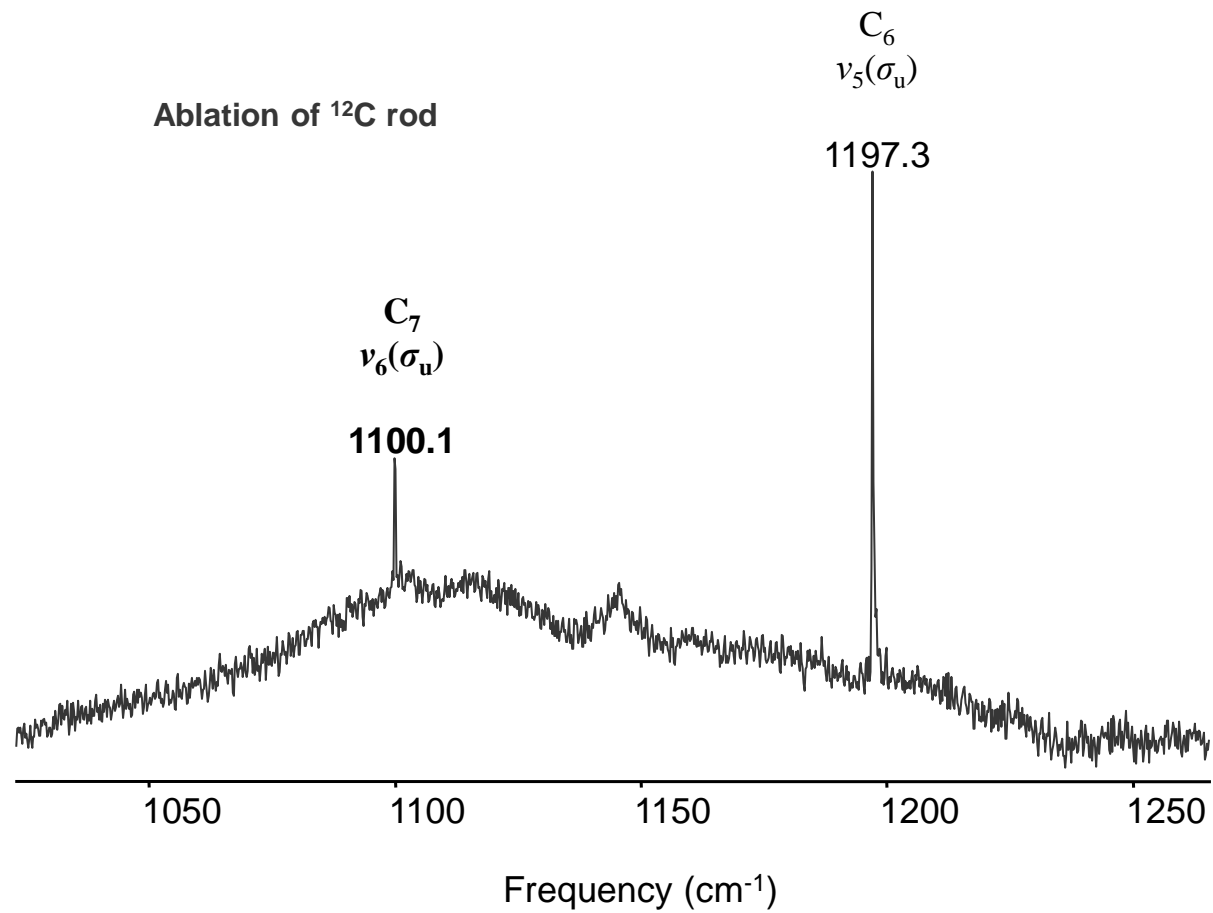
Figure 7.1   FTIR spectra produced by the laser ablation of a carbon rod.
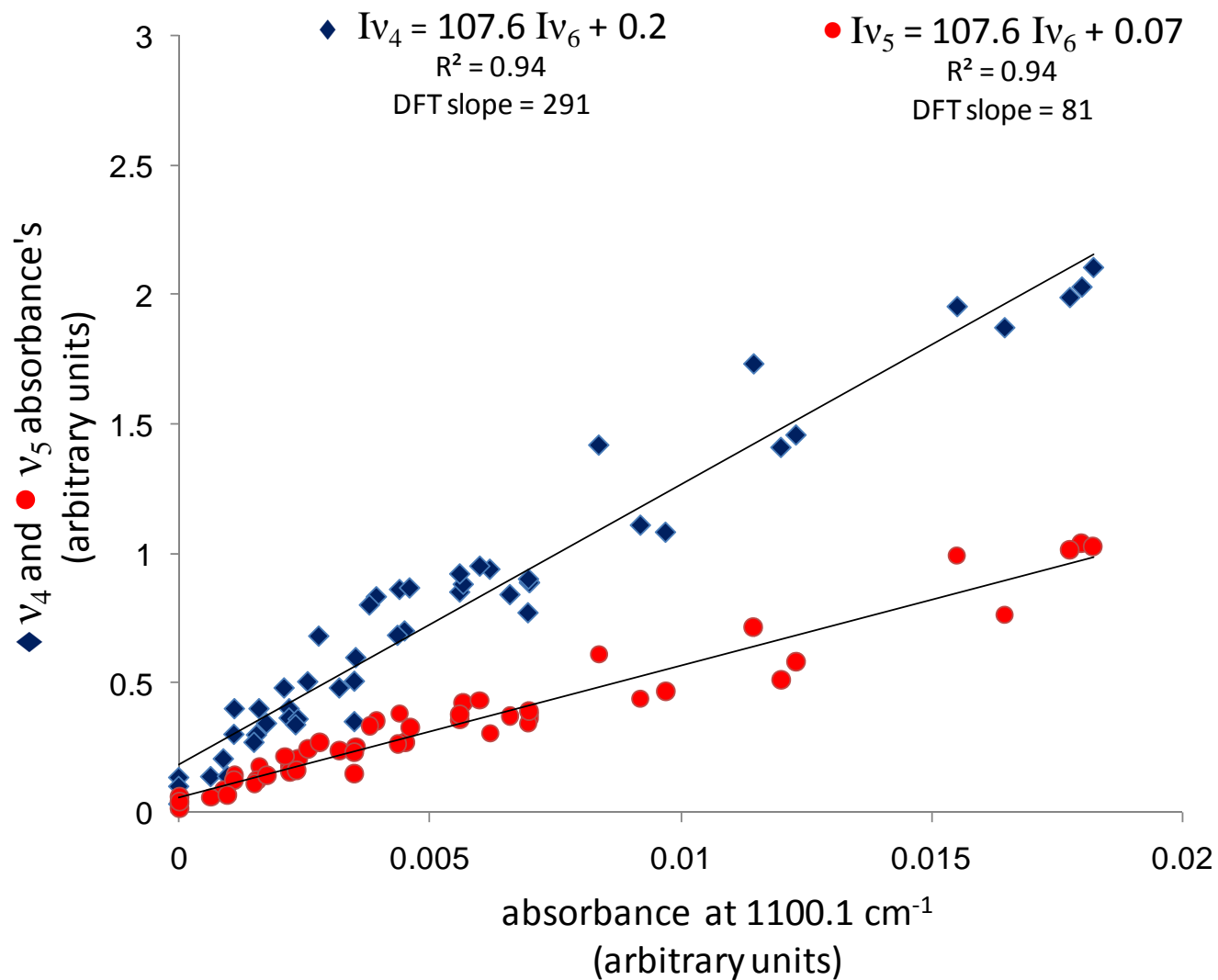
Figure 7.2   Intensity correlation plot of the $\nu_4(\sigma_u)$ and $\nu_5(\sigma_u)$, absorbance vs. the absorbance at 1100.1 cm^{-1}. The integrated intensities are in arbitrary units.

pattern for linear C_7 when 10% ^{13}C enrichment is used. A detailed comparison of these shifts with the theoretical predictions for linear C_7 is presented in Table 7.2. As expected, the absorptions labeled B, C and D correspond to the 12-13-12-12-⋯, 12-13-12-12-⋯ and 12-12-13-12-⋯ isotopomers, each with two equivalent sites, and D is the absorption of the 12-12-12-13-⋯ isotopomer with the unique central site. As seen in Table 7.2, the agreement between the measured isotopic shifts and the DFT predictions is good, confirming our conclusion that the 1100.1 cm^{-1} absorption can be assigned to the $v_6(\sigma_u)$ fundamental of linear C_7..

7.6   Conclusion

The $v_6(\sigma_u)$ weakest asymmetric stretching mode of linear C_7 has been detected for the first time and has been assigned at 1100.1 cm^{-1} in solid Ar. The assignment is supported by the intensity correlation of this mode with the previously observed $v_4(\sigma_u)$ and $v_5(\sigma_u)$ modes and the good agreement between the observed and simulated isotopic shifts pattern. The isotopic shifts were observed with sintered rods doped with silicon or germanium, which allowed them to resist high laser powers for long periods of times, allowing the observation of the very weak isotopomer bands necessary for this assignment.
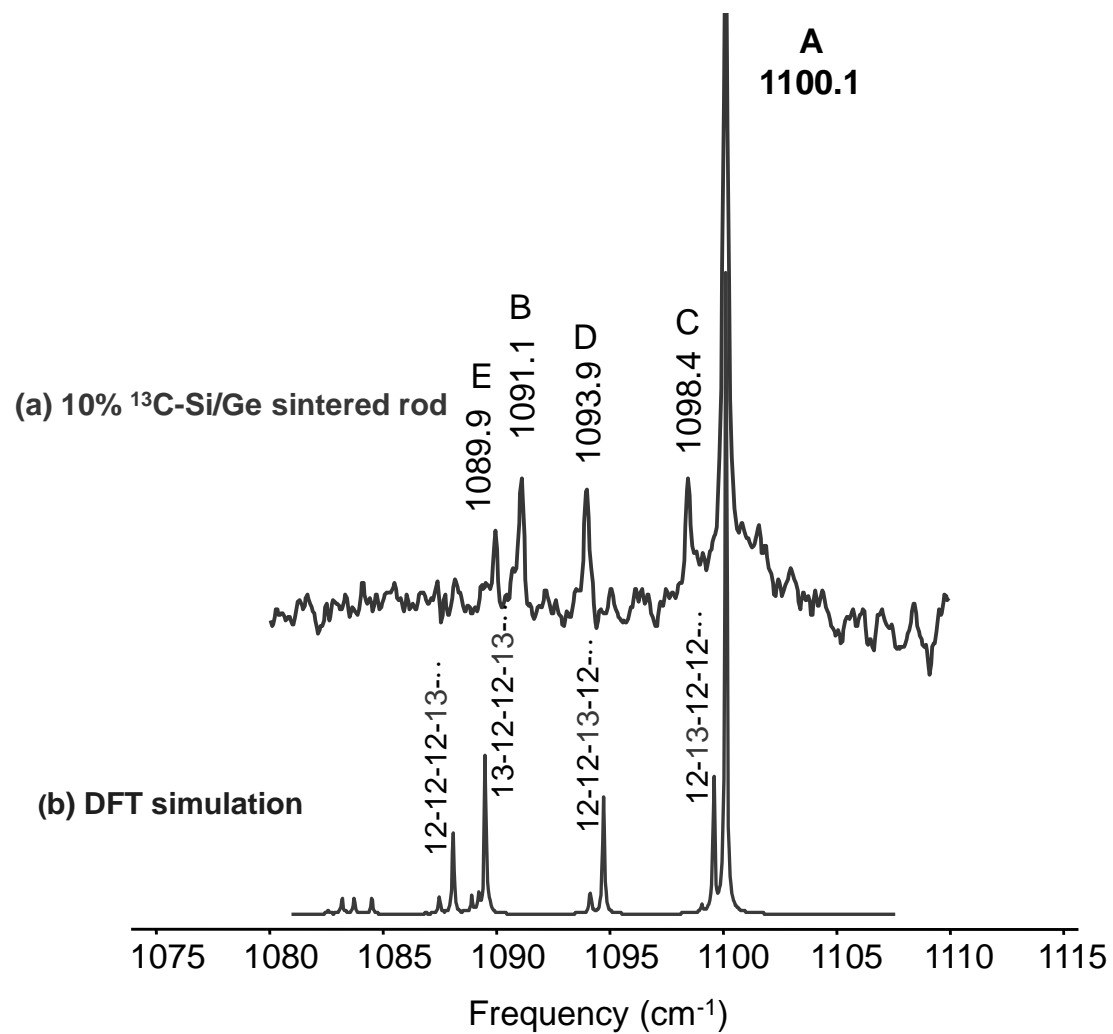
Figure 7.3 (a) FTIR spectra produced by the ablation of sintered silicon/germanium-carbon rod, the carbon powder used had 10% [13]C enrichment. (b) DFT simulation with B3LYP/cc-pVDZ level of theory for the $\nu_6(\sigma_u)$ fundamental of linear C_7

Table 7.2 Comparison of observed and predicted harmonic DFT (B3LYP/cc-pVDZ) frequencies for single ^{13}C-substituted isotopomers of the v_6 mode of linear C_7

Isotopomers	Observed (cm^{-1})	B3LYP/cc-pVDZ harmonic	Scaled[a]	Difference v_{obs} - v_{scaled}
12-12-12-12-12-12…(A)	1100.1	1118.8	1100.1	…
13-12-12-12-12-12... (B)	1091.1	1106.6	1089.5	1.6
12-13-12-12-12-12... (C)	1098.4	1118.3	1099.6	-1.2
12-12-13-12-12-12... (D)	1093.9	1113.3	1094.7	-0.8
12-12-12-13-12-12... (E)	1089.9	1108.0	1088.1	1.8

[a] scaling factor 1100.1/1118.8=0.983285

CHAPTER VIII

INTENSITY CALCULATIONS

8.1   Introduction

The calculation of the molecular dipole-moment derivatives, necessary for predicting the infrared intensities has been a research area of interest.[135] Many models have been developed for the calculation of the molecular dipole-moment derivatives.[136]

In earlier work, presented in ref.137, expressions were derived for the intensities of fundamentals, overtones, binary combination and difference bands as explicit functions of the temperature and force constants and dipole-moment derivatives. Some of these expressions were tested against experimental data for N_2O and CO_2 for the binary combination and different bands in ref. 138. The objective of this work was to test the expressions not to compute the dipole-moment derivatives from *ab initio* calculations. Developing models for computing the dipole-moment derivatives analytically has been the focus of more recent research work; to my knowledge there is no work putting recent and earlier works together.

This work presents the calculation of the second derivatives of the dipole-moment by numerical differentiation of the first derivatives which are computed analytically in the *Gaussian 03* suites of programs[2] which utilizes a method similar to the one presented in ref. 135. The levels of theory used are a density functional theory method, the B3LYP[51,52,53] functional, a Moller-Posset second order many body perturbation method (MP2), and the Coupled Cluster method (CCSD). These results are compared with available experimental data[139] for CO_2.

8.2   The Physics of the Infrared Absorption

The absorption of quanta by a molecule can be described with time-dependent perturbation theory. The perturbation is the electric dipole Hamiltonian,[140] where an electric plane wave is used for the incident radiation and $\mathbf{\mu}$ is the molecular dipole-moment, see Eq. 8.1.

$$W(t) = -\mathbf{\mu} \cdot \mathbf{\varepsilon_o} e^{-i\omega t} \qquad \text{Eq. 8.1}$$

Then, the transition probability in the first order approximation between vibrational states $|\,i\,\rangle$ and $|\,f\,\rangle$ is

$$P_{i \to f}(t) = \tfrac{1}{\hbar^2} \left| \langle f \left| \mathbf{\mu} \right| i \rangle \right|^2 \varepsilon_o^2 \, \mathrm{sinc}\left(\tfrac{1}{2} \omega_{fi} t \right)$$
$$\text{where} \;\; \omega_{fi} = \frac{E_f - E_i}{\hbar} \qquad \text{Eq. 8.2}$$

The infrared intensity can be considered as the average of the number of transitions per unit time multiplied by the energy of the incident quanta

$$I_{\omega_{fi}}(\omega) = \hbar \omega \times \lim_{t \to \infty} \frac{P_{i \to f}(t)}{t} = \frac{\omega}{\hbar} \left| \langle f \left| \mathbf{\mu} \right| i \rangle \right|^2 \varepsilon_o^2 \, \delta(\omega - \omega_{fi}) \qquad \text{Eq. 8.3}$$

Equation 8.3 shows that the resonance effect, the frequency of the quanta absorbed, is very close to the vibrational states transition frequency ω_{fi}. In addition, the molecular dipole's matrix element will determine if the particular transition is allowed or not, and how intense it is relative to other transitions. Eq. 8.3 could be multiplied could by the appropriate Boltzman factor to account for temperature dependence, this factor is dominant for the difference bands, see Table 8.3

8.2   Calculation of the Intensity of Fundamentals and Simultaneous Transitions

In order to compute the infrared intensity of vibrational states transitions it is necessary to find the molecular dipole's matrix elements with the involved states. Since the molecular dipole

is a function of the nuclear coordinates, hence also the normal modes coordinates, it can be Taylor expanded around the equilibrium position in the normal mode coordinates, see Eq. 8.4. Because the normal modes coordinates can be expressed in terms of the ladder operators ($Q_t \sim a_t^\dagger + a_t$), the desired matrix elements of the dipole-moment, hence the intensities can be found. This work is going to be restricted to fundamentals transitions: $|0\rangle \to |1_i\rangle$, first overtones ($i=j$) and combination and difference bands transitions: $|0\rangle \to |1_i, 1_j\rangle$, $|1_i\rangle \to |1_j\rangle$,.

$$\boldsymbol{\mu} = \boldsymbol{\mu_o} + \sum_i \boldsymbol{\alpha_i} Q_i + \tfrac{1}{2} \sum_{i,j} \boldsymbol{\beta_{ij}} Q_i Q_j + \tfrac{1}{6} \sum_{i,j,k} \boldsymbol{\gamma_{ijk}} Q_i Q_j Q_k + O(h^4)$$

$$\boldsymbol{\alpha_i} = \left. \frac{\partial \boldsymbol{\mu}}{\partial Q_i} \right|_0, \boldsymbol{\beta_{ij}} = \left. \frac{\partial^2 \boldsymbol{\mu}}{\partial Q_i \partial Q_j} \right|_0, \text{ and } \boldsymbol{\gamma_{ijk}} = \left. \frac{\partial^3 \boldsymbol{\mu}}{\partial Q_i \partial Q_j \partial Q_k} \right|_0$$

Eq. 8.4

where the Q_t are linear combination of the cartesian nuclei coordinates.

For the fundamentals transitions, the even terms in the matrix elements of the dipole's Taylor expansion are zero since the integration of the matrix element involves an odd function. The first dipole derivative term is the first approximation for the fundamental intensity and has an accuracy of $O(h^3)$ in the dipole-moment expansion if the mechanical anharmonicity is ignored. Using this term, the resulting intensity doesn't depend on the frequencies and an appropriate unit could be the square of the dipole first derivative in atomic units. All calculated fundamental intensities presented in this work are computed only using the first derivatives of the molecular dipole. The next correction to the fundamental using the cubic term of the dipole expansion was derived; see Eq. 8.5. Now the intensity depends on the dipole cubic derivatives $\boldsymbol{\gamma}$ and the frequencies. Another improvement to the calculation of the fundamentals intensity is the mechanical anharmonicity, see ref.137.

$$\langle 1_i | \mu | 0 \rangle = \sqrt{\frac{\hbar}{2\omega_i}} \left(\boldsymbol{\alpha}_i + \tfrac{1}{4} \sum_j \boldsymbol{\gamma}_{ijj} \frac{\hbar}{\omega_j} \right) + O(h^5)$$

$$I_{\omega_i} = \boldsymbol{\alpha}_i^2 \left(1 + \tfrac{1}{4} \sum_j \frac{\boldsymbol{\gamma}_{ijj}}{\boldsymbol{\alpha}_i} \frac{\hbar}{\omega_j} \right)^2$$

Eq. 8.5

In the case of the first overtones ($i = j$) or combination or difference bands ($i \neq j$) transitions, the matrix elements of the odd terms of the Taylor's expansion are zero. The dipole second derivatives term is the first approximation for the intensities of these binary transitions[141] and is exact up to $O(h^4)$, see Eq. 4.6.

$$I_{\omega_i \pm \omega_j} = \frac{\hbar(\omega_i \pm \omega_j)}{2\omega_i \omega_j} \boldsymbol{\beta}_{ij}^2 + O(h^4)$$

Eq. 8.6

Notice that when the quadratic or cubic terms of the dipole expansion are considered, the intensity depends on the frequencies, see Eq. 4.5 and 4.6. In those expressions, there is a factor of the Plank's constant divided by the infrared frequency which have order of magnitude:

$$\frac{\hbar}{\omega_i} = \frac{10^{-34} Kg\, m^2 s^{-1}}{\sim 10^{13} s^{-1}} \sim \frac{10^{-34} 10^{27} amu\, 10^{20} \overset{\circ}{A}^2}{10^{13}} \sim 1\, a.m.u\, \overset{\circ}{A}^2$$

The value of this term might not be considerable small, and the higher derivatives of the molecular dipole are not necessarily smaller than the lower ones. Thus the intensities of combination bands are not significantly smaller than the fundamental counterparts; these intensities could be at the orders of weak stretching modes or strong bending modes. Coming across this fact motivated me to do a series of experiments trying to identify novel combination bands of carbon clusters, see Chapter VII.

8.3   Computation of the Infrared Intensities of the Binary Transitions of CO_2

The combination bands intensities are not computed in quantum chemistry suite of programs. In order to compute them it is necessary to have the second derivatives of the molecular dipole in the normal modes coordinates. This work presents the computation of the second derivatives of the molecular dipole for CO_2 by the numerical differentiation of the cartesian first derivatives which are provided by *Gaussian 03* suite of programs. The numerical differentiation was carried out using the four point derivative formula, Eq. 8.7. The value of the step-size h selected was such that the molecular energy changed by ~1 mHartrees from the optimized geometry.[142] If the molecule is highly symmetric or contain few atoms the task of computing the first derivatives for each step-size is not very laborious. It is necessary to calculate the first derivatives, $\boldsymbol{\alpha}$, for each of the few non-equivalent nuclei coordinates, $\mathbf{x}$; for CO_2 only for one terminal oxygen atom and the carbon atom.

$$\boldsymbol{\beta}_{ij} = \frac{8\left[\boldsymbol{\alpha}_j(x_i+h)-\boldsymbol{\alpha}_j(x_i-h)\right]-\left[\boldsymbol{\alpha}_j(x_i+2h)-\boldsymbol{\alpha}_j(x_i-2h)\right]}{12h}+O(h^4) \qquad \text{Eq. 8.7}^{\ddagger}$$

A code was written to import the first dipole's derivatives from the *Gaussian 03* output files, compute the second dipole-moment's cartesian derivatives and transform them to normal modes coordinates using the transformation matrix of ref. 143. Finally, the intensities were predicted using Eq. 8.6. The second derivatives of the molecular dipole of CO_2 are presented in Table 8.1, the intensities are presented in Table 8.2, and the comparison with experimental data is shown in Table 8.3.

[‡] I am abusing notation in this equation, now the *i* and *j* indexes run over the cartesian nuclei coordinates. The second derivatives are the cartesian derivatives which are later transformed to the normal modes coordinates.

Table 8.1   First derivatives of the molecular dipole-moment for CO_2 computed analytically by Gaussian 03 using three levels of theory: B3LYP, MP2, and CCSD with cc-pVTZ basis set.

$\mu_{Q_i}^{(x,y,z)}$	Theoretical predictions (B3LYP/cc-pVTZ) (e a.m.u$^{-1/2}$)	Theoretical predictions (MP2/cc-pVTZ)	Theoretical predictions (CCSD/cc-pVTZ)
$\mu_{Q_3}^{x}$	-0.128	-0.158	0.176
$\mu_{Q_4}^{x}$	0.127	0	0.064
$\mu_{Q_3}^{y}$	0.127	0	0.064
$\mu_{Q_4}^{y}$	0.128	-0.158	-0.176
$\mu_{Q_2}^{z}$	-0.803	0.736	-0.851

Table 8.2   Second derivatives of the molecular dipole of CO_2 computed using Eq. 8.7 with the first derivatives computed by Gaussian using three levels of theory: B3LYP, MP2, and CCSD with cc-pVTZ basis set.

$\mu_{Q_iQ_j}^{(x,y,z)}$	Theoretical predictions (B3LYP/cc-pVTZ) (e Å^{-1} a.mu$^{-1/2}$)	Theoretical predictions (MP2/cc-pVTZ)	Theoretical predictions (CCSD/cc-pVTZ)
$\mu_{Q_2Q_3}^{x}$	-0.0135	0.0304	0.0178
$\mu_{Q_2Q_4}^{x}$	0.0135	0.0000	0.0065
$\mu_{Q_2Q_3}^{y}$	0.0135	0.0000	0.0065
$\mu_{Q_2Q_4}^{y}$	0.0135	0.0304	0.0178
$\mu_{Q_2Q_2}^{z}$	-0.0107	-0.0147	-0.0099
$\mu_{Q_1Q_1}^{z}$	-0.0489	-0.0540	-0.0449
$\mu_{Q_1Q_2}^{z}$	0.1641	-0.1787	0.1506

Table 8.3   Fundamentals intensities provided by Gaussian 03, and first overtones, and combination/difference bands intensities computed using the second derivatives of the dipole presented in Table 8.1 using Eq. 8.6. The equation used to estimate the error is Eq. 8.10, see Appendix section.

Intensities of fundamentals and combination/diff. bands	Theoretical predictions (B3LYP/ cc-pVTZ) (km/mol)	Theoretical predictions (MP2/ cc-pVTZ)	Theoretical predictions (CCSD/ cc-pVTZ)	Experiment Gas phase 300 K ref. 139[a]
$I\nu_2$	629.2	528.7	706.5	567.4
$I\nu_3$	31.9	24.3	34.2	53.9
$I_{2\nu_1}$	1.4 ± 0.4	1.7 ± 0.8	1.2 ± 0.5	…
$I_{2\nu_2}$	0.04 ± 0.06	0.07 ± 0.11	0.03 ± 0.06	…
$I_{2\nu_3}$	0	0	0	…
$I\nu_{1+}\nu_2$	12.3 ± 1.0	14.8 ± 2.0	9.9 ± 1.3	9.6 ± 0.4
$I\nu_{1+}\nu_3$	0	0	0	$(3.7\pm0.7)\times10^{-2}$
$I\nu_{2+}\nu_3$	0.3 ± 0.2	0.7 ± 0.6	0.27 ± 0.26	…
$I\nu_{2-}\nu_1{}^{b}$	$(4.6 \pm 0.4)\times10^{-3}$	$(7.2 \pm 1.0)\times10^{-3}$	$(3.9 \pm 0.4)\times10^{-3}$	$(6.6\pm0.3)\times10^{-3}$
$I\nu_{1-}\nu_3$	0	0	0	2.0 ± 0.4^{c}
$I\nu_{2-}\nu_3$	0.19 ± 0.12	0.4 ± 0.3	0.15 ± 0.15	…

[a] In Table II of ref. 139 the units for the intensity is $cm^{-2}atm^{-1}$, to converted to km/mol it was multiplied by 0.24616596 conversion factor obtained from the same reference

[b] Multiplied by the appropriate Boltzman factor $exp(hc\nu_1/kT)$. See text. A resonance occurred, the denominator $2\omega_1-\omega_2$ of Eq. 8.8 is small. The mechanical anharmonicity, which is not included in this work, also contributes

[c] A resonance occurred, the denominator $2\omega_3-\omega_1$ is considerable small, and $\mu_{Q_1Q_3}^{(x,y,z)}=0$, so the contribution to the intensity is only due to the mechanical anharmonicity, which is not included in this work.

8.4   Conclusions and remarks

A correction involving the third derivatives of the molecular dipole-moment for the fundamentals intensity was derived using the ladder operators to find matrix elements as shown in ref. 145. This correction appears in the expressions presented in ref. 137 which were derived using a contact transformation.

The second derivatives of the molecular dipole-moment of CO_2 were computed by numerical differentiation of the first derivatives which are calculated analytically in *Gaussian 03*. They allow predicting the intensities of the combination and difference bands. The v_1+v_2 intensity is predicted to be 9.9 km/mol using CCSD/cc-pVTZ level of theory. This is very close to the 9.6 km/mol experimental value, a 4% difference. On the other hand, the difference band v_1-v_2 intensity data differs 26% (CCSD) from the experimental value, see Table 8.3. This difference can be explained using the ref. 138 mechanical anharmonicity correction in which a term has a denominator of $2\omega_1$-ω_2 which might imply the same order as the second derivative of the dipole-moment term, see Eq. 8.8 below. When using[144] $k_{122} = -249.1 \, cm^{-1}$ and the fundamental frequencies ($v_1 = 1388 \, cm^{-1}$ and $v_2 = 2349 \, cm^{-1}$) the mechanical anharmonicity term for the difference band will be twice bigger than the corresponding combination band.[§] This might explain why the prediction for the combination band is good but not so good for the difference band, see Table 8.3. These terms were not included in the calculation of Table 8.3 because not having available the cubic mechanical anharmonicity and not having expressed Eq. 8.8 in the appropriate units. It will be interested to calculate the combination band intensities

---

[§] 249·2349/1388(2·2349-1388)=0.12;   249·2349/1388(2·2349+1388)=0.06

measured in Ar at 10 K for C_5, and C_6,[**] which are resented in Chapter VI adding the mechanical anharmonicity in the code I wrote and compared with the available measurements.

$$\left\langle 1_i \left| \boldsymbol{\mu}' \right| 1_j \right\rangle = \boldsymbol{\beta}'_{ij} - \frac{2k_{iij}\omega_i\boldsymbol{\alpha}'_i}{\omega_j(2\omega_i - \omega_j)} - \frac{2k_{ijj}\omega_j\boldsymbol{\alpha}'_j}{\omega_i(2\omega_j - \omega_i)}$$

$$\left\langle 1_i 1_j \left| \boldsymbol{\mu}' \right| 0 \right\rangle = \boldsymbol{\beta}'_{ij} + \frac{2k_{iij}\omega_i\boldsymbol{\alpha}'_i}{\omega_j(2\omega_i + \omega_j)} + \frac{2k_{iij}\omega_i\boldsymbol{\alpha}'_i}{\omega_j(2\omega_i + \omega_j)}$$

Eq. 8.8

Where the k_{ijk} are the cubic anharmonic terms; the primes indicates that the derivatives are respect to a dimensionless normal mode variables.[138]

Recently, great effort has been put in computing the dipole-moment and its first derivatives by analytical methods. In the 1970s expressions were derived which included mechanical and electrical anharmonicity[††] corrections to the fundamental and combination/difference bands. This work suggests that the second derivatives computed numerically from the first derivatives are precise enough to predict intensities of combination/difference bands with magnitudes of order >~5 km/mol. Therefore, computing the fundamentals intensities using the mechanical (up to the quartic term) and electrical (up to the second term) anharmonicity corrections presented in ref. 137 might clarify why the intensity predictions using only the first dipole-moment derivatives with pure harmonic states are so inexact.

[**] There are available two modes for C_5 and four modes for C_6, so the intensity ratios can be used for the comparison
[††] Earlier papers on this topic refer to electrical anharmonicity as the terms other than the first derivatives of the dipole-moment

8.5   Appendix

This section will briefly include part of the derivations of some expressions present in this chapter.   The matrix elements involved were obtained using the ladder operators as presented in ref. [145].

Equations 8.5 present the correction of the fundamental intensity using the cubic term of the dipole-moment Taylor's series expansion with pure harmonic states, the γ are the third derivatives of the dipole-moment in the normal modes coordinates and are mass weighted.

$$\langle 1_i | \mu | 0 \rangle = \boldsymbol{\alpha}_i \sqrt{\frac{\hbar}{2\omega_i}} + \langle 1_i | \tfrac{1}{6} \sum_{j,k,l} \boldsymbol{\gamma}_{jkl} Q_j Q_k Q_l | 0 \rangle$$

$$\langle 1_i | \tfrac{1}{6} \sum_{j,k,l} \boldsymbol{\gamma}_{jkl} Q_j Q_k Q_l | 0 \rangle = \tfrac{1}{6} \sum_{j,k,l} \boldsymbol{\gamma}_{jkl} \langle 0 | a_i Q_j Q_k Q_l | 0 \rangle$$

using $Q_s = \sqrt{\frac{\hbar}{2\omega_i}} (a_s^\dagger + a_s),\ a_s a_t^\dagger = \delta_{st} + a_t^\dagger a_s,\ \text{and}\ a_s |0\rangle = 0$

$$\langle 0 | a_i Q_j Q_k Q_l | 0 \rangle = \langle 0 | a_i (a_j^\dagger + a_j)(a_k^\dagger + a_k)(a_l^\dagger + a_l) | 0 \rangle = \delta_{ij}\delta_{kl} + \delta_{il}\delta_{kj} + \delta_{ik}\delta_{jl}$$

$$\langle 1_i | \mu | 0 \rangle = \boldsymbol{\alpha}_i \sqrt{\frac{\hbar}{2\omega_i}} + \langle 1_i | \tfrac{1}{6} \sum_{j,k,l} \boldsymbol{\gamma}_{jkl} Q_j Q_k Q_l | 0 \rangle = \boldsymbol{\alpha}_i \sqrt{\frac{\hbar}{2\omega_i}} + \tfrac{1}{6} \sum_j \left(\boldsymbol{\gamma}_{ijj} + \boldsymbol{\gamma}_{jij} + \boldsymbol{\gamma}_{jji} \right) \sqrt{\frac{\hbar^3}{8\omega_i\omega_j^2}}$$

$$= \sqrt{\frac{\hbar}{2\omega_i}} \left(\boldsymbol{\alpha}_i + \tfrac{1}{4} \sum_j \boldsymbol{\gamma}_{ijj} \frac{\hbar}{\omega_j} \right)$$

thus using Eq. 4.3 an appropiate unit for the intensity is $\left(\frac{\partial \mu}{\partial Q}\right)^2$ which are e^2

$$I_{\omega_i} = \left(\boldsymbol{\alpha}_i + \tfrac{1}{4} \sum_j \boldsymbol{\gamma}_{ijj} \frac{\hbar}{\omega_j} \right)^2 = \boldsymbol{\alpha}_i^2 \left(1 + \tfrac{1}{4} \sum_j \frac{\boldsymbol{\gamma}_{ijj}}{\boldsymbol{\alpha}_i} \frac{\hbar}{\omega_j} \right)^2$$

The vector matrix in bold mean three (x,y,z) independent sums, and the sums run over all fundamentals. If the fundamentals are in the units obtained upon the diagonalization the mass-weighted cartesian force constants matrix which are in *Hartrees Bohr^{-2} a.m.u$^{-1/2}$*, the above expression becomes:

$$I_{\omega_i} = \boldsymbol{\alpha}_i^2 \left(1 + \tfrac{1}{16\pi^2} \sum_j \frac{\boldsymbol{\gamma}_{ijj}}{\boldsymbol{\alpha}_i} \frac{1}{v_j} \right)^2 \qquad\qquad \text{Eq. 8.5}'$$

and the units are e^2, the conversion from e^2 to km/mol is 42.2561 from refs. 146 and 145.

For small molecules the sum doesn't contain many terms the correction might be $\sim \boldsymbol{\alpha}_i^2 / 70$ and the bending modes terms of the sum might be the higher contributions. Above correction was also obtained in ref. 137 using a contact transformation on the vibrational-Hamiltonian and dipole-moment operators which is constructed empirically. The above derivation is the straightforward and tedious calculation of the matrix elements the transformation of the dipole-moment derivatives in cartesian coordinates to the normal modes coordinates are carried out using the transformation matrix given in ref. 143. The work presentesd in ref. 137 also includes the mechanical anharmonicity correction (limited to the cubic term); now the second derivatives of the dipole-moment are present in the expression.

Similarly to obtain Eq. 8.6 the dipole moment matrix elements involved for the combination and difference bands are: $\langle 1_i 1_j | \mu | 0 \rangle, \langle 1_i | \mu | 1_j \rangle$. Then the first contribution is the second term of the dipole-moment expansion so these expressions

$$\langle 0 | a_i a_j (a_k^\dagger + a_k)(a_l^\dagger + a_l) | 0 \rangle = \delta_{ik}\delta_{jl} + \delta_{jk}\delta_{il}$$

$$\langle 0 | a_i (a_k^\dagger + a_k)(a_l^\dagger + a_l) a_j^\dagger | 0 \rangle = \delta_{ik}\delta_{jl} + \delta_{jk}\delta_{il} + \delta_{ij}\delta_{kl}$$

are needed. Equation 8.6 in atomic units becomes:

$$I_{\nu_i \pm \nu_j} = \frac{1}{8\pi^2} \frac{\nu_i \pm \nu_j}{\nu_i \nu_j} \boldsymbol{\beta}_{ij}^2 \qquad \text{Eq. 8.6}$$

Some third cartesian derivatives,($\frac{\partial^3 \boldsymbol{\mu}}{\partial^2 z_j \partial x_i}$), can be computed numerically by:

$$\gamma_{jji} = \frac{\left[\boldsymbol{\alpha}_i(x_j + 2h) + \boldsymbol{\alpha}_i(x_j - 2h) \right] - \left[\boldsymbol{\alpha}_i(x_j + h) + \boldsymbol{\alpha}_i(x_j - h) \right]}{3h^2} \qquad \text{Eq. 8.9}$$

The error due to the numerical differentiation can be estimated by:

$$\delta I_{v_i \pm v_j} = \frac{1}{8\pi^2} \frac{v_i \pm v_j}{v_i v_j} 2|\boldsymbol{\beta_{ij}}| \, \delta\boldsymbol{\beta_{ij}} = 2 I_{v_i \pm v_j} \frac{\delta\boldsymbol{\beta_{ij}}}{|\boldsymbol{\beta_{ij}}|}, \text{ and } \delta\boldsymbol{\beta_{ij}} = \sum \gamma_{ijk} \delta Q_k \approx \frac{\max[\gamma]}{m} h$$

$$\delta I_{v_i \pm v_j} \approx 2 I_{v_i \pm v_j} \frac{\max[\gamma]}{m|\boldsymbol{\beta}_{ij}|} h \qquad \text{Eq. 8.10}$$

$h = 0.01 \overset{\circ}{A}$ (step-side in the numerical differentiation)

$m = 16.0$ (oxygen's mass)

CHAPTER IX

CONCLUSIONS AND FUTURE WORK

9.1   GeC$_5$Ge

The linear GeC$_5$Ge germanium-carbon chain has been detected for the first time through the dual laser evaporation of graphite and germanium. FTIR isotopic shift measurements and DFT calculations at the B3LYP/cc-pVDZ level confirm the identification of the $v_4(\sigma_u)$ vibrational fundamental at 2158.0 cm^{-1}.

These results were presented to the 61st International Symposium on Molecular Spectroscopy, Ohio State University, Columbus, OH, June 2006 and were published in the Journal of Chemical Physics [J. Chem. Phys. **125**, 044504 (2006)]

9.2   GeC$_3$Ge

Two new vibrational fundamentals of linear GeC$_3$Ge, $v_4(\sigma_u) = 735.3$ cm^{-1} and $v_6(\pi_u) = 580.1$ cm^{-1}, have been assigned based on the results ^{13}C and ^{70,72,73,74,76}Ge isotopic shift measurements and comparison with the predictions of DFT calculations at the B3LYP/cc-pVDZ level. This is apparently the first observation of germanium isotopic shifts in vibrational spectra.

These results were presented to the Physics and Chemistry of Matrix Isolated Species, Gordon Research Conference, Bates College, Lewiston, ME, July 2007.and were published in the Journal of Physical Chemistry A [J. Phys. Chem. A **2008**, 112 (43)]

9.3 GeC_3

Linear GeC_3 has been formed by the dual laser ablation of germanium and carbon rods and by single laser ablation of a sintered germanium-carbon rod, and trapped in Ar matrices. Two vibrational fundamentals of linear GeC_3, $v_1(\sigma) = 1903.9$ cm^{-1} and $v_2(\sigma) = 1279.6$ cm^{-1}, have been assigned based on the comparison of ^{13}C isotopic shift measurements and the predictions of DFT calculations at the B3LYP/cc-pVDZ level. Although the $v_1(\sigma) = 1903.9$ cm^{-1} mode lies in a congested region that makes its analysis more complicated, the $v_2(\sigma) = 1279.6$ cm^{-1} mode is in a region with no other absorptions making its assignment straightforward and presenting unambiguous experimental evidence that linear GeC_3 has been synthesized.

Evidence accumulated from previous studies indicates that the laser ablation technique favors the formation of linear structures and cyclic structures with transannular metal-carbon bond over cyclic structures with transannular C-C bond. In the present work there is no spectroscopic evidence of cyclic structures for GeC_3 with either the transannular Ge-C or C-C bond although at the coupled cluster level of theory they are both predicted to be ~7-9 kcal/mol lower in energy than the linear isomer. This result suggests a need for further theoretical studies of GeC_3 to see if the cyclic isomers are indeed more stable than the linear.

These results were presented to the 63rd International Symposium on Molecular Spectroscopy, Ohio State University, Columbus, OH, June 2008 and were published in the Journal of Chemical Physics [J. Chem. Phys. **130**, 194511 (2009)]

9.4   Observation of Novel Spectroscopy Data for Linear C_5, C_9, and C_7

New combination bands of carbon chains have been observed, $(v_1+v_4) = 3388.8$ cm^{-1} of linear C_5 and $(v_2+v_7) = 3471.8$ cm^{-1} of linear C_9. These assignments are based on very good agreement

between measured isotopic shifts and DFT predictions at the B3LYP/cc-VDZ level of theory and the correlation of the intensities of the combination bands with vibrational fundamentals of the same molecule Since the asymmetric stretching modes involved in these absorptions have been measured previously[110,119] it has been possible to assign the infrared inactive symmetric stretching modes, the $v_1(\sigma_g)$ mode of linear C_5 at 1942 cm^{-1} and the $v_2(\sigma_g)$ mode of linear C_9 at 1870 cm^{-1}. The close agreement of the measured $v_1(\sigma_g)$ fundamental of linear C_5 and $v_2(\sigma_g)$ of linear C_9 and the frequencies predicted from the B3LYP anharmonic calculation gives further support to the identifications of the fundamentals and combination bands.

The $v_6(\sigma_u)$ weakest asymmetric stretching mode of linear C_7 has been detected for the first time and has been assigned at 1100.1 cm^{-1} in solid Ar. The assignment is supported by the intensity correlation of this mode with the previously observed $v_4(\sigma_u)$ and $v_5(\sigma_u)$ modes and the good agreement between the observed and simulated isotopic shifts pattern. The isotopic shifts were observed with sintered rods doped with silicon or germanium, which allowed them to resist high laser powers for long periods of times, allowing the observation of the very weak isotopomer bands necessary for this assignment

These results were presented to the Physics and Chemistry of Matrix Isolated Species, Gordon Research Conference, Magdalen College, Oxford, July 2009.and they are going to be submitted to the Journal of Physical Chemistry A

9.5   Intensity Calculations

The work presented in Chapter VIII suggests that the second derivatives computed numerically from the first derivatives are precise enough to predict intensities of combination/difference bands with magnitudes of order >~5 km/mol. Therefore, computing the

fundamentals intensities using the mechanical (up to the quartic term) and electrical (up to the second term) anharmonicity corrections presented in ref. 137 might clarify why the intensity predictions using only the first dipole-moment derivatives with pure harmonic states are so inexact.

Table II of ref. 139 includes measurements of combination/difference bands for many molecules: CO_2, H_2O, N_2O, O_3, SO_2, and NH_3, which provide vast experimental data to compare with the calculations presented in Chapter VIII. If the results are good, they indicate that the inaccuracy of intensity calculations is the exclusion of mechanical and electrical anharmonicity terms rather than the *ab initio* models for computing the first derivatives analytically. To my knowledge, there is not work on calculating the intensities of fundamental and combination/difference bands including these terms.

9.6   Incomplete work on linear GeC_3Si, a method for producing molecules with three elements XC_3Y

Linear GeC_3Si was first synthesized by the laser evaporation of sintered germanium-silicon-carbon rods.[7]   The $v_1(\sigma)$ fundamental was assigned at 1939.0 cm^{-1}. Theoretical calculations predict that the $v_3(\sigma)$ vibration is at 832.2 cm^{-1} with an intensity of ~200 km/mol, see Table 9.1. Effort was put into experimental techniques to try to increase the yield of the molecule in order to observe this fundamental. This was partially achieved: the mode was observed with pure carbon but not with rods with ^{13}C enrichment. Figure 9.1 shows a survey spectrum of the products of the laser evaporation of germanium-carbon-silicon rods (10%Ge/10Si/80%C atomic percentage using Eq. 2.2 of Chapter II). The most prominent species produced in these types of experiments are GeC_3Ge, GeC_3Si and SiC_3Si. Figure 9.2

shows the same experiment in the 700-900 cm^{-1} region, where the $v_4(\sigma_u)$ mode of GeC$_3$Ge is at 735.3 cm^{-1} discussed in detail in Chapter IV and the only the $v_4(\sigma_u)$ mode of SiC$_3$Si at 898.8 cm^{-1} are present. Thus, is tempting to suppose that the absorption at 824.7 cm^{-1}, which is the only remaining feature in this region, is the $v_3(\sigma)$ mode of GeC$_3$Si. The theoretical calculations of the fundamentals of GeC$_3$Si indicate that the germanium and silicon atoms participate in this vibration, and thus it is expected to have an envelope of five peaks due to the germanium natural isotopes: ^{70}Ge (21.23%), ^{72}Ge(27.66%), ^{73}Ge (7.73%), ^{74}Ge (35.94%),and ^{76}Ge (7.44%). This feature was discussed in detail for the case of two germanium atoms in Chapter IV related to $v_4(\sigma_u)$ mode of GeC$_3$Ge at 735.3 cm^{-1}. A closer look around the absorption at 824.7 cm^{-1}(see Fig. 9.3) shows the typical envelope of one germanium atom participating in the vibration. Table 9.2 shows a comparison between the observed and calculated germanium isotopic shifts, both resemble the same pattern.

This work did not observe the ^{13}C isotopic shifts of this mode in order to unambiguously assign the 824.7 cm^{-1} absorption to GeC$_3$Si, but provides a technique on how to produce three element molecules (XC$_3$Y). The best yield of GeC$_3$Si was produced by one sintered rod with the three elements. This technique could be repeated using transition metals or a combination of transition metals and semiconductor elements.

Table 9.1   DFT-B3LYP/cc-pVDZ predicted vibrational frequencies and band intensities for linear GeC_3Si.

Vibrational mode	Frequency (cm^{-1})	Infrared intensity (km/mol)
$v_1(\sigma)$	2040.4	2280.3
$v_2(\sigma)$	1549.9	0.7
$v_3(\sigma)$	832.2	208.9
$v_4(\sigma)$	362.9	3.4
$v_5(\pi)$	578.2	15.9
$v_6(\pi)$	198.9	0.0
$v_7(\pi)$	76.1	3.4

Figure 9.1   FTIR spectra produced by the laser ablation of a sintered germanium/carbon/silicon rod with atomic ratio ~10%/10%/80% respectively
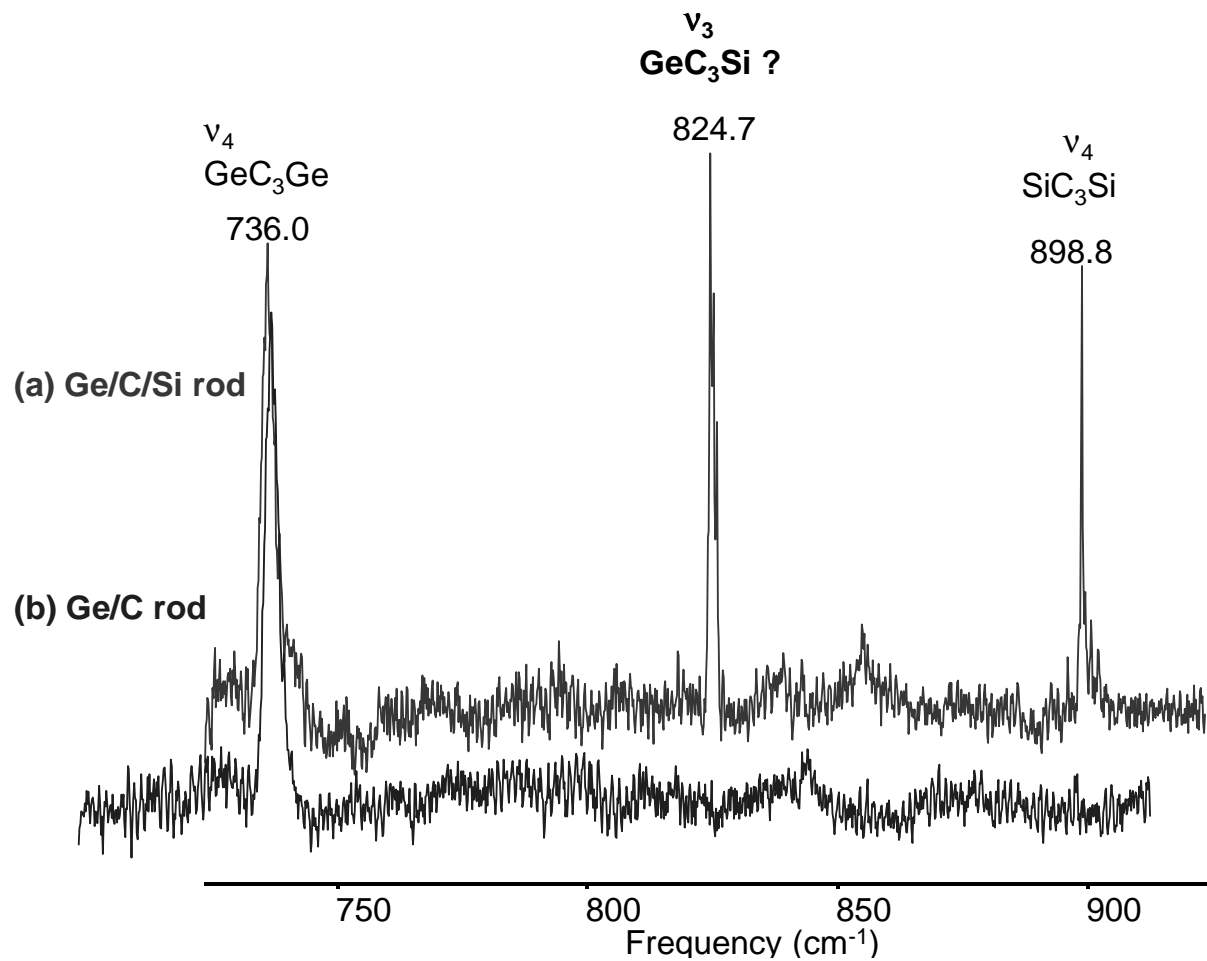
Figure 9.2   FTIR spectra produced by the laser ablation of a sintered (a) germanium/carbon/silicon rod with atomic ratio ~10%/10%/80% respectively and (b) a sintered germanium/carbon rod with atomic ratio ~20%/80% respectively
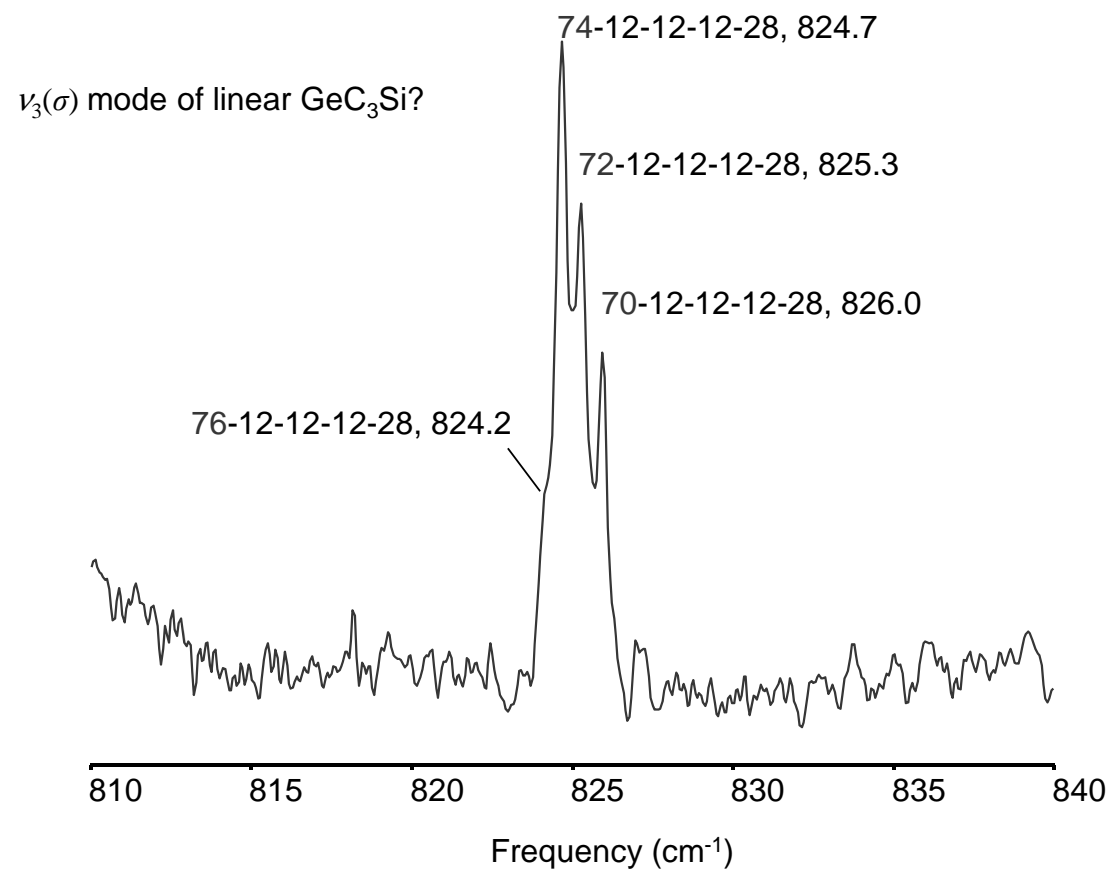
Figure 9.3   Closer look around the 824.7 cm^{-1} absroption showing the participation of one germanium atom in the vibration. Table 9.1 shows the comparison of these shifts with the DFT simulation.

Table 9.2 Comparison of observed and predicted harmonic DFT (B3LYP/cc-pVDZ) frequencies for [70,72,73,74,76]Ge natural isotopomers of the v_3 mode of linear GeC$_3$Si.

Isotopomer Ge-C-C-C-Si		Observed (cm^{-1})	Calculation B3LYP/cc-pVDZ	Scaled[a]	Difference Obs.-Scaled
74-12-12-12-28	(A)	824.7	832.2	824.7	…
72-12-12-12-28	(B)	825.3	832.8	825.3	0
70-12-12-12-28	(C)	826.0	833.6	826.1	-0.1
73-12-12-12-28	(D)	…	832.5	…	…
76-12-12-12-28	(E)	824.2	831.5	824.0	0.2

[a] calculations scaled by 824.7/832.2

REFERENCES

[1] E. S. Imes, *Astrophysical J.,* **50**, 251-256 (1919)

[2] Gaussian 03, Revision A.1, M. J. Frisch, G. W. Trucks, H. B. Schlegel, G. E. Scuseria, M. A. Robb, J. R. Cheeseman, J. A. Montgomery, Jr., T. Vreven, K. N. Kudin, J. C. Burant, J. M. Millam, S. S. Iyengar, J. Tomasi, V. Barone, B. Mennucci, M. Cossi, G. Scalmani, N. Rega, G. A. Petersson, H. Nakatsuji, M. Hada, M. Ehara, K. Toyota, R. Fukuda, J. Hasegawa, M. Ishida, T. Nakajima, Y. Honda, O. Kitao, H. Nakai, M. Klene, X. Li, J. E. Knox, H. P. Hratchian, J. B. Cross, V. Bakken, C. Adamo, J. Jaramillo, R. Gomperts, R. E. Stratmann, O. Yazyev, A. J. Austin, R. Cammi, C. Pomelli, J. W. Ochterski, P. Y. Ayala, K. Morokuma, G. A. Voth, P. Salvador, J. J. Dannenberg, V. G. Zakrzewski, S. Dapprich, A. D. Daniels, M. C. Strain, O. Farkas, D. K. Malick, A. D. Rabuck, K. Raghavachari, J. B. Foresman, J. V. Ortiz, Q. Cui, A. G. Baboul, S. Clifford, J. Cioslowski, B. B. Stefanov, G. Liu, A. Liashenko, P. Piskorz, I. Komaromi, R. L. Martin, D. J. Fox, T. Keith, M. A. Al-Laham, C. Y. Peng, A. Nanayakkara, M. Challacombe, P. M. W. Gill, B. Johnson, W. Chen, M. W. Wong, C. Gonzalez, and J. A. Pople, Gaussian, Inc., Wallingford CT, 2004.

[3] C.M.L. Rittby Simulated Spectra for Ge_n (n=3-5) clusters, unpublished

[4] X. D. Ding, S. L. Wang, W. R. M. Graham, and C. M. L. Rittby, J. Chem. Phys. **110**, 11214 (1999), and references cited therein.

[5] D. L. Robbins, C. M. L Rittby, and W.R. M. Graham, J. Chem. Phys. **114**, 3570 (2001)

[6] D. L. Robbins, C. M. L Rittby, and W.R. M. Graham, J. Chem. Phys. **120**, 4664 (2004)

[7] D. L. Robbins, C. M. L Rittby, and W.R. M. Graham, J. Chem. Phys. **117**, 3811 (2002)

[8] J. D. Presilla-Marquez and W. R. M Graham, J. Chem. Phys. **100**, 181 (1994); C. M. L. Rittby, *ibid.*, **100**, 175 (1994)

[9] J. D. Presilla-Marquez, S. C. Gay, C. M. L. Rittby, and W. R. M. Graham, J. Chem. Phys. **102**, 6354 (1995)

[10] J. D. Presilla-Marquez, C. M. L. Rittby, and W. R. M. Graham, J. Chem. Phys. **104**, 2818(1996)

[11] X. D. Ding, S. L. Wang, C. M. L. Rittby, and W. R. M. Graham, J. Chem. Phys. **104**, 3712 (2000)

[12] R. W. Schmude, Jr., K. A. Gingerich, J. E. Kingcade, J. Chem. Phys. **99**,15294 (1995)

[13] R A. Shepherd and W. R. M. Graham, J. Chem. Phys. **82**, 4788 (1985); *ibid.*, **88**, 3399 (1988)

[14] L. Sari, K.A. Peterson, Y. Yamaguchi, H. F. Schaefer III, J. Chem. Phys. **117**, 10008 (2002)

[15] J. Drowart, R. P. Burns, g. De Maria, and M. G. Inghram, J. Chem. Phys. **31**, 1299(1959)

[16] G.V. Chertihin, L. Andrews, and P.R.Taylor, J. Am. Chem. Soc., **116**, 3513(1994)

[17] W. Lauterborn and T. Kurz, *Coherent Optics*, pgs 36-70, Springer(2003)

[18] D.W. Ball, Zakya H. Fafafi, *et al., A Bibliography of Matrix Isolation Spectroscopy, 1954-1985,* Rice University Press, Huston(1988)

[19] M. Murdock, private communication (2004-2006).

[20] G. Katchinska, private communication (2004-2006).

[21] S. Wang, *Spectroscopy Study of Novel Silicon and Carbon Clusters Formed by the Laser Ablation Technique,* Disertation (1997)

[22] P. Withey and W.R.M. Graham, J. Chem. Phys. **95**, 820 (1991)

[23] J. Karolczak, W.W. Harper, R.S. Grev, and D. J. Clouthier, J. Chem. Phys. **103**, 2840 (1995)

[24] O. Leifeld, R. Hartmann, E. Miller, E. Kaxiras, K. Kern, and D. Grützmacher, Nano. **10,** 122(1999)

[25] O. Leifeld, R. Hartmann, E. Miller, E. Kaxiras, K. Kern, and D. Grützmacher, Appl. Phys. Lett.**74,** 994 (1999)

[26] R. Hartmann, U. Gennser, H. Sigg, K. Ensslin, and D. Grützmacher, Appl. Phys. Lett. **73,**1257(1998)

[27] X.D. Ding, S.L. Wang, W.R.M. Graham, and C.M.L. Rittby, J. Chem, Phys. **110**, 11214 (1999), and references cited therein

[28] D.L. Robbins, C.M.L. Rittby, and W.R.M. Graham, J. Chem. Phys. **114**, 3570 (2001)

[29] D.L. Robbins, C.M.L. Rittby, and W.R.M. Graham, J. Chem. Phys. **120**, 4664 (2004)

[30] D.L. Robbins, C.M.L. Rittby, and W.R.M. Graham, J. Chem. Phys. **117**, 3811 (2002)

[31] J.D. Presilla-Márquez and W.R.M. Graham, J. Chem. Phys. **100**, 181 (1994); C.M.L. Rittby, *ibid.*, **100**, 175 (1994)

[32] J.D. Presilla-Márquez, S.C. Gay, C.M.L. Rittby, and W.R.M. Graham, J. Chem. Phys. **102**, 6354 (1995)

[33] J.D. Presilla-Márquez, C.M.L. Rittby, and W.R.M. Graham, J. Chem. Phys. **104**, 2818 (1996)

[34] X.D. Ding, S.L. Wang, C.M.L. Rittby, and W.R.M. Graham, J. Phys. Chem. A **104**, 3712 (2000)

[35] R.E. Kinzer, C.M.L. Rittby, and W.R.M. Graham, J. Chem. Phys., *submitted* (2006)

[36] S.L. Wang, C.M.L. Rittby, and W.R.M. Graham, J. Chem. Phys. **107**, 6032 (1997)

[37] S.L. Wang, C.M.L. Rittby, and W.R. M. Graham, J. Chem. Phys. **107,** 7025 (1997); *ibid.*, **112**, 1457 (2000)

[38] P.A. Withey and W.R.M. Graham, J. Chem. Phys. **96**, 4068 (1992)

[39] J.D. Presilla-Márquez, C.M.L. Rittby, and W.R.M. Graham, J. Chem. Phys. **106**, 8367 (1997)

[40] L.N. Shen, T.J. Doyle, and W.R.M. Graham, J. Phys. Chem. **93**, 1597 (1990)

[41] X.D. Ding, S.L. Wang, C.M.L. Rittby, and W.R.M. Graham, J. Chem. Phys. **112**, 5113 (2000)

[42] R.H. Kranze and W.R.M. Graham, J. Chem. Phys. **96**, 2517 (1992)

[43] R.H. Kranze, C.M.L. Rittby, and W.R.M. Graham, J. Chem. Phys. **105**, 5313 (1996)

[44] X.D. Ding, S.L. Wang, C.M.L. Rittby, W.R.M. Graham, *J. Chem. Phys.* **110**, 11214 (1999) and references cited therein

[45] X.D. Ding, S.L. Wang, C.M.L. Rittby, and W.R.M. Graham, *J. Phys. Chem. A.* **104**, 3712 (2000), and references cited therein

[46] D.L. Robbins, C.M.L. Rittby, W.R.M. Graham, *J. Chem. Phys.*, **120**, 4664 (2004)

[47] D.L. Robbins, C.M.L. Rittby, W.R.M. Graham, *J. Chem. Phys.*, **117**, 3811 (2002)

[48] J.D. Presilla-Márquez, W.R.M. Graham, *J. Chem. Phys.*, **100**, 181 (1994); Rittby, C.M.L. *ibid.*, **100**, 175(1994)

[49] J.D. Presilla-Márquez, S.C. Gay, C.M.L. Rittby, W.R.M. Graham, *J. Chem. Phys.* **102**, 6354(1995)

[50] J. D. Presilla-Márquez, C. M. L. Rittby, W. R. M. Graham, *J. Chem. Phys.* **104**, 2818(1996)

[51] A.D. Becke, Phys. Rev. A. **38**, 3098 (1988)

[52] J. P. Perdew, Phys. Rev. B **33**, 8822 (1986)

[53] C. Lee, W. Yang, and R.G. Parr, Phys. Rev. B **37**, 785 (1988)

[54] C.M.L. Rittby (unpublished calculations for carbon chains -C_n , n=3 to 21)

[55] X.D. Ding, S.L. Wang, C.M.L. Rittby, and W.R.M. Graham, J. Chem. Phys. **112**, 5113 (1999), and references cited therein.

[56] P. Wielgus, S. Roszak, D. Majumdar, J. Leszczynski, *J. Chem. Phys.* **2005,** *123*, 234309.

[57] P.A. Withey, L.N Shen, and W.R.M. Graham, J. Chem. Phys. **95**, 2 (1991)

[58] P. Thaddeus, S. E. Cummins, and R. A. Linke, Astrophys. J. **283**, L45 (1984)

[59] A. J. Apponi, M. C. McCarthy, C. A. Gottlieb, and P. Thaddeus, Astrophys. J. **516,** L103 (1999)

[60] W. R. M. Graham, K. I. Dismuke, and W. Weltner, Jr., Astrophys. J. **204**, 301 (1976)

[61] L. N. Shen and W. R. M. Graham, J. Chem. Phys. **91**, 5115 (1989)

[62] P. A. Withey, L. N. Shen, and W. R. M. Graham, J. Chem. Phys. **95**, 820 (1991)

[63] J. R. Heath and R.J. Saykally, J. Chem. Phys. **94**, 3271 (1991)

[64] N. Moazzen-Ahmadi and J. J. Thong, Chem. Phys. Lett. 233, **471** (1995)

[65] D. E. Bernholdt, D. H. Magers, and R. J. Bartlett, J. Chem. Phys. **89,** 3612 (1988)

[66] J. D. Watts, J. Gauss, J. F. Stanton, and R. J. Bartlett, J. Chem. Phys. **97**, 8372 (1992)

[67] I. L. Alberts, R.S. Grev, and H.R. Shaefer III, J. Chem. Phys. **93**, 5046 (1990)

[68] M. C. McCarthy, A. J. Apponi, and P. Thaddeus, J. Chem. Phys. **110**, 10645, (1999)

[69] M. C. McCarthy, A. J. Apponi, and P. Thaddeus, J. Chem. Phys. **111**, 7175 (1999)

[70] M. Gomei, R. Kishi, A. Nakajima, S. Iwata, and K. Kaya, J. Chem. Phys. **107**, 10051 (1997)

[71] J. M. Rintelman and M. S. Gordon, J. Chem. Phys. **115**, 1795 (2001)

[72] K. W. Sattelmeyer, H. F. Schaefer III, and J. F. Stanton, J. Chem. Phys. **116**, 9151 (2002)

[73] J. M. Rintelman, M. S. Gordon, G. D. Fletcher, and J. Ivanic, J. Chem. Phys. 124, 034303 (2006)

[74] G. E. Davico, R. L. Schwartz, and W. C. Lineberger, J. Chem. Phys. **115**, 1789 (2001)

[75] P. Wielgus, S. Roszak, D. Majumdar, and J. Leszczynski, J. Chem. Phys. **123,** 234309 (2005)

[76] R. W. Schmude, Jr., K. A. Gingerich, and J. E. Kingcade, J. Phys. Chem. **99**,15294 (1995)

[77] D. L. Robbins, C. M. L. Rittby, and W. R. M. Graham, J. Chem. Phys. **114,** 3570 (2001)

[78] E. Gonzalez, C. M. L. Rittby, and W. R. M. Graham, J. Phys. Chem. A, **112**, 10831 (2008)

[79] E. Gonzalez, C. M. L. Rittby, and W. R. M. Graham, J. Chem. Phys. **125,** 044504 (2006)

[80] D. L. Robbins, K.-C. Chen, C. M. L. Rittby, and W. R. M. Graham, J. Chem. Phys. **120**, 4664 (2004)

[81] S. A. Bates, C. M. L. Rittby, and W. R. M. Graham, J. Chem. Phys. **125**, 074506 (2006)

[82] S. A. Bates, C. M. L. Rittby, and W. R. M. Graham, J. Chem. Phys. **127**, 064506 (2007)

[83] S. A. Bates, J. L. Rhodes C. M. L. Rittby, and W. R. M. Graham, J. Chem. Phys. **128**, 234301 (2008)

[84] R. E. Kinzer, Jr., C. M. L. Rittby, and W. R. M. Graham, J. Chem. Phys. **125**, 074513 (2006)

[85] R.E. Kinzer, Jr., C.M.L. Rittby, and W.R.M. Graham, J. Chem. Phys. **129**, 184309 (2008)

[86] R. E. Kranze and W. R. M. Graham, J. Chem. Phys. **98**, 71 (1993)

[87] S. L. Wang, C. M. L. Rittby, and W. R. M. Graham, J. Chem. Phys. **107,** 6032 (1997)

[88] J. Szczepanski, S. Ekern, C. Chapo, and M. Vala, Chem. Phys. **211,** 359 (1996)

[89] S. L. Wang, C. M. L. Rittby, and W. R. M. Graham, J. Chem. Phys. **107,** 7025 (1997)

[90] D. L. Robbins, C. M. L. Rittby, and W. R. M. Graham, J. Chem. Phys. **117**, 3811 (2002)

[91] R. H. Kranze and W. R. M. Graham, J. Chem. Phys. **98**, 71 (1993)

[92] J. Szczepanski, S. Ekern, M. Vala, J. Phys. Chem. A **101**, 1841(1997)

[93] R. H. Kranze, C. M. L. Rittby, and W. R. M. Graham, J. Chem. Phys. **105**, 5313 (1996)

[94] L. Zhang, J. Dong, and M. Zhou, J. Chem. Phys. **113**, 8700 (2000)

[95] R. H. Kranze, P. A. Withey, C. M. L. Rittby, and W. R. M. Graham, *J. Chem. Phys.* **103**, 6841 (1995)

[96] W. Weltner, Jr., D. McLeod, Jr., *J. Chem. Phys.*, **40**, 1305(1964)

[97] H.W. Kroto, J.R. Heath, S.C. O'Brien, R.F. Curl, R.E.Smalley, *Nature* (London), **318**, 162(1985)

[98] D.W. Arnold, S.E. Bradforth, T.N. Kitsopoulos, D.M. Neumark, *J. Chem. Phys.*, **95**, 8753(1991)

[99] T.N. Kitsopoulos, C.J. Chick, Y.Zhao, D.M. Neumark, *J. Chem. Phys.*, **95**,5479(1991)

[100] P.F. Bernath, K.H. Hinkle, J.J. Keady, *Science*, **244**, 562(**1989)**

[101] N. Moazzen-Ahmadi, A.R.W. McKellar, T. Amano, *Chem. Phys. Lett.*, **157**, 1(1989)

[102] J.R. Heath, A.L. Cooksy, M.H.W. Gruebele,C.A. Schmuttenmaer, R.J. Saykally, J., *Science*, **244**, 564(1989)

[103] N. Moazzen-Ahmadi, A.R.W. McKellar, T. Amano, *J. Chem. Phys.*, **91**, 2140(1989)

[104] Dismuke, W.R.M.Graham.K.I. W. Weltner, Jr., *Astrophys. J.*, **204**, 301(1976)

[105] A.M. Smith, J. Agreiter, M. Hartle, C. Engel, V.E.Bondybey, *Chem. Phys.*, **189**, 315(1994)

[106] S. Tam, M. Macler, M.E. Fajardo, *J. Chem. Phys.*, **106**, 8955(1997)

[107] K.R.Thompson, R.L DeKock, W. Weltner, W., Jr., *J. Am. Chem. Soc.*, **93**,4688(1971)

[108] M. Vala, T.M. Chandrasekhar, J. Szczepanski, R. Van Zee, W. Weltner, Jr., *J. Chem. Phys.*, **90**, 595(1989)

[109] M. Miki, T. Wakabayashi, T. Momose, T. Shida, *J. Phys. Chem.*, **100**,12135(1996)

[110] R.H. Kranze, W.R.M. Graham, *J. Chem. Phys.*, **96**, 2517(**1992)**

[111] S. Gakwaya, Z. Abusara, N. Moazzen-Ahmadi, *Chem. Phys. Lett.*, **398**, 564(2004)

[112] A. Van Orden, R.A. Provencal, F.N. Keutch, R.J. Saykally, *J. Chem. Phys.*, **105**, 6111(1996)

[113] P. Freivogel, M. Grutter, D. Forney, J.P. Maier, *Chem. Phys.*, **216**, 401(1997)

[114] J.C. Hayes, R.S. Sheridan, *J. Am. Chem. Soc.*, **112**, 5879(1990)

[115] A. Van Orden, H.J. Hwang, E.W. Kuo, R.J. Saykally, *J. Chem. Phys.*, **98**, 6678(1993)

[116] R. Casaes, R. Provencal, J. Paul, R.J. Saykally, *J. Chem. Phys.*, **116**, 6640(2002)

[117] M. Vala, T.M. Chandrasekhar, J. Szczepanski, R. Pellow, *High Temp. Sci.*, **27**, 19(1988)

[118] J. Szczepanski, M. Vala, J. Phys. Chem. **95**, 2792(1991)

[119] R.H. Kranze, P.A. Withey, C.M.L. Rittby, W.R.M. Graham, *J. Chem. Phys.* **103**, 6841(1995)

[120] J, Szczepanski, M.Vala, *J. Chem. Phys.* **1993**, 99, 7371

[121] F. Fuller, J. Szczepanski, M. Vala, *Chem. Phys. Lett.* **323**, 86(2000)

[122] J.L. Duncan, *Spectrochim. Acta*, **47A** ,1(1991**)**

[123] D. W. Arnold, S.E. Bradforth, T.N. Kitsopoulos, D.M. Neumark, *J. Chem. Phys.* **95**, 8753(1991)

[124] G. Garcia-Navarro, *An Investigation into the Limitations of the Harmonic Approximation in the Calculations of Vibrational Isotopic Shifts*, Dissertation(2008)

[125] F. Fuller, J. Szczepanski, M. Vala, *Chem. Phys. Lett*. **2000**, 323, 86.

[126] J. R. Heath, R. A. Sheeks, A.L. Cooksy, R. J. Saykally,. *Science*, **249**, 895 (1990)

[127] J. R. Heath, R. J. Saykally, *J. Chem. Phys.*, **94**, 1724 (1991)

[128] P. Neubauer-Guenther, T. F. Giesen, S. Schelemmer, k.M.T. Yamada, *J. Chem. Phys.,***127**, 014313 (2007)

[129] A. M. Smith, J. Agreiter, M. Hartle, C. Engel, V. E. Bondybey, *Chem. Phys.*, **189**, 315 (1994)

[130] S. Tam, M. Macler, M.E. Fajardo, . *Chem. Phys.,***105**, 5313 (1996)

[131] J. R. Heath, A. Van orden, E. Kuo, R. J. Saykally, *Phys Lett.*, **182**, 17 (1991)

[132] M. E. Jacox, *Vibrational and electronic energy levels of polyatomic transient molecules,* American Chemical Society, Washington DC, 464(1994)

[133] M. E. Jacox, *Vibrational and electronic energy levels of polyatomic transient molecules: supplement A, J. Phys. Chem. Ref. Data,* **27**, 115-393(1998)

[134] M. E. Jacox, *Vibrational and electronic energy levels of polyatomic transient molecules: supplement B, J. Phys. Chem. Ref. Data,* **32**, 1-141(2003)

[135] L. Roberto, A. Hiduke and R. E. Bruns, *J. Phys. Chem. A* **109**, 2680 (2005) and references therein

[136] These models are referenced in ref. 141

[137] S. Y. Yao and John Overend, *Spectrochimica Acta*, **32A**, 1059 (1976)

[138] K. G. Brown and W. B. Person, *J. Chem. Phys.* **65**, 2367 (1976)

[139] L. A. Pugh and K. N. Rao, *Molecular Spectroscopy: Modern Research Volume II,* Chapter IV, pg 165-2009 (1976)

[140] C. Cohen-Tannoudji and B. Frank Laloe, *Quantum* Mechanics, Volume II, pg 1306

[141] Y. Kakiuti, J. Chem. Phys. **25**, 777, (1956)

[142] R. Burcl, S. Carter, and N. C. Handy, *Phys.Chem.Chem.Phys.*, **6**, 340(2004)

[143] J.W. Ochterski, *Vibrational Analysis in Gaussian*, 1999, a retrieved from: http://www.gaussian.com/g_whitepap/vib/vib.pdf

[144] I. Susuki, J. Mol. Spectrosc. **25**, 479(1968)

[145] C.M.L. Rittby, *An Analysis of Isotopically Shifted Harmonic Frequencies,* unpublished

[146] A. Frisch, M. J. Frisch, and G. W. Trucks, *Gaussian 03* User's Reference , 2nd Edition

ABSTRACT

INFRARED SPECTROSCOPY AND THEORETICAL STUDIES OF GROUP
IV MOLECULES

by Eric Gonzalez
Department of Physics
Texas Christian University

Dissertation Advisor: Dr. W.R.M. Graham, Professor of Physics

This research involved the formation of novel molecules, and the first observation of infrared active modes and infrared active combination bands of already discovered molecules. The molecules were produced by the laser evaporation of germanium, germanium-carbon, and carbons rod previously sintered in a new built vacuum furnace. The infrared spectra were taken using Bomem FTIR spectrometer with an interface infrared optics toward the formation chamber. These molecules were theoretically simulated using commercial quantum chemistry suites of programs and homemade codes.

The linear GeC_5Ge germanium-carbon chain has been detected for the first time through the dual laser evaporation of graphite and germanium, the $v_4(\sigma_u)$ vibrational fundamental was observed at 2158.0 cm^{-1}.

Two new vibrational fundamentals of linear GeC_3Ge, $v_4(\sigma_u) = 735.3$ cm^{-1} and $v_6(\pi_u) = 580.1$ cm^{-1}, have been observed. This is apparently the first observation of germanium isotopic shifts in vibrational spectra

Linear GeC_3 has been formed by the dual laser ablation of germanium and carbon rods and by single laser ablation of a sintered germanium-carbon rod, and trapped in Ar matrices. Two

vibrational fundamentals of linear GeC_3, $v_1(\sigma) = 1903.9$ cm^{-1} and $v_2(\sigma) = 1279.6$ cm^{-1}, have been observed. In the present work there is no spectroscopic evidence of cyclic structures for GeC_3 with either the transannular Ge-C or C-C bond although at the coupled cluster level of theory they are both predicted to be ~7-9 kcal/mol lower in energy than the linear isomer. This result suggests a need for further theoretical studies of GeC_3 to see if the cyclic isomers are indeed more stable than the linear.

   New combination bands of carbon chains have been observed, $(v_1+v_4) = 3388.8$ cm^{-1} of linear C_5 and $(v_2+v_7) = 3471.8$ cm^{-1} of linear C_9. Since the asymmetric stretching1 modes involved in these absorptions have been measured previously it has been possible to assign the infrared inactive symmetric stretching modes, the $v_1(\sigma_g)$ mode of linear C_5 at 1942 cm^{-1} and the $v_2(\sigma_g)$ mode of linear C_9 at 1870 cm^{-1}. The $v_1(\sigma_g)$ mode of linear C_5 is the last undetected fundamental of this molecule.

        The $v_6(\sigma_u)$ weakest asymmetric stretching mode of linear C_7 has been detected for the first time and has been assigned at 1100.1 cm^{-1} in solid Ar.

        The calculation of the intensities of combination bands presented in this work suggests that the second derivatives computed numerically from the first derivatives are precise enough to predict intensities of combination/difference bands with magnitudes of order >~5 km/mol. Therefore, computing the fundamentals intensities using the mechanical (up to the quartic term) and electrical (up to the second term) anharmonicity corrections might clarify why the intensity predictions using only the first dipole-moment derivatives with pure harmonic states are so inexact. To my knowledge, the inexactness of the calculated fundamental intensities is attributed to the method used for the calculation of the first derivatives of the dipole-moment rather than including anharmonic terms.

VITA

ERIC GONZALEZ

PERSONAL

Born April 6th, 1975, Havana, Cuba
Son of Nilda Cecilia Estévez Rodríguez and Eloy Arnaldo González González
Other name used, Eric González Estévez
Naturalized US citizen (2005)
Married to Danely Gonzalez, one daughter Anna Elena Gonzalez

EDUCATION

Ph. D. (Physics) Texas Christian University, August 2009
M.S. (Physics) Texas Christian University, May 2007
B.S. (Physics) University of Havana, June 1998

Ph. D. Dissertation

Infrared Spectroscopy and Theoretical Studies of Group IV Molecules

This research involved the formation of novel molecules, and the first observation of infrared active modes and infrared active combination bands of already discovered molecules. The molecules were produced by the laser evaporation of germanium, germanium-carbon, and carbon rods previously sintered in a new built vacuum furnace. The infrared spectra were taken using Bomem FTIR spectrometer with an interface infrared optics toward the formation chamber. These molecules were theoretically simulated using commercial quantum chemistry suites of programs and homemade codes.

PROFESSIONAL MEMBERSHIPS
- American Physical Society (APS)
- American Chemical Society (ACS)

PREPRINTS

> *Infrared observation and isotopic study of combination bands of linear* C_5 *and* C_9, **Eric Gonzalez**, C.M.L. Rittby, and W.R.M. Graham. New spectroscopy data observed, to be submitted to Journal of Physical Chemistry A

REFEREED PUBLICATIONS

> *Infrared Observation of linear* GeC_3 *trapped in solid Ar*, **Eric Gonzalez**, C.M.L. Rittby, and W.R.M. Graham. Journal of Chemical Physics, **130**, 194511 (2009)

FTIR identification of the $\nu_4(\sigma_u)$ and $\nu_6(\pi_u)$ modes of linear GeC_3Ge *trapped in solid Ar*, **Eric Gonzalez**, C.M.L. Rittby, and W.R.M. Graham, Journal of Physical Chemistry A, **2008**, *112* (43)

Vibrational spectra of germanium-carbon clusters in solid Ar: Identification of the $\nu_4(\sigma_u)$ mode of linear GeC_5Ge, **E. Gonzalez**, C.M.L. Rittby, and W.R.M. Graham, Journal of Chemical Physics, **125**, 044504 (2006)

PRESENTATIONS

- *Recent Results on the Vibrational Spectroscopy of Carbon Clusters,* **Eric Gonzalez** and W.R.M. Rittby, Physics and Chemistry of Matrix Isolated Species, Gordon Research Conferences, Magdelan, Oxford, July 2009.
- *Infrared Spectroscopy and Theoretical Studies of Group IV Molecules*, **Eric Gonzalez**, dissertation lecture, Texas Christian University, July 2009.
- *Infrared Observation of the $\nu_2(\sigma)$ Stretching Mode of Linear* GeC_3, **Eric Gonzalez**, C.M.L. Rittby, and W.R.M. Graham, 63rd International Symposium on Molecular Spectroscopy, Ohio State University, Columbus, OH, June 2008.
- *Identification of the $\nu_4(\sigma_u)$ and $\nu_6(\pi_u)$ modes of linear* GeC_3Ge *and $\nu_3(\sigma)$ mode of linear* GeC_3Si*"*, **E. Gonzalez**, Physics and Chemistry of Matrix Isolated Species, Gordon Research Conferences, Bates College, Lewiston, ME, July 2007.
- *Infrared spectroscopy of germanium-carbon clusters*, **E. Gonzalez**, pre-dissertation lecture, Texas Christian University, February 2007.
- *FTIR spectroscopy of germanium-carbon clusters,* **Eric Gonzalez**, C. M. L. Rittby, and W. R. M. Graham. Fall Meeting, Texas Section, American Physical Society, October 2006, University of Texas at Arlington.
- *Vibrational spectra of germanium-carbon clusters in solid Ar*, **E. Gonzalez**, C.M.L. Rittby, and W.R.M. Graham, 61st International Symposium on Molecular Spectroscopy, Ohio State University, Columbus, OH, June 2006.
- *FTIR and DFT Studies of Carbon Chains and Metal-Carbon Species of Astrophysical Interest*, Rafael Cardenas, S. A. Bates, **Eric Gonzalez**, R.E. Kinzer, Jr., C.M.L. Rittby, and W.R.M. Graham, Matrix 2005: The Physics and Chemistry of Matrix-Isolated Species, Funchal, Madeira, Portugal, July 2005.